Development of Water Purification Systems Based on Reverse Osmosis

United States Department of the Interior

Office of Saline Water • Research and Development Progress Report No. 410

Research and Development Progress Report No. 410 • April 1969

Development of Water Purification Systems Based on Reverse Osmosis

By R. C. Ellington, Pratt and Whitney Aircraft Division of United Aircraft Corporation, East Hartford, Connecticut, for Office of Saline Water, J. A. Hunter, Director; W. Sherman Gillam, Assistant Director, Research; Sidney Johnson, Chief, Applied Science Division; Raymond H. Horowitz, Project Monitor

Contract No. 14–01–0001–1113

UNITED STATES DEPARTMENT OF THE INTERIOR • Walter J. Hickel, Secretary
Carl L. Klein, Assistant Secretary for Water Quality and Research

For sale by the Superintendent of Documents, U.S. Government Printing Office
Washington, D.C. 20402 - Price $2.25

As the Nation's principal conservation agency, the Department of the Interior has basic responsibilities for water, fish, wildlife, mineral, land, park, and recreational resources. Indian Territorial affairs are other major concerns of America's "Department of Natural Resources".

The Department works to assure the wisest choice in managing all our resources so each will make its full contribution to a better United States—now and in the future.

FOREWORD

This is one of a continuing series of reports designed to present accounts of progress in saline water conversion and the economics of its application. Such data are expected to contribute to the long-range development of economical processes applicable to low-cost demineralization of sea and other saline water.

Except for minor editing, the data herein are as contained in a report submitted by the contractor. The data and conclusions given in the report are essentially those of the contractor and are not necessarily endorsed by the Department of the Interior.

TABLE OF CONTENTS

TABLE OF CONTENTS (Cont'd.)

LIST OF FIGURES

LIST OF FIGURES (Cont'd.)

LIST OF FIGURES (Cont'd.)

LIST OF FIGURES (Cont'd.)

LIST OF FIGURES (Cont'd.)

LIST OF TABLES

LIST OF TABLES (Cont'd)

I. INTRODUCTION

Pratt & Whitney Aircraft has conducted an applied research program for the Office of Saline Water, U. S. Department of the Interior, to demonstrate the concept of a compact factory-assembled disposable reverse-osmosis cartridge. Three major activities were carried out. These were: 1) a search for suitable membrane supporting structures and materials during which the hydrodynamic characteristics of a number of potential materials were evaluated, 2) the evaluation of reverse-osmosis membranes cast directly on support materials and on reinforcing materials, and 3) the design, fabrication and testing of a small reverse-osmosis cartridge.

The concept of a disposable compact cartridge reduces capital costs and operating costs. Capital costs are reduced by minimizing the high-pressure volume of the reverse-osmosis plant and also the size of the pumping facilities. The operating costs are reduced because the replacement cost of the membranes is minimized, labor cost for membrane replacement is minimized, and the energy cost is minimized because the brine-side pressure drop is low. The primary objective of these investigations was to identify components and processes that would be adequate for the demonstration of the cartridge concept. The investigations were not exhaustive and were generally terminated after a successful approach to a cartridge component had been demonstrated. Some of the approaches that were not carried out to a successful completion could probably be demonstrated with additional effort.

All investigations were performed with solutions of NaCl in water. For the most part tap water was used, although distilled water was used in a few cases.

II. SUMMARY

Two compact cartridges were fabricated and tested. The first cartridge consisted of three "composite membranes" and had a total membrane surface area of 2.4 square feet. This unit operated at a recovery factor* of 8 percent on a NaCl feed of 10,000 ppm; the performance of this unit was 23 gallons per square foot per day at 93 percent salt rejection. The second unit consisted of 10 composite membranes with a total surface area of 8.0 square feet. This unit operated at a recovery factor of 50 percent. The performance of this unit on 5,000 ppm NaCl would be 30 gfd at a salt rejection of 95 percent. Concentration polarization effects on these cartridges were minimal.

A process was developed for manufacturing reverse-osmosis membranes reinforced with nylon cloth. The performance of these membranes under the standard test conditions established by OSW for brackish water is 25 to 30 gfd at a salt rejection of 98 to 95 percent.

During a 500-hour test the performance of three membranes decreased from 25 gfd at a salt rejection of 97 percent to 23 gfd at a salt rejection of 93 percent. Either a linear or a logarithmic function of time is consistent with this data. The decay rate is low enough for the design of practical reverse-osmosis systems, only if the decay is logarithmic. The data does not support a conclusion with respect to the type of decay, and 1,500-hour tests are recommended to resolve this question which is crucial for any reverse-osmosis membrane or device.

The hydrodynamics of a number of porous support materials and structures were evaluated.

A grooved plastic support plate for use with reinforced membranes was selected for the cartridge demonstration. The combination of a plate grooved on both sides and supporting membranes on both sides is referred to in this report as a composite membrane. This configuration offers considerable latitude in design because it permits very long flow paths for the product water with negligible pressure drop.

* Recovery factor is defined as the percentage of the feedwater stream recovered as product-water flux

III. HYDRODYNAMICS OF POROUS MEDIA

A. Requirements of Porous Materials

One of the major components of reverse-osmosis systems is the porous material used in the formation of composite membranes. The porous material is necessary to support the reverse-osmosis membranes and to remove the product water produced by the membranes. Two properties of the porous material dominate the design of a reverse-osmosis plant: the porous material thickness and its product-water flow resistance. The membrane surface area density of a compact cartridge is strongly dependent upon the thickness of the porous material. For the best product-water economy the thickness of the porous material should be a minimum in order to obtain a high membrane surface area density. Also, in the interests of good plant economy, the back pressure of the product water flowing through the porous material should be a minimum. The back pressure is strongly dependent upon the thickness of the porous material and its flow resistance coefficient. For a given material, back pressure can be minimized by going to greater thicknesses. In order to achieve a practical design, a compromise must be made between porous-material thickness and product-water back pressure. Since flow resistance is a function of the composition of the porous material, a material must be found which has a suitably low flow resistance so that it can be used in thin sections. This material must also have sufficient mechanical strength, long-term resistance to creep, and be of low cost.

The objective of this section of the program was to evaluate the hydrodynamics and flow resistance of porous materials for use in the design of a compact reverse-osmosis system. The porous material specimens were encapsulated with RTV silicone rubber and inserted into an evaluation cell. A compressive loading was applied by a hydraulic system to the test cell to simulate the effect of brine pressure and to force a positive seal between the porous material and the cell components. Evaluation was accomplished by experimentally measuring the pressure loss across specimens of known length at a series of purified water flow rates and at compressive loads expected in actual operation. A complete description of the evaluation cell and test system used during the evaluation is presented in Appendix 1. To fulfill the objectives of the contract the following program was performed:

1) Basic analytical and experimental evaluations were performed in order to select 15 porous materials for detailed investigations. The materials evaluated were subdivided into engineered, commercial and zero-loss materials. The engineered materials consist of an aggregate composite molded from sand using phenolic resin, phenoxy resin, terpolymer resin (acrylonitrile butadiene styrene),and Portland cement as binders. These materials are easily formed, they are porous, and their cost is low.

The commercial materials varied from expensive materials such as sintered stainless-steel screen developed for the aerospace industry, to inexpensive materials such as Flexboard, an asbestos-cement composite developed for the building industry. The zero-loss materials contained surface grooves to provide for product-water transport. They were formed from inexpensive solid materials such as phenolic resin, polyvinylchloride and the cement-asbestos building materials.

2) The pressure drop across the 15 materials under several simulated feed-water pressures was measured at controlled water flow rates.

3) Based on the above screening tests, the six most promising materials were evaluated further in 100-hour tests.

4) Four specimens were then endurance-tested for 500 hours. The endurance test was performed to determine whether there was any significant change in the flow resistance of the materials as a function of time. The compressive load, water flow rate, and water temperature were varied during the tests.

The major experimental study was the determination of the flow resistance coefficient α of the materials selected. The pressure gradient in a porous material is given by

$$\frac{dp}{dx} = \alpha \mu V + \beta \rho V^2$$

where V is the velocity of the water, μ the viscosity, ρ the density and where α and β are two undetermined coefficients. The first term of the equation describes the viscous effects and the second term accounts for the inertial effects. For low rates of water flow the second term can be neglected and the equation becomes

$$\frac{dp}{dx} = \alpha \mu V$$

The undetermined coefficient α is the flow resistance coefficient. It is a function of the porosity and the pore texture of the material, and is independent of the overall dimensions of the porous material[1]. Analytical studies have shown that the flow resistance coefficient must not exceed a range of 10^{10} to $10^{12} ft^{-2}$ to be considered as a feasible support material in a desalination system. At values greater than 10^{12} ft^{-2}, the back pressures created would cause flux reductions in excess of 20 percent.

1 See Page 124 for numbered list of references

B. Evaluation of Porous Materials

The fifteen materials selected for evaluation are listed in Table 1 and are shown in Figures 1, 2 and 3.

TABLE 1

Porous Materials

A) Engineered Materials

sand-phenolic
sand-phenolic-Fiberglas
sand-phenoxy
sand-cement-asbestos
sand-terpolymer (ABS)

B) Commercial Materials

sintered glass (20-25 μ)
sintered stainless-steel screen
sintered stainless steel
resin bond - cellulose fibers
porous ceramic (10 μ)
porous ceramic (100 μ)

C) Zero-Loss Materials

phenolic resin
polyethylene
sintered glass (5 μ)
Flexboard

The support material samples were fabricated or purchased to the dimensions of 4 inches long, 1.5 inches wide and 0.062 inch thick. A complete description of the procedures and processes employed to fabricate the six engineered porous support materials is presented in the second quarterly report, PWA-3042. A photograph of a zero-loss material is shown in Figure 4. Twenty grooves were machined into these materials so that a measurable pressure drop across the sample could be obtained. A groove 6 mils square with 20-mil spacing between grooves was used for the phenolic resin and Flexboard samples, and a groove 4 mils square for the sintered-glass specimens. The calculated pressure losses were 18 psi for the specimens with 6-mil square grooves and 91 psi for the 4-mil specimens.

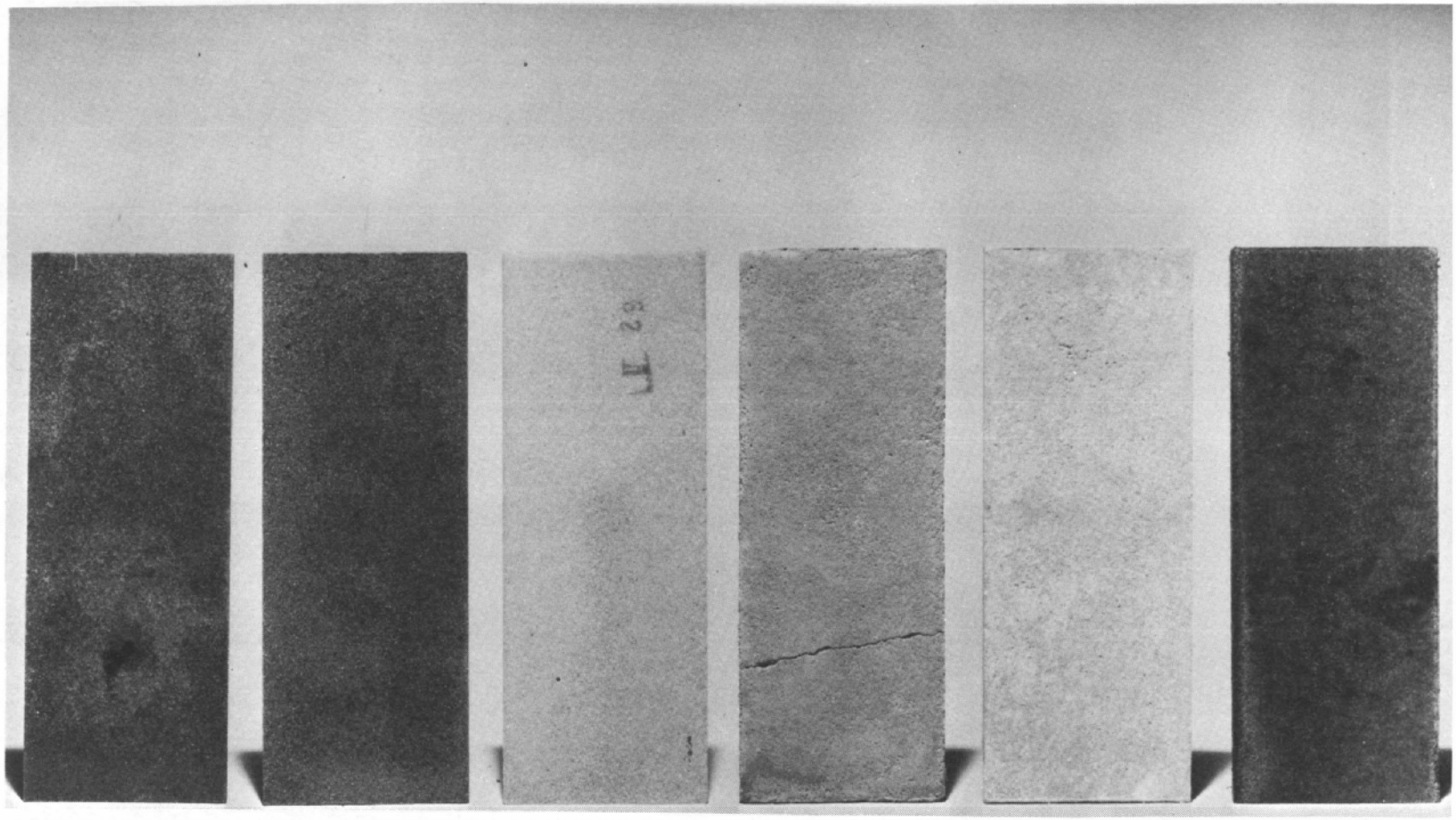

sand-phenolic

sand-phenolic-Fiberglas

sand-phenoxy

sand-Portland cement

sand-Portland cement-asbestos

sand-terpolymer

Figure 1 Engineered Porous Support-Material Specimens XP-74456

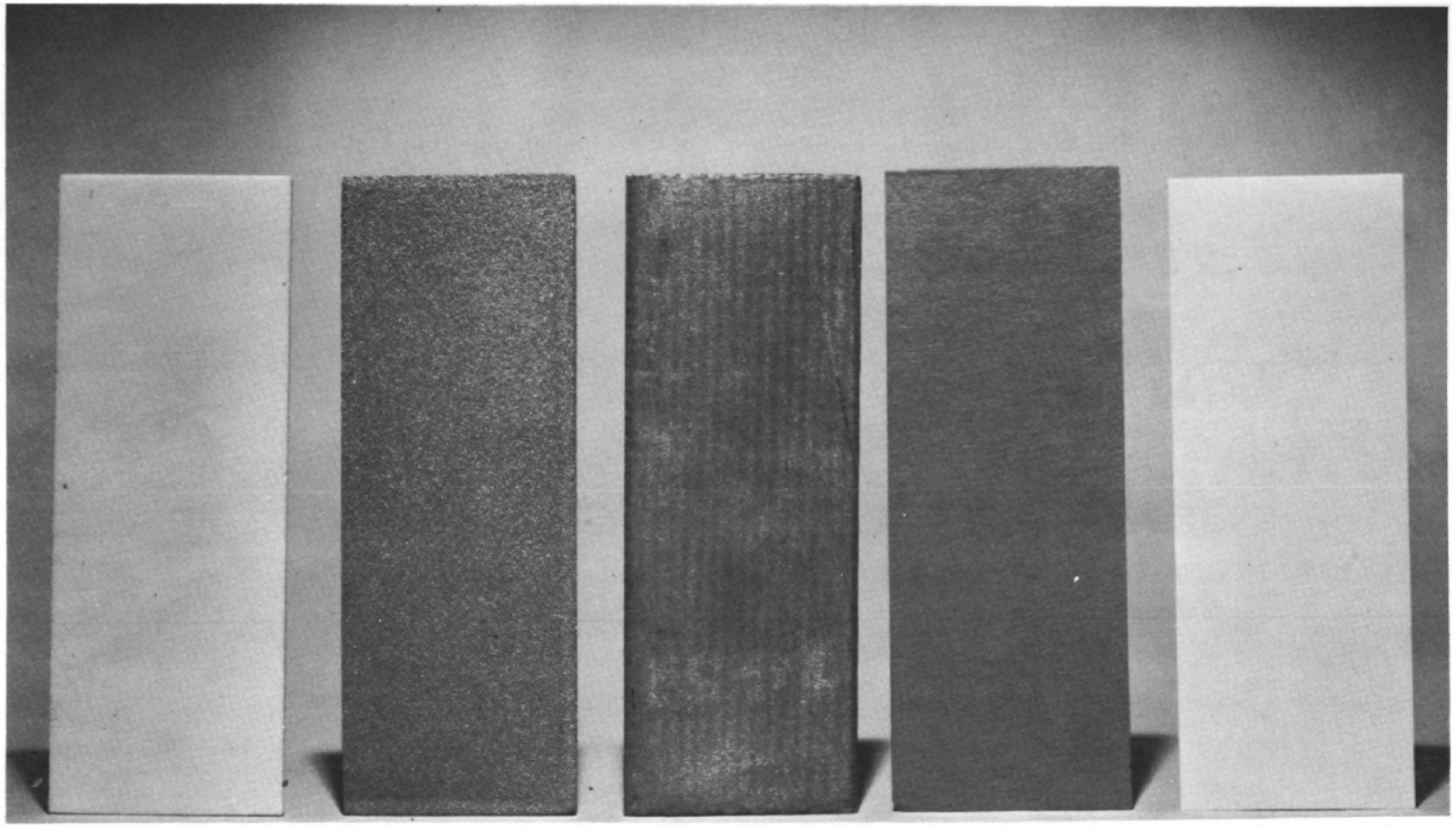

sintered glass

sintered stainless steel

sintered laminated stainless steel screen

resin-bonded cellulose fiber

porous alumina

Figure 2 Commercial Porous Support-Material Specimens XP-74451

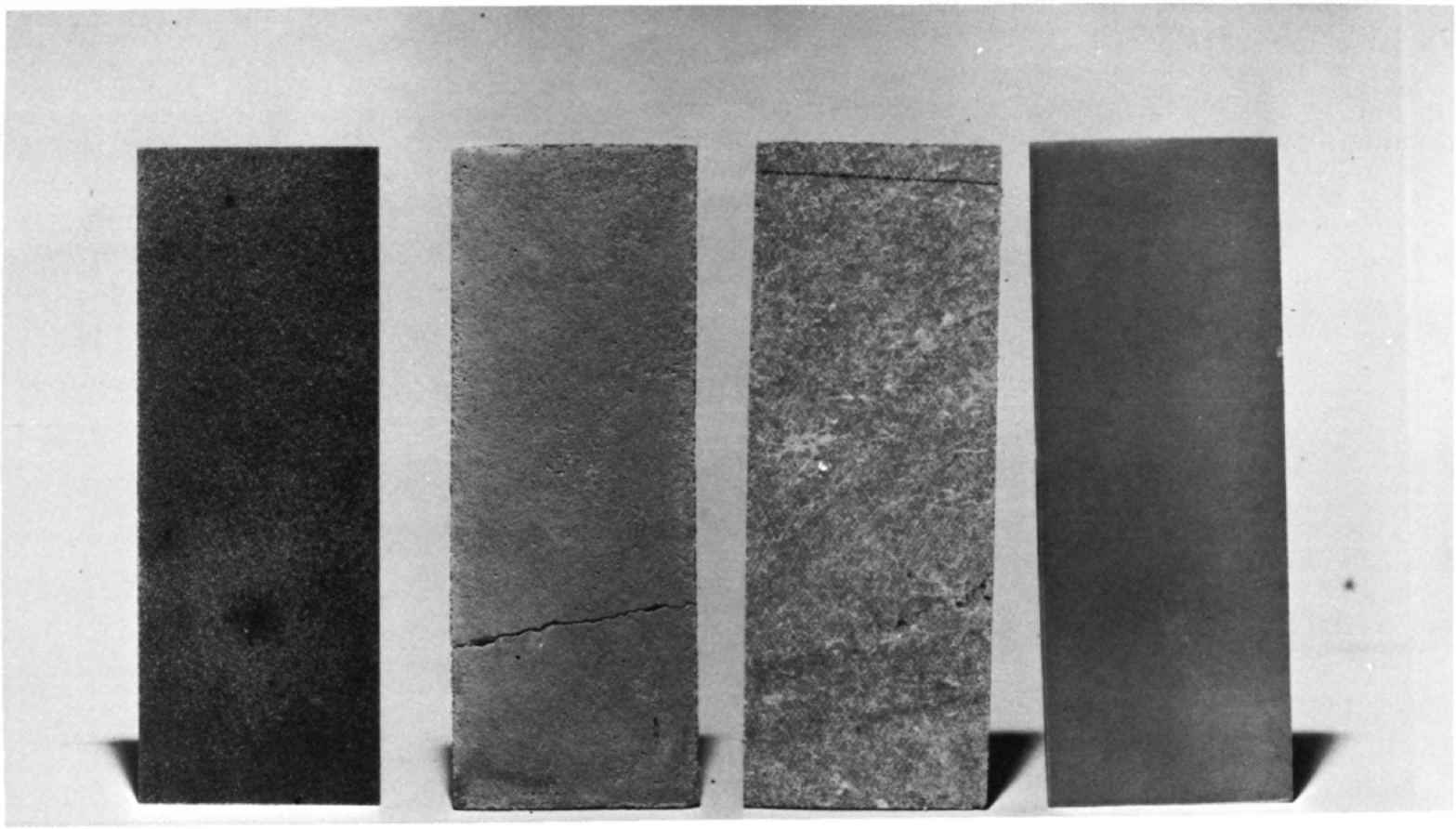

sand–phenolic

sand–Portland cement

Flexboard

phenolic resin

Figure 3 Zero-Loss Support-Material Specimens XP-74450

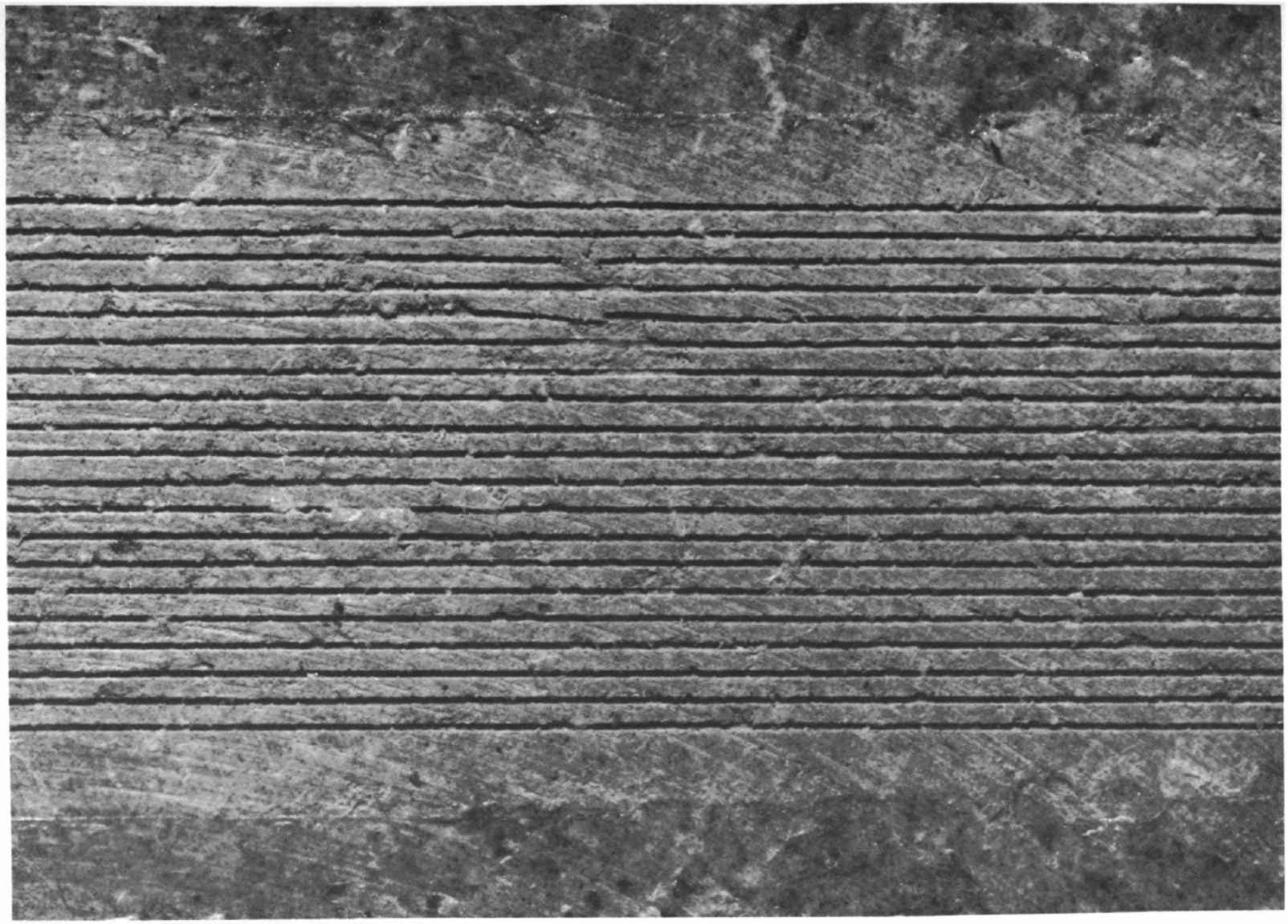

Figure 4 Grooved Flexboard Specimen XP-77671

1. Screening Tests

The test conditions for the support materials selected for evaluation were 0.5 gph product-water flow rate, 750 psi simulated feedwater pressure, and 77°F feedwater temperature. Two specimens of each material were evaluated for approximately 12 hours. Based on early test results, the materials were subdivided into two groups, high-pressure materials and low-pressure materials. High-pressure materials were evaluated at 0.5 gph product-water flow rate, 1500 psi compressive load, and 77°F feedwater temperature. The low-pressure materials were evaluated at the same conditions except that the compressive load was 400 psi. The tests were normally conducted for 10 hours.

A summary of the major results is presented in Table 2. This table presents the values of average pressure loss and flow resistance coefficient for the two specimens evaluated at a compressive load of 750 psi. The zero-loss configuration appeared to have the most desirable flow characteristics for reverse-osmosis support materials. Several commercial porous materials such as sintered stainless steel, porous alumina and sintered stainless-steel screen had reasonable performance, but were much too expensive for further consideration (about $\$50/ft^2$).

A complete tabulation of the data recorded for the screening tests can be found in Appendix 1.

TABLE 2
Support-Material Summary

	Calculated psi	$P_1 - P_2$, psi	α ft^{-2}	Cost	Remarks
Grooved Materials					
phenolic resin	18	20.0		inexpensive	-
Flexboard	18	45.0		inexpensive	-
sintered glass (5μ)	91	98.6		moderate	brittle
Porous Materials					
stainless-steel screen	-	5.3	8.80×10^9	expensive	
100μ porous ceramic	-	20.5	1.30×10^{10}	moderate	brittle
sand-terpolymer	-	21.8	2.25×10^{10}	inexpensive	exhibited creep
sintered stainless-steel	-	73.7	5.50×10^{10}	expensive	-
sand-Fiberglas-phenolic	-	62.5	6.20×10^{10}	inexpensive	-
25μ sintered glass	-	203.0	1.40×10^{12}	moderate	brittle
resin-bonded cellulose fibers	-	233.8	4.10×10^{11}	inexpensive	compressed
sand-phenolic	-	220.7	2.10×10^{12}	inexpensive	-
10μ porous ceramic	-	232.5	2.20×10^{12}	moderate	brittle
sand-phenoxy	-	*	-	inexpensive	-
sand-cement	-	*	-	inexpensive	-
sand-asbestos-cement	-	*	-	inexpensive	-

* The desired water flow rate could not be attained

2. 100-Hour Tests

As a result of the screening tests, six materials were selected to be tested for 100 hours. Table 3 lists the materials selected and the compressive load at which they were evaluated.

TABLE 3
100-Hour Evaluation of Porous Materials

Material	Compressive load, psi
sand-phenolic- Fiberglas	1500
sand-terpolymer (ABS)	750
sintered stainless-steel screen	1500
sintered glass (5 μ) zero-loss	1500
phenolic resin zero-loss	1500
porous ceramic (100 μ)	750

The basic operating conditions were a water flow rate of 0.5 gph and a water temperature of 77°F. Variable water flow and pressure programs were performed on all samples. A temperature variable program was performed on the sintered stainless-steel screen sample.

Figure 5 presents a plot of pressure loss as a function of time for the six materials. The curves shown represent the average of two specimens except for the sand-phenolic-Fiberglas and the sintered-glass zero-loss specimens, where the performance of one sample is shown. These specimens were eliminated from discussion as a result of high pressure losses due to experimental sealing problems.

Typical performance curves for the variable flow, compressive load, and temperature programs are shown in Figure 6. The results of the variable programs were as follows:

1) The pressure loss was a linear function of flow rate, demonstrating that the flow resistance coefficients were constant and independent of velocity in the range investigated.

2) The pressure loss was independent of the compressive load for all specimens except for the sand-terpolymer and the sintered-glass zero-loss specimens. As previously mentioned, this is attributed to material creep and experimental sealing problems.

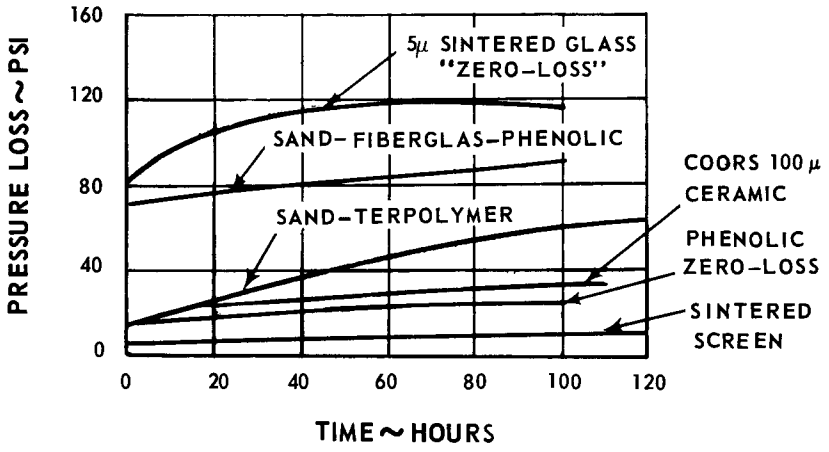

Figure 5 Pressure Loss as Function of Time. 100-Hour Endurance

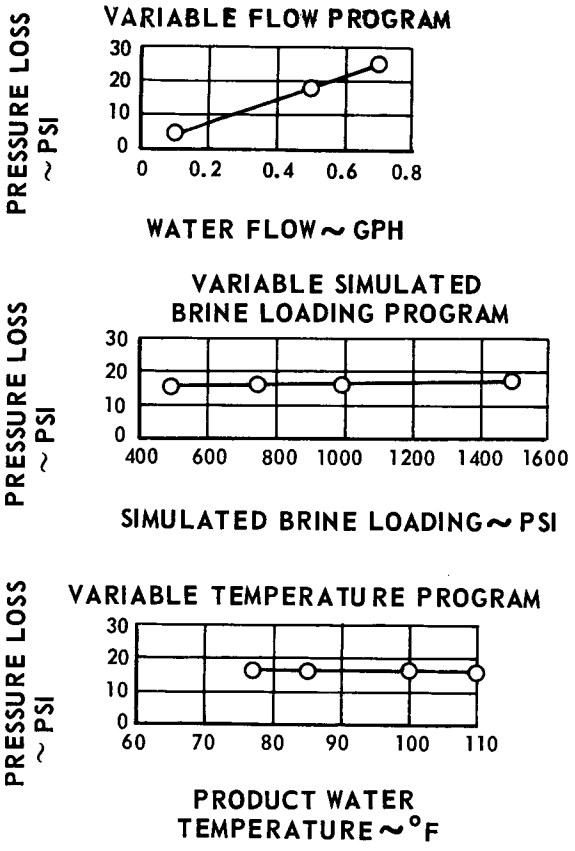

Figure 6 Performance of Sintered Stainless-Steel Screen in Variable-Flow, Pressure and Temperature Programs

3) Pressure loss as a function of increasing water temperature is relatively constant. The data obtained showed that there was a slight decrease in the pressure loss as the water temperature was increased. This change is smaller than the measurement accuracy.

3. 500-Hour Endurance Tests

The four specimens selected for the 500-hour test were: two phenolic resin zero-loss specimens, one Flexboard specimen, and one sand-phenolic-Fiberglas specimen. The sintered stainless-steel screen was not included because it was felt that since the material had performed so well during the 100-hour test, it would not generate much more useful data compared to that generated by the engineered material sand-phenolic-Fiberglas. The operating conditions were 0.5 gph and 77°F. All four specimens were high pressure materials and the simulated feedwater pressure was 1500 psi. A variable water flow and simulated brine pressure program was performed.

Figure 7 presents the pressure loss as a function of time. The pressure loss increase of the phenolic-resin zero-loss specimens is attributed to partial clogging of the grooves with small air bubbles, or possibly to system contamination.

Figure 8 presents a curve of the data obtained from a typical variable water flow rate and simulated brine pressure program. As can be seen, the pressure loss is independent of the simulated brine loading. The flow resistance coefficients are constant and independent of water velocity, as demonstrated by the linearity of the curve.

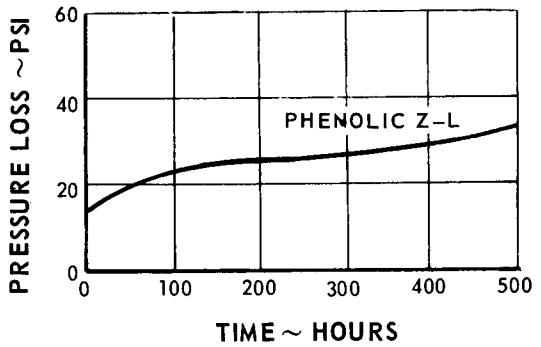

Figure 7 Pressure Loss as Function of Time. 500-Hour Endurance

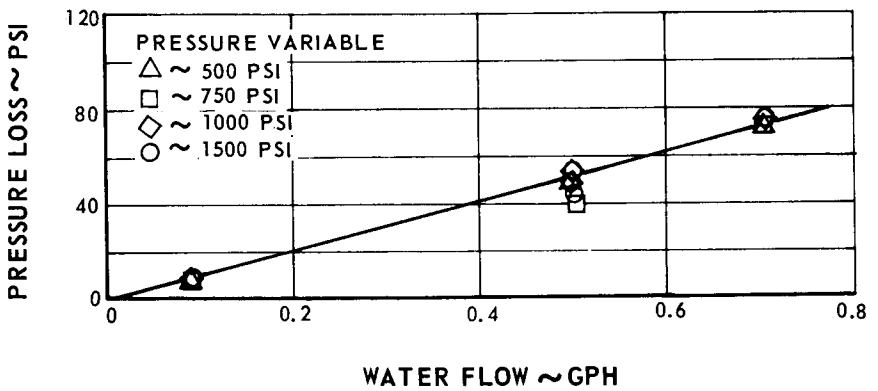

Figure 8 Pressure Loss as Function of Water Flow with Simulated Brine Pressures. Flexboard Specimen

IV. REINFORCED MEMBRANE STUDIES

One of the principal problems associated with casting a membrane on a glass plate is that it is relatively low in structural strength and is easily torn. As a means of overcoming this weakness, reinforced membranes were formed by casting membranes on thin substrates, such as cloth fabrics and porous materials, and the membranes were thus given added strength and resistance to tearing. Reinforced membranes are simpler to attach to a porous support material, and they permit a designer more flexibility in the design of an actual reverse-osmosis desalination system. The use of a reinforcing fabric provides a more uniform support to the membrane if the membrane support material has a relatively large pore size. This is important since it has been observed experimentally that a degradation in membrane performance will result unless the membrane is supported uniformly by a smooth material.

The purpose of this program was to study the problems of forming modified cellulose-acetate reverse-osmosis membranes on the surfaces of both thin reinforcing fabrics and on porous support materials. They were evaluated to define the best method of membrane formation for the manufacturing of composite membranes in large volume. A detailed description of the membrane preparation area, membrane cast area and the membrane evaluation facilities is presented in Appendices 2 and 3.

In order to fulfill the above objectives the following program was performed:

1) The performance characteristics of modified cellulose-acetate membranes cast on reinforcing fabrics and on porous materials were measured. The reinforcing fabrics selected for evaluation were acetate, nylon, Dacron, Dynel, Fiberglas, Saran Mono, Polymax B, cotton, acrylic and rayon. The porous materials selected for evaluation were sintered glass, molded sand, nylon felt and Dacron felt. The most promising type of reinforcing material was selected for further studies.

2) Variations were made in the membrane formulation, formation, processing and evaluation techniques in order to optimize the desalination performance characteristics of the reinforced membranes. The performance characteristics of the optimized membranes were determined as a function of operating conditions.

3) Twenty of the best performing membranes were then lifetime-measured to define their product-water flux decay as a function of operating time.

A. Membrane-Coated Reinforcing Materials

Twenty-eight potential reinforcing fabrics were screened in order to identify six fabrics that had desalination performance characteristics similar to or superior to membranes cast on glass plates. The reinforcing fabrics selected for evaluation were acetate, nylon, Dacron, Dynel, Fiberglas, Saran Mono, Polymax B, cotton, acrylic and rayon. Membranes were cast on these fabrics and were evaluated with respect to membrane adhesion, cast solution bleed-through and membrane integrity. Properties such as material wetability, weave count, thread fiber count, gauge, mono or multi filament, woven or fused interstices and surface finish were considered.

With a few exceptions, fabric material contributed little to the behavior of membrane-coated composites. Membrane adhesion was, in general, strictly mechanical in nature and was related more to fabric structure than to chemical composition.

There were three notable exceptions:

1) Membranes cast on cotton were unsatisfactory due to absorption of casting solution which prevented the formation of a continuous cast film.

2) Membranes cast on Dynel (vinylchloride acrylonitrile copolymer) fabrics failed to achieve satisfactory film continuity, apparently due to incomplete wetting of the fabric surface.

3) The bond of membranes on cellulose-acetate fabric was better than on other reinforcing materials. This superiority probably resulted from the chemical similarity of the membrane and reinforcing materials, which may have produced a chemical bond between them.

The structure of fabric reinforcing materials appeared to exert a marked effect on the attachment, integrity and performance of cast membranes. Coarse-textured fabrics, such as acrylic S/40726, provided poor surfaces for casting which resulted in membrane discontinuities and craters. In most instances, open-weave fabrics containing large interstices were prone to a high degree of cast solution bleed-through and entrapped gas bubbles, while membranes cast on close-weave fabrics showed negligible bleed-through. Apparent membrane adhesion was better on the open-weave fabrics due to the mechanical advantage derived from enveloping of the fibers. Two exceptions to the bleed-through behavior were observed, one with Dacron and one with Fiberglas. These exceptions cannot be fully explained, but they appear to be related to fabric thickness. A detailed summary of the twenty-eight fabrics evaluated is presented in Table 4.

TABLE 4

Experimental and Analytic Study of Reinforced Membrane Composites

Material	Designation	Weave	Wt/sq yd	Fiber Count	Gauge, in.	Mono or Multi Filamented	Woven (or) Fused Interstices	Finish	Bleed Through, %	Adhesion	Appearance	Surface		Vendor	Remarks
												Top	Bottom		
nylon	5055	satin	4.0 oz	270 x 112	0.0075	multi	woven		0	poor	trans.	smooth	unaffected	Travis	
Dacron	601	plain	3.0 oz	112 x 76	0.0050	multi	woven		0	poor	trans.	smooth	unaffected	Travis	
Dynel	821	twill	6.0 oz	100 x 52	0.0016	multi	woven		0	fair-good	trans.	rough	unaffected	Travis	coarse fibers
Fiberglas	EM-30			40 x 34	0.0070	multi	woven	heat-cleaned	0	poor	trans.	smooth	unaffected	Millikin	
Saran mono	1440133			113 x 45	0.019	mono	fused		0	good	trans.	smooth with flaws	unaffected	Nat. Filter Media	entrapped air pits
Polymax B	224-019-04			114 x 122	0.012	mono	woven		0	poor	trans.	smooth	unaffected	Nat. Filter Media	
acetate No. 400 L-9535	26194-5			205 x 73	0.0068	multi	woven		0	good	trans.	smooth	unaffected	Stevens	chemical attachment
Dacron polyester	S/91669		220 oz	46 x 50	0.0055	multi	woven		4	good	trans.	smooth	unaffected	Burlington	
Fiberglas	EM-16			55 x 51	0.004	multi	woven	G-500	10	good	trans.	smooth	lumpy	Millikin	
Dynel	815	plain	3.75 oz	23 x 21	0.0017	multi	woven		50	good	trans.	rough with flaws	rougher with flaws	Travis	many flaws
cotton	M1550		35.0 gm	37 x 28	0.004	multi	woven		75	fair-good	trans.	smooth	many flaws	Kendall	bottom 25% flaws
Fiberglas	116(175-6507)			61 x 58	0.004	multi	woven		80	good	stripped	smooth	large craters	Millikin	
Fiberglas	116 Garan			52 x 52	0.004	multi	woven		90	good	trans.	smooth	craters	Millikin	crater effect
nylon	5183	twill	1.6 oz	84 x 84	0.0055	mono	woven		90	good	trans.	smooth	large craters	Travis	
Saran	901	plain	6.8 oz	32 x 32	0.0185	mono	woven		95	good	opaque	pitting	pitting		pitting breakthrough
acrylic	S/40726	100%	acrylic	flag bunting	0.0095	multi	woven		95	good	opaque	rough	rough craters	Burlington	
nylon	S/G9560	---	210 oz	18 x 17	0.0065	multi	woven		98	good	trans.	striated	pits and striations	Burlington	striated in line of cast
nylon	501	leno	0.92 oz	56 x 32	0.0055	multi	woven		100	good	trans.	smooth	pin holes and pits	Travis	wrinkling in line of cast
nylon	M-1A	plain	4.2 oz	45 x 40	0.017	mono	woven		100	good	trans.	smooth	smooth	Travis	
nylon	RFL S-11471		400 oz	25 x 25	0.0165	multi	woven		100	good	trans.	uneven coat	uneven coat	Burlington	uneven-thick and thin
Dacron	606	plain	1.3 oz	110 x 98	0.0035	multi	woven		100	good	trans.	smooth-entrapped air	smooth-pits	Travis	
Fiberglas	EM-10			32 x 26	0.005	multi	woven		100	good	trans.	smooth	large and small pits	Millikin	
Polymax B	224-007-98			32 x 30	0.0225	mono	fused		100	good	trans.	smooth-entrapped air	smooth	Nat. Filter Media	entrapped air pockets
Saran mono	144-008-99			63 x 57	0.022	multi	woven		100	good	opaque	smooth with pits	many entrapped air pockets	Nat. Filter Media	entrapped air pockets
nylon	15401099				0.009				100	no film		weave too large - no film			
rayon	ST 381		32 gm		pressed into sheet				100	good	trans.	smooth	flaws	Kendall	
cotton	R2801		200 gm	41 x 34	0.023	single fibers pressed into sheet				good	opaque	rough	soggy cotton	Burlington	cotton backing
rayon	M1702		778 gm		fiber mat backed by cotton thread				100	good	opaque	smooth	rough	Kendall	coarse fibers

As a result of the initial screening the following fabrics were selected for a more thorough evaluation:

Material	Manufacturer
acetate 26194-5	J. P. Stevens
Dacron 601	Travis Mills
Fiberglas EM-30	Milliken
nylon 5055	Travis Mills
Polymax B 224-019-04	National Filter Media
Dacron S/91669	Burlington Mills

A membrane was cast on two samples of each fabric. All samples were hot-bath treated at 185°F for 4 minutes. The specimens were evaluated for 4 hours at the conditions of 800 psi feedwater pressure, 2.0 gpm feedwater flow rate (turbulent), 77°F feedwater temperature and 5500 ppm NaCl feedwater concentration. The results of the evaluation are presented in Table 5.

TABLE 5

Performance of Membrane-Coated Fabrics

Fabric Designation	Fabric Thickness, mils	Coated Material Thickness, mils		Bleed-Through, %	Product-Water Flow Rate, gfd/ft^2	Salt Rejection, %
		Pretest	Post-test			
Dacron S-91669	5	13	10	slight	18	96
acetate 26194-5	-	16	12	0	16	98
Dacron 601	5	12	9	0	23	94
Fiberglas EM30	7	14	11	0	19	98
nylon 5055	7.5	15	11	0	14	97
Polymax B 224019-4	12	24	17	0	14	97

Travis Mills nylon 5055 was selected as the fabric for further investigation. Selection of this fabric was based on the above tests and the following desirable properties:

1) excellent membrane adhesion,

2) zero membrane bleed-through,

3) excellent membrane appearance, and

4) repeatable membrane performance.

This fabric should be considered typical rather than superior to the other five fabrics.

The characteristics of Travis Mills nylon 5055 fabric are as follows:

thread count	270 x 112
thickness	7.5 mils
density	4 oz per sq yd
fiber	multi-filament, woven interstices

1. Membrane-Coated Support Materials

Seventeen engineered and commercial porous materials were coated with membranes and their performance evaluated. The evaluation tests were performed at the previously-mentioned test conditions. A tabulation of the materials evaluated and the performance obtained is presented in Table 6.

TABLE 6

Performance of Membrane-Coated Porous Materials

Material	Product-Water Flow Rate, gfd	Salt Rejection, %
sand-asbestos-phenolic	15	93
sand-phenolic	failure	
sintered glass	failure	
Corfam	12	1
cellulose-acetate fiber composite	16	93
Fiberfrax	73	58
Dacron felt 4005	40	25

TABLE 6 (Cont'd)

Material	Product-Water Flow Rate, gfd	Salt Rejection, %
Dacron felt 4024	failure	
nylon felt 2020	failure	
nylon felt 2014	failure	
sand-Fiberglas-phenolic resin		
Sample No. 1	29	82
Sample No. 2	25	97
Sample No. 3	18	78
Sample No. 4	27	88
asbestos Flexboard		
Sample No. 1	4.9	63.8
Sample No. 2	36.8	10.4
Sample No. 3	11.2	11.1
resin-bonded cellulose fiber		
Sample No. 1	116	44
Sample No. 2	20	85
Amerace rubber separator	failure	
Eccofoam	failure	
rigidified material	failure	
cement-sand-asbestos	failure	

One sand-Fiberglas-phenolic resin specimen had performance characteristics similar to those obtained with reinforced membranes, however, performance repeatability could not be achieved. Further work in this direction was discontinued as no membrane-coated porous material performed better than the membrane-coated fabrics. Also, the failure rate of these specimens was high and it became obvious that a long development program would be required. This program demonstrated that acceptable performance could be obtained by directly casting a membrane on a porous support material. If a membrane could be directly cast on both sides of a porous support material, a sizable reduction in the fabrication cost of a composite membrane would result. A photograph of a membrane-coated engineered material is shown in Figure 9.

B. Study of Membrane Processing

The second phase of the reinforced membrane study was to evaluate the effects of different cast-process parameters on the performance of the modified cellulose-acetate membranes. The casting process employed was essentially that developed by Manjikian[2] except that the membranes were cast on Travis Mills nylon 5055 instead of a glass plate. The membrane processing studies

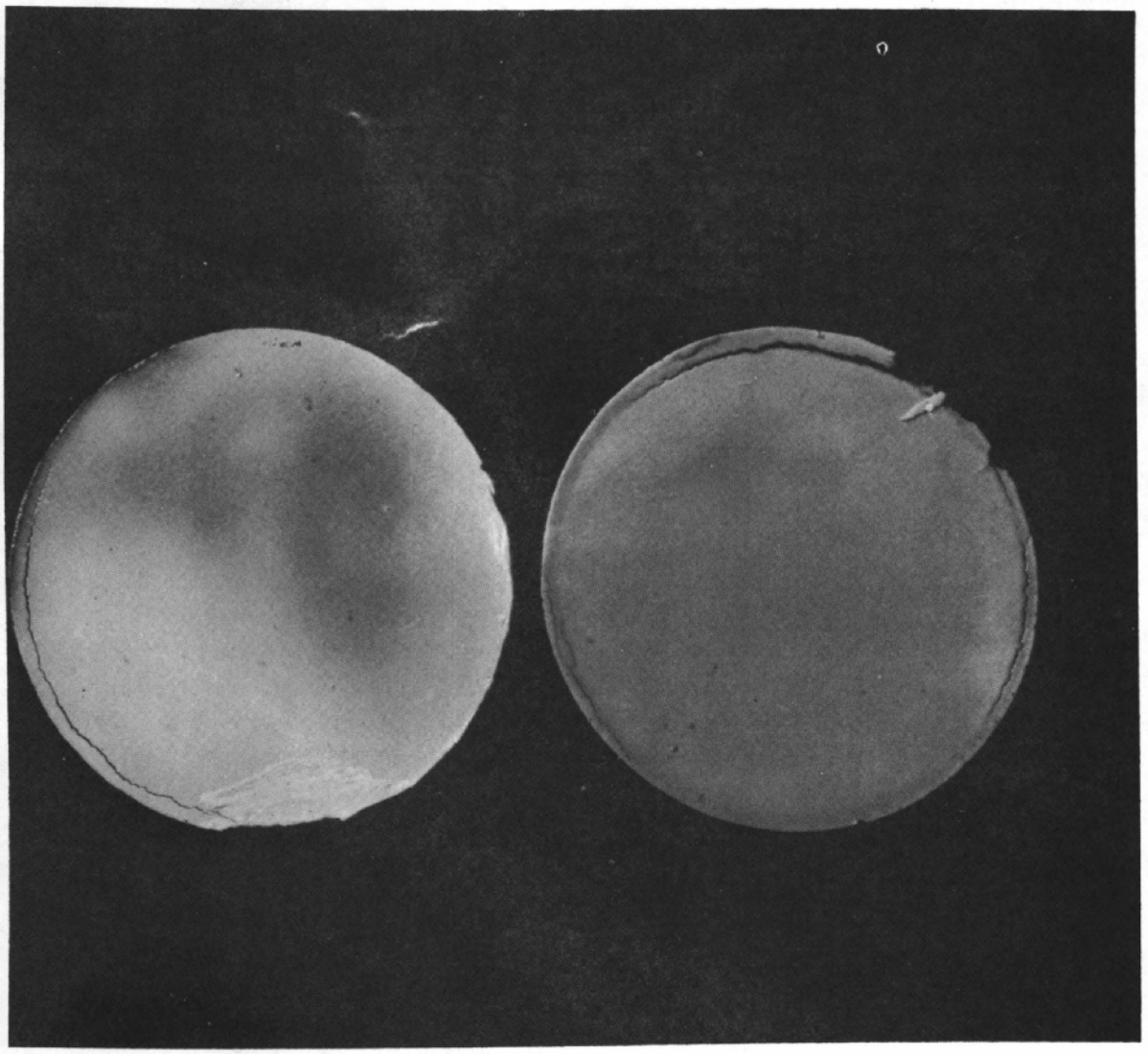

Figure 9 Membrane-Coated Sand-Phenolic Resin-Fiberglas Specimens H-61607

were directed towards, 1) producing high-performance repeatable membranes, 2) identifying the significant cast-processing parameters, and 3) obtaining a performance map as a function of the cast-processing parameters. It was hoped that the performance map would yield an optimum membrane. It was found that many formulations could yield high-performing membranes and no one formulation was significantly better than the others. For this reason the following formulation and processing conditions were selected for all further studies:

Membrane Formulation - percent by weight

cellulose acetate	25
acetate	45
formamide	30

Processing Conditions

cellulose acetate type	Eastman Kodak E-398-3
reinforced membrane thickness	15 mils
cast temperature	70°F
evaporation time	30 seconds
cold-bath temperature	35°F
cold-bath time	1 hour
hot-bath temperature	180°F
hot-bath time	4 minutes

1. Membrane Formation Technique

The reinforced membranes formed during these studies were cast in a facility designed and developed by Pratt & Whitney Aircraft. The cast facility offered the advantages of mechanized casting and a controlled and variable cast environment. The characteristics of the facility were as follows:

Cast Chamber

controlled temperature	0-70°F
controlled humidity	0-70%
recovery rate	30 min.
atmosphere	as desired
stainless-steel lined	

Cast Knife

cast speed - variable	0.1 to 8.0 ft/sec
cast capabilities	
membrane width	9.0 in.
membrane length	28.0 in.
film thickness	0.093 in.

A detailed description of the membrane preparation area and cast facility is presented in Appendix 2. The cast technique used to obtain high-performance membranes will be presented below. This technique should be considered the standard procedure for processing reinforced membranes for this contract. It was also used as the baseline for comparison studies for the entire program.

Details of the cast-process technique are as follows:

1) The acetone and formamide are added to the cellulose-acetate powder and slowly tumbled (5 to 6 rpm) for 16 hours to insure proper mixing. The solution is filtered and stored at 65°F until it is used. A cast solution containing E-398-10 cellulose acetate is tumbled for 32 hours.

2) The reinforcing fabric is wrapped around a glass plate and placed in the cold-bath pan which is located in the cast chamber.

3) The atmosphere of the cast chamber is conditioned to 70°F with a 30 percent relative humidity.

4) The cast chamber is allowed to stabilize.

5) When a membrane is to be cast, the cast solution is removed from storage and permitted to reach room temperature. A sample is removed and a viscosity check is performed using a Cannon-Fenske Viscometer.

6) The remainder of the cast solution is introduced into the cast-knife solution reservoir.

7) A film approximately 7.5 mils thick is cast onto the fabric at a rate of 0.2 foot per second.

8) The membrane is inundated with a 35°F cold-bath solution 30 seconds from the start of cast. The cold-bath pan is placed in a refrigerator at 35°F for 1 hour.

9) Six 3 x 4 inch samples are cut from the center portion of the membrane sheet and are hot-bath treated at 185°F for 4 minutes. Clips are attached to the bottom of the samples to reduce curling.

10) The sample is stored in tap water at room temperature until it is experimentally evaluated.

A description of the membrane evaluation apparatus is presented in Appendix 3.

2. Membrane-Processing Studies

The first task in the membrane-processing studies was to select the cast-process parameters to be investigated. A large number of parameters influence the performance of cellulose-acetate films, so that it was necessary to select a reasonable number to initiate the study. After a comprehensive review of Pratt & Whitney Aircraft data and published data, the following variables were selected:

1) type of cellulose acetate,
2) percentage of solvent in cast solution,
3) temperature of cast atmosphere,
4) evaporation time,
5) cold-bath temperature,
6) cold-bath composition, and
7) hot-bath temperature.

The investigation of the effect of cast-process variables was a statistically-planned program which used a full factorial matrix. Before presenting the matrix and the initial set of data, the reason for selecting each parameter will be explained and the variations of the parameters will be identified.

1) Type of cellulose acetate - Eastman Kodak cellulose acetate E398-3 and E398-10 were used for the program in order to determine if an increase in polymer chain length would have a noticeable performance effect for a membrane-coated fabric.

2) Percentage of cast-solution solvent - At least one variation of the cast-solution composition was desired. The membrane-coated fabric showed sensitivity to solution viscosity as solution penetration into the weave became the prime variable of the screening program. Solutions of 45 and 48.8 percent by weight acetone were used on the program.

3) Temperature of cast atmosphere - This parameter was selected to vary the acetone evaporation rate, thus controlling the rate at which the skin was formed. The temperature levels selected were 50 and 70°F.

4) Evaporation time - This parameter controls the total amount of acetone that evaporates in the cast chamber if the acetone evaporation rate is constant, and therefore tends to control the skin depth. Variations of 29 to 21 seconds were used in this program.

5) Cold-bath temperature - The cold-bath solution leaches the solvent and swelling agent from the membrane, causing the cellulose acetate to precipitate into a solified structure. The cold-bath temperature variations permit control of the leaching rate. Temperatures of 50 and 35°F were chosen.

6) Cold-bath composition - Composition of the cold bath also affects the leaching rate of the solution, but it was chosen for a different reason. The two compositions used were 100 percent water and 95 percent water - 5 percent acetone by volume. Previous studies had shown that a marked change in performance occurs for a water-acetone cold-bath composition. Apparently the skin structure is partially dissolved or reformed if a small amount of acetone is introduced into the bath.

7) Hot-bath temperature - The membrane must be compacted to achieve a reasonable desalting property. This parameter controls the rate of shrinkage or compaction. Levels of 195, 185, and 175°F were chosen for the initial studies.

The full factorial matrix is shown in Table 7. The columns of the matrix can be used to examine the effect of cast-atmosphere temperature, type of cellulose acetate and percentage of acetone in the cast solution. The rows of the matrix permit examination of the hot-bath temperature, the cold-bath temperature, and cold-bath composition parameters. The matrix is a five-factorial 2-level matrix with the hot-bath temperature and the evaporation time treated in a special fashion.

Thirty-two membrane sheets were made by modifying the type of cellulose acetate, the acetone content of the casting solution, the cast-atmosphere temperature, the cold-bath temperature, the cold-bath solution composition, the evaporation time prior to immersion in the cold bath, and the hot-bath temperature. Six repeat sheets were formed to establish the repeatability of the process. The number of sheets cast under a given set of conditions are presented in Table 7. This series of reinforced membranes constitutes the basic study of cast-process variables.

TABLE 7

Matrix for Cast-Process Variables

Cold-Bath Composition, $\%H_2O$	Cold-Bath Temperature, °F	Hot-Bath Temperature °F	Sheets Processed							
			45% Acetone				48.8% Acetone			
			Cellulose Acetate Type E398-3		Cellulose Acetate Type E398-10		Cellulose Acetate Type E398-3		Cellulose Acetate Type E398-10	
			Cast Temperature		Cast Temperature		Cast Temperature		Cast Temperature	
			50°F	70°F	50°F	70°F	50°F	70°F	50°F	70°F
100	35	175								
		185	2	2	1		1	2	1	1
		195								
	50	175								
		185	1	2	1	1	1	1	1	1
		195								
95	35	175								
		185	1	1	1	1	1	1	1	2
		195								
	50	175								
		185	1	1	1	1	1	1	1	1
		195								

The basic cast process has been described previously. The membrane formation apparatus and the evaluation apparatus is described in Appendices 2 and 3, respectively. The data was subdivided for detailed analysis into two classes, screened and unscreened. The screened data contains only those samples which do not contain major defects. The unscreened data contains all membrane samples. On this basis 59 specimens were excluded, leaving the data from 165 samples. This data then was considered screened data and was used for the analysis. The specimens whose data was excluded had visible defects and were not considered representative of the performance achievable at the given set of cast conditions. The defects normally were cracks in the cellulose-acetate membrane. Cracks occur because the cellulose acetate tends to shrink during processing and the nylon fabric retains its original dimensions, so that the membrane experiences a tensile load because of the presence of the fabric. Excessive bending of reinforced membranes also caused defects in the cellulose-acetate material. A complete listing of the data for each sample was given in the fifth quarterly report, PWA-3256. This report also identified each sample that was considered defective.

The full factorial matrix was analyzed statistically as shown in Table 8. Each set of values of product-water flux and salt rejection listed in the table represent the average performance of from 1 to 4 specimens. All process variable variations are shown in this table except evaporation time. Six membrane specimens were obtained from each membrane sheet that was processed. The evaporation time for these specimens ranged from 29 seconds for Specimen Number 1 to 21 seconds for Specimen Number 6. To minimize the effect of the evaporation time variation, the performance characteristics, product-water flux and salt rejection for Specimens 1 and 4, 2 and 5, and 3 and 6 were averaged. For this matrix, it would have been desirable to consider evaporation rate as one of the prime variables and randomize it accordingly.

The data in Table 8 was processed by a computer to perform a correlation analysis of the independent variables, a correlation analysis of some performance parameters, and a regression analysis of some performance parameters. A correlation analysis of independent variables is shown in the Table 9.

TABLE 8

Screened Matrix Data

Cold-Bath Composition, % H_2O	Cold-Bath Temperature, °F	Hot-Bath Temperature, °F	45% Acetone								48.8% Acetone							
			Cellulose Acetate Type E398-3				Cellulose Acetate Type E398-10				Cellulose Acetate Type E398-3				Cellulose Type E398-10			
			Cast Temperature 50°F			70°F	Cast Temperature 50°F			70°F	Cast Temperature 50°F			70°F	Cast Temperature 50°F			70°F
			gfd	%	gfd	%	gfd	%	gfd	%	gfd	%	gfd	%	gfd	%	gfd	%
100	35	175	80	55	52	85	66	67	44	85	64	70	47	84	45	57	25	87
		185	41	84	29	96	35	92	27	95	39	87	30	95	29	80	23	93
		195	17	96	13	94	17	96	15	92	20	96	18	91	15	96	15	96
	50	175	62	68	46	88	43	60	36	91	68	58	40	84	38	61	26	62
		185	36	88	29	95	25	84	27	95	46	74	24	98	25	93	20	86
		195	15	95	19	94	13	16	16	97	26	85	21	96	17	93	14	95
95	35	175	57	76	61	79	54	75	39	92	67	60	39	94	43	73	27	90
		185	37	90	50	75	33	92	27	96	42	81	27	98	32	78	21	96
		195	18	98	32	58	16	95	18	93	23	93	18	96	18	95	15	96
	50	175	65	69	39	92	46	60	26	92	58	89	40	82	22	76	32	64
		185	42	87	26	95	24	92	24	88	27	95	26	94	17	91	17	95
		195	23	91	19	92	16	92	15	96	20	96	26	82	14	92	11	92

TABLE 9

Correlation of Independent Variables

	Cellulose Acetate	Acetone Content	Cast Temp.	Cold-Bath Temp.	Hot-Bath Temp.	Spec. No.	Solu. Vis.	Solu. Temp.	Rel. Hum.	Cold-Bath Cont.
Cellulose Acetate	100	5	0	-1	0	0	86	29	0	-10
Acetone Content		100	1	-1	0	0	-32	-13	0	-10
Cast Temperature			100	-4	0	0	2	-13	-100	4
Cold-Bath Temperature				100	0	0	-1	9	4	3
Hot-Bath Temperature					100	-2	0	0	0	0
Specimen Number						100	0	0	0	0
Solution Viscosity							100	33	-1	-3
Solution Temperature								100	13	-21
Relative Humidity									100	-4
Cold-Bath Content										100

The numbers in the above table are correlation coefficients and they can vary from 0 to 100 percent. A correlation coefficient of zero indicates no correlation between the variables, whereas 100 percent indicates perfect correlation. This latter condition indicates that every data point falls exactly on a line when plotting one variable against the other. The line beneath a correlation coefficient indicates that the correlation is mathematically significant with respect to the level of confidence chosen. A 95 percent level of confidence was chosen. Hence, whenever a correlation is defined as significant there is a mathematical probability of 19 in 20 that the correlation really exists rather than being a fictitious correlation within the tolerance of experimental error. The sign before the correlation coefficient signifies the direction of the slope between the two variables. For example a -100 percent correlation exists between relative humidity and cast-atmosphere temperature. The negative sign indicates that the relative humidity decreases as the cast-atmosphere temperature increases. This high degree of correlation should exist since the relative humidity was controlled to 60 percent at a cast temperature of 50°F, and to 30 percent at a temperature of 70°F.

There is only one correlation coefficient that has meaningful significance. This is 86 percent between solution viscosity and cellulose-acetate type. This correlation was anticipated as solutions prepared with E398-10 material produce viscosity levels over 400 stokes, whereas E398-3 solutions yield values less than 300 stokes.

The purpose of performing the correlation analysis shown in Table 9 was to investigate the possibility that some cast-process or independent variables were in fact dependent on other cast-process variables. The first six variables were those studied in this program and the low correlation coefficients indicate that the cast-process parameters were truly independent variables for this data.

A correlation analysis of performance parameters with cast-process parameters is shown in Table 10.

TABLE 10

Correlation of Performance Parameters with Cast-Process Parameters

	Cellulose Acetate Type	Acetone Content	Cast Temperature	Cold-Bath Temperature	Cold-Bath Content	Hot-Bath Temperature
product water	-32	-14	-23	-15	5	-75
reduced product water	-40	-19	-13	-19	2	-75
leakage	-15	-4	-32	-6	7	-60
salt rejection	2	-3	29	-1	-5	58

The performance parameters or dependent variables are listed vertically and the cast-process parameters or independent variables are listed horizontally. The performance parameters are strongly dependent on hot-bath temperature. The product-water flux and reduced product-water flux are higher using E398-3 cellulose acetate than with E398-10 material. Three of the four performance parameters correlate with the cast-temperature variable. It is felt that this particular correlation is representative of a relative humidity effect but because of the high correlation between cast temperature and relative humidity, this could not be verified.

A regression analysis of the performance parameters was also performed. The detailed results are given in the fifth quarterly report, PWA-3322. They merely point up the fact that a variety of different levels exist which yield a given performance level. A partial factorial matrix was performed prior to the full factorial matrix. It is described in detail in the third quarterly report, PWA-3100.

The performance of reinforced membranes using Eastman E398-3 cellulose acetate was superior to that recorded for samples using E398-10 material. The basic difference between the two cellulose acetates is that the E398-3 material has shorter average polymer chain length and forms a less viscous solution than the E398-10 material.

The effect of hot-bath temperature was similar to that expected for modified cellulose-acetate membranes if a 100 percent water cold-bath solution was used. The product-water flux decreased and the salt rejection increased as hot-bath temperature was increased. A hot-bath temperature of 185°F normally

yielded salt rejection values approaching or greater than 90 percent. Hot-bath treatment at 195°F produced extremely poor salt rejection and high product-water flux performance for some samples. This is mentioned to reassert that the membrane tends to crack or split if formed using certain combinations of the processing parameters. A much larger percentage of those membranes processed at 195°F hot-bath temperature exhibited this characteristic than samples processed at the lower hot-bath temperatures. These cracks or surface defects were observed under microscopic examination. The above comments only apply to samples processed in a cold bath of 100 percent water.

Insufficient data was accumulated on reinforced membranes to define the effect of cast temperature or cold-bath temperature. These parameters did not appear to exert as strong an influence on the performance as the other parameters investigated.

These studies emphasized the need for careful judgment in forming conclusions as to the effect of various process variables on the performance of reinforced membranes. The reinforcing fabric tends to stress the membrane because the membrane shrinks during processing, whereas the attached fabric retains its basic configuration. Thus, the poor salt-rejection data must be divided into two classifications as follows:

1) The processing conditions were such that a homogeneous membrane was produced but these processing conditions also created a poor cellulose-acetate structure for use as a semipermeable membrane.

2) The processing conditions were such that the cellulose-acetate structure contained defects. These defects permitted the passage of the brackish solution, resulting in the poor salt-rejection data.

For the latter case, a simple change of the reinforcing material may reduce or eliminate the defects in the cellulose-acetate structure, because the stresses on this structure are modified.

A second series of comments should be made with respect to performance comparisons of the various reinforced membranes. At least two sets of comparisons should be performed with caution. These are as follows:

1) The choice of the basic cellulose acetate material (E398-3 or E398-10) has been discussed for the short-term tests. It is quite possible that E398-10 material may yield performance comparable to that of the E398-3 material if the evaporation period were reduced for the E398-10 material. Hence the comparison made between these two cellulose-acetate materials is only applicable to the conditions investigated in this program.

2) It is difficult to compare the samples formed in a dilute acetone cold-bath solution with those formed in a water cold-bath solution. One can hypothesize as to the effect of the cast-solution parameters, the cast-technique parameters, the cold-bath parameters, and the hot-bath parameters for films made in a water cold bath. The data recorded on this program suggests that a dilute acetone cold-bath solution reacts with the cellulose acetate structure. This implies that cold-bath time and temperature and the concentration and activity of the additive (acetone for this program) determine the degree of reaction with the cellulose acetate. Studies conducted prior to this contract effort and not reported in literature suggested that a 5 percent acetone concentration combined with a 1-hour time period and 35 and 50°F temperatures might produce beneficial modification to the membrane structure. Further studies would be required to evaluate the interactions of these cold-bath variables.

The reinforced membrane-processing studies defined the performance level of this composite membrane structure using state-of-the-art techniques. The studies indicated that the stress pattern within the modified cellulose-acetate membrane is modified because of the fabric. The studies also identified potential techniques which may improve the state of the art for cellulose-acetate membrane formation.

C. Performance Characteristics

The third phase of the reinforced membrane studies was to investigate the performance of cellulose-acetate membranes as a function of operating time and operational variables such as temperature, pressure and brine concentration.

1. Lifetime Measurements

Twenty specimens having various levels of salt rejection and product-water flux were evaluated at standard brackish water conditions for periods from 77 to 489 hours. The specimens were selected from specimens formed for the cast-process variables study. The decay rate of the product-water flux was not markedly affected by such cast-process parameters as cellulose-acetate type, cold-bath temperature or hot-bath temperature. A correlation analysis indicated that performance decay cannot be conclusively described as being either linear or logarithmic with respect to time. It is very important to establish which is the proper hypothesis: if a linear variation is correct, then with respect to membrane compaction a practical reverse-osmosis system may not be possible with the membranes developed to date. However, if the logarithmic variation is correct, then a practical reverse-osmosis system for brackish water can be made using the developed membranes. It is therefore necessary to continue the evaluation of membranes for extended periods to properly identify the mode of decay. Fifteen hundred hours would be an appropriate endurance goal.

The method of selecting the membrane specimens for lifetime measurements is described in detail in the fifth quarterly report PWA-3256. These membranes received either a 4-hour evaluation at standard brackish-water conditions or a 3-hour evaluation using a 5500 ppm NaCl solution, operating at 750 psi pressure and 77°F solution temperature, under turbulent-flow conditions. The membranes were stored in tap water until required for the endurance evaluation. Table 11 summarizes the data from the short-duration tests.

TABLE 11

Short-Duration Performance of Membranes

Specimen No.	Product-Water Flux, gfd	Salt Rejection, %
88A-4*	23	99
88A-1*	23	98
88A-2*	23	99.8
142A-3	24	98
140B-3	24	97
140B-5	27	96
103B-6	14	96
98B-2	16	96
105A-5	19	96
77A-6*	21	96
113B-1	25	96
109A-6	30	96
109B-1	39	95
112A-3	36	91
82B-3*	37	91
86A-6*	49	92
109A-5	52	86
86B-1*	58	84
79A-2*	59	82
86B-4*	69	81

*These specimens were evaluated for three hours

Figure 10 shows a plot of membrane performance as a function of time for three membranes whose initial product-water flux was at different levels. The membrane which had the highest initial product-water flux (Specimen 109A-5) experienced a decreasing rate of decay for the first 20 hours and then exhibited a constant decay rate. Specimen 112A-3, which had an intermediate initial product-

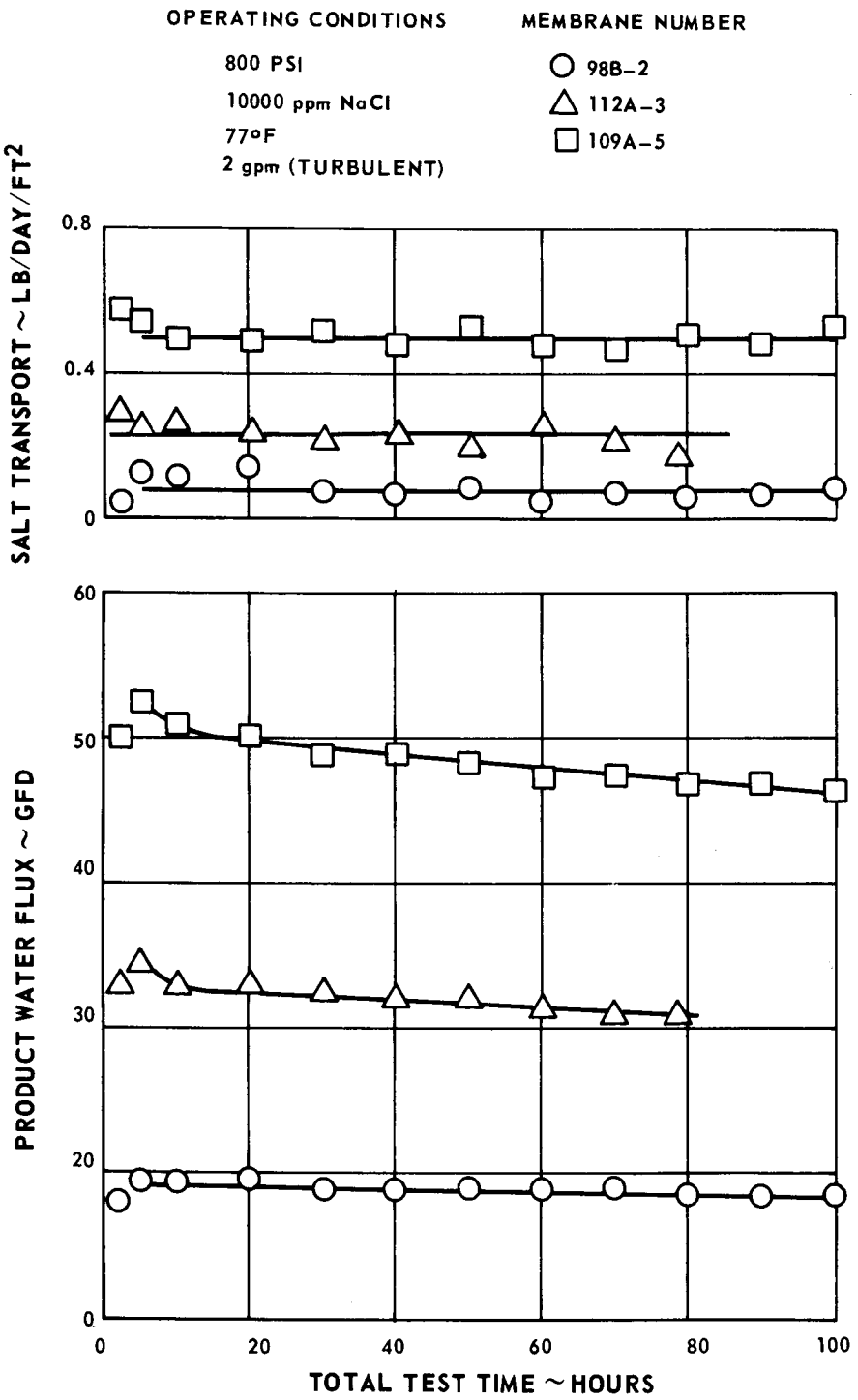

Figure 10 Preliminary Lifetime Performance

water flux followed the same pattern, however, the permeability decay rate was lower. Specimen 98B-2, which had an initial value of 18 gfd, had a very low decay rate and it appeared to be constant for the duration of the test. The water permeability decrease appeared to be a linear relation with test time for all three membranes. The salt-transport characteristic of the specimens remained constant. The product-water decay rate was a direct function of initial product-water flux, as shown in Figure 11. This relationship indicates that a specimen which exhibits high initial product-water flux will decay more rapidly and eventually will achieve the product-water level of a specimen with lower initial product-water flux.

In order to determine the mode of membrane decay, three membranes were tested for 489 hours at standard brackish-water conditions. The membranes selected for evaluation are identified as Specimen Numbers 140B-3, 140B-5 and 142A-3. The test was normally conducted for 16 hours per day. Consequently, the specimens were subjected to a minimum of 35 pressure cycles.

In an effort to identify the product-water flux decay of the three membranes, both a correlation analysis and a curve fit were performed. A correlation analysis involves finding a measure of the dependence of one variable upon another. The data was fitted using the method of least squares. The types of curves investigated in detail were:

1) Linear: $Y = mt + b$

2) Logarithmic: $Y = m(\log t) + b$

where Y = dependent variable

m = slope of the line

b = y (intercept)

t = time

Other curves investigated were:

3) Exponential: $\text{Ln } y = mt + b$

and $Y = m(e^{-0.01t}) + b$

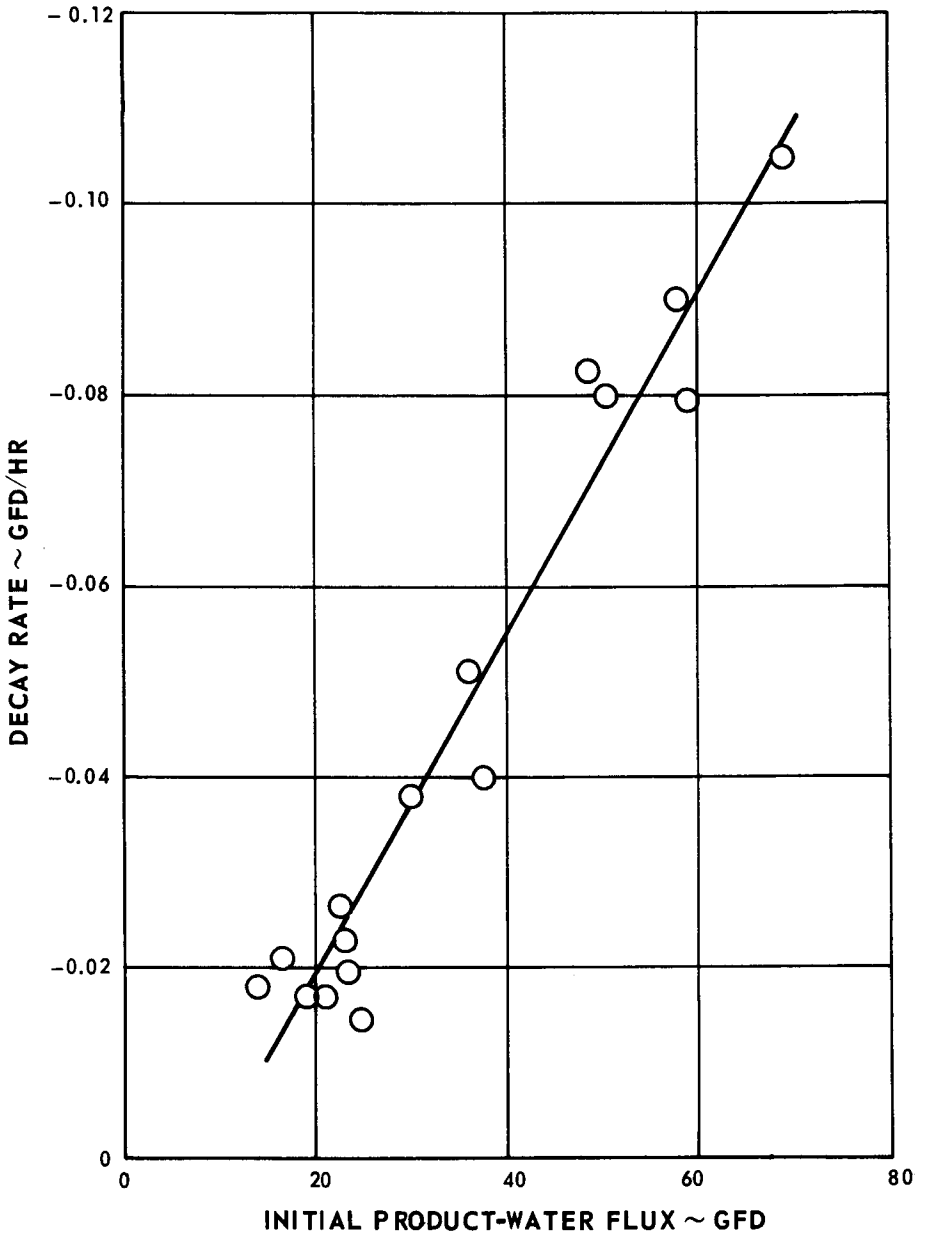

Figure 11 Correlation of Decay Rate and Initial Product-Water Flux

Test time was the independent variable, while product-water flux was the dependent variable. Four other dependent variables, reduced product-water flux, product-water concentration, salt rejection and salt transport were considered. However, the major effort was expended on the correlation analysis between product-water flux and linear time or logarithmic time.

The results of the correlation analysis indicated that a high correlation exists between time and product-water decay for both the linear and logarithmic cases. Table 12 presents the correlation coefficients and slopes for time and product-water flux for the linear and logarithmic cases.

TABLE 12

Correlation Analysis Results

Membrane Specimen	Linear		Logarithmic	
	Correlation Coefficient, r	Slope, gfd/hr	Correlation Coefficient, r	Slope, gfd/log time
140B-3	-0.364	-0.0064	-0.392	-2.316
140B-5	-0.637	-0.0057	-0.712	-2.137
142A-3	-0.655	-0.0058	-0.629	-1.983

A confidence level of 99+% was obtained for a correlation coefficient, $r \geq |0.26|$ for the number of data points obtained from the lifetime test. The correlation analysis indicated significant curve fits for both the linear and logarithmic cases. Therefore, based on the 489 hours of evaluation, it could not be conclusively determined whether product-water flux decay is linear or logarithmic.

Figure 12 shows a plot of product-water flux and salt rejection of Membrane 140B-5 as a function of linear time. The data points shown represent an average product-water flux over a 20-hour period. The slope of the curve was obtained by the method of least squares from a linear fit. Very little scatter with the data points and the calculated curve slope is in evidence. Figure 13 shows the product-water flux of Membrane 140B-5 as a function of time on a logarithmic scale. The slope of the line was calculated from the equation $y = m (\log t) + b$. The data points shown represent a product-water flux over a 20-hour period.

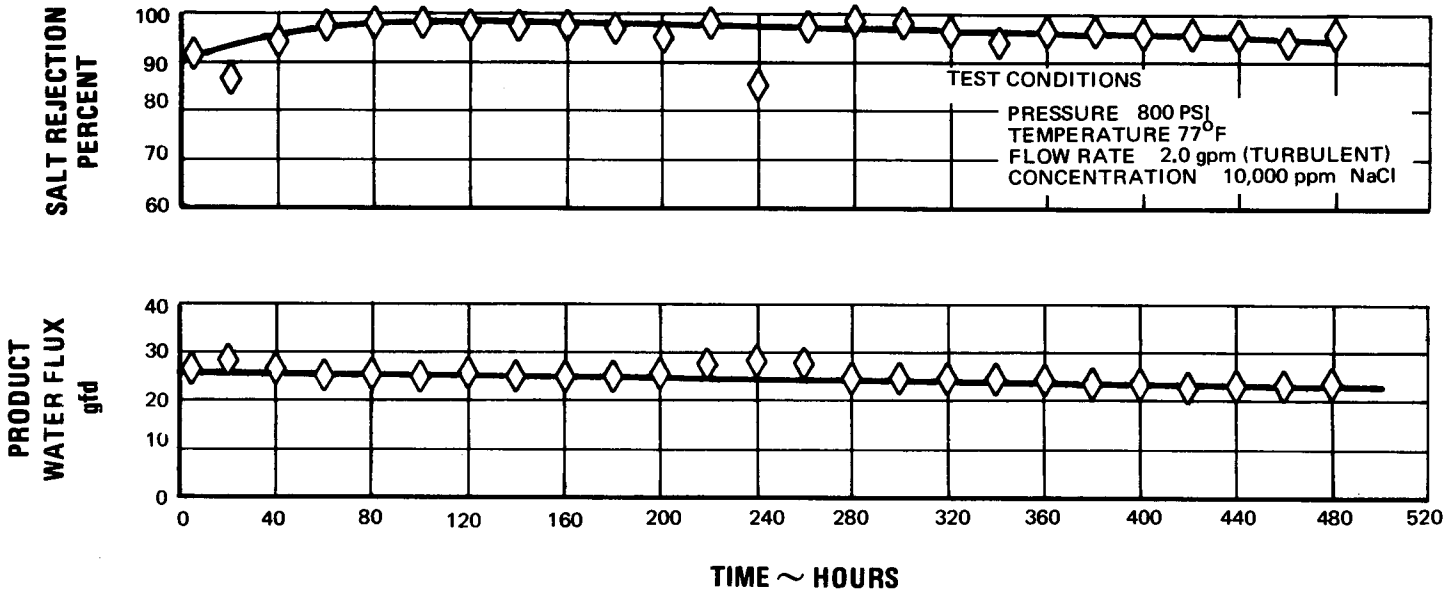

Figure 12 Product-Water Flux as Function of Time - Membrane 142A-3

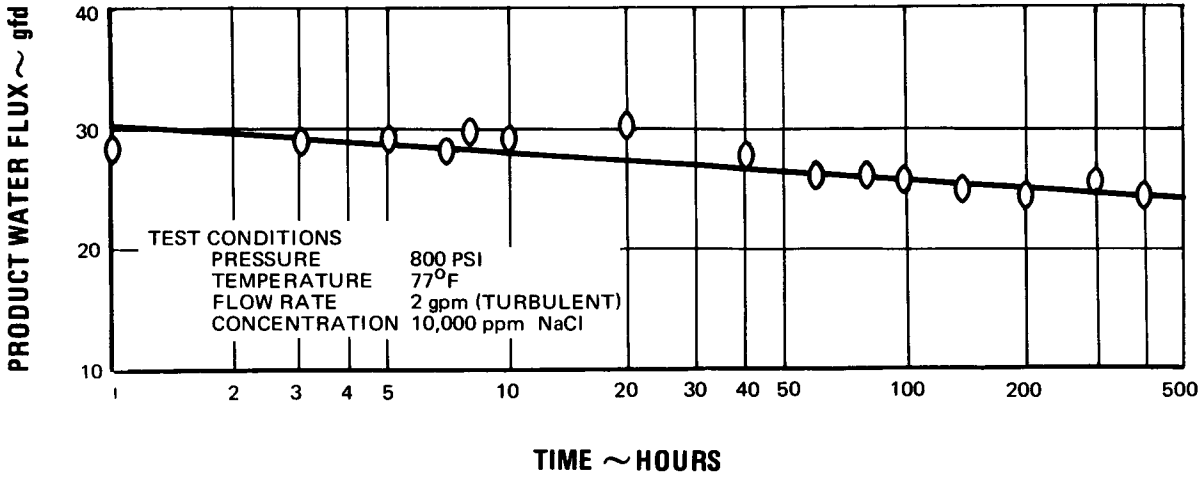

Figure 13 Product-Water Flux as Function of Time - Membrane 140B-5

Again very little scatter between product-water flux and time is in evidence. These curves should be considered typical for the membranes evaluated. Table 13 presents the performance characteristics, product-water flux, salt rejection and salt transport of the membranes evaluated.

The importance of identifying the functional form of the product-water flux decay can be best illustrated by considering the performance of Membrane 140B-5. The initial product-water flux of 28 gfd will decay to 21 gfd after 1000 hours, if the flux decay with time were linear. On the other hand, if the flux decay were a logarithmic function of time, the product-water flux after 1000 hours would be 24 gfd. The same membrane after 2000 hours would have a product-water flux of 15 gfd for the linear case and 23 gfd for the logarithmic case. Figure 14 shows the best linear and best logarithmic fit of the product-water flux for Membrane 140B-5 as a function of time. It is typical of the three membranes evaluated. There is very little difference between the linear and logarithmic curves up to about 500 hours. It can therefore be concluded that it is necessary to continue the evaluation of membranes for extended periods to properly identify the mode of decay. Fifteen hundred hours would be an appropriate endurance goal. A photograph of the three membranes evaluated for 489 hours is shown in Figure 15. A description of the lifetime measurement program is presented in detail in the fourth, fifth, sixth and eighth quarterly reports PWA-3181, 3256, 3320 and 3510, respectively.

2. Operating Variables Study

In addition to the lifetime performance characteristics it is necessary to know the variation of performance with the operating variables. The operating variables chosen as most important were pressure, temperature and concentration. Merten[3] and others have shown that the permeation flux can be expressed by

$$j_1 = A\,(\Delta P - \Delta \pi)$$

and that salt permeation flux can be given by

$$j_2 = \frac{D_s}{\lambda}\,\Delta C + C_b\, j_L$$

The salt concentration used in this equation should be the concentration of the solution adjacent to the membrane, as opposed to the bulk-solution concentration. The second term of the equation recognizes that some membranes have pores or defects sufficiently large to permit flow which is pressure-dependent. The quantity of water passing through the membrane normally is quite small with respect to water passage by the diffusion process as given by the previous equation, however the salt transported in this leakage term can be quite significant when compared to salt transport by diffusion.

TABLE 13

Preliminary Lifetime Measurements

Time, Hours	Membrane Specimen 140B-3			Membrane Specimen 140B-5			Membrane Specimen 142A-3		
	Product-Water Flux, gfd	Salt Rejection, %	Salt Transport, lb/day/ft^2	Product Water Flux, gfd	Salt Rejection, %	Salt Transport, lb/day/ft^2	Product Water Flux, gfd	Salt Rejection, %	Salt Transport, lb/day/ft^2
Initial Screen	24	97	—	27	96	—	24	98	—
5	27	91	0.212	29	95	0.139	27	92	0.182
20	26	90	0.235	30	86	0.374	29	87	0.321
40	25	93	0.155	28	94	0.149	27	95	0.122
60	23	96	0.068	26	97	0.068	25	98	0.050
80	24	97	0.056	26	98	0.034	25	98	0.036
100	24	97	0.057	26	98	0.052	25	98	0.036
120	24	96	0.073	26	98	0.057	25	98	0.052
140	23	98	0.041	25	98	0.050	26	98	0.052
160	22	97	0.049	25	97	0.063	25	97	0.063
180	23	97	0.048	25	97	0.063	25	97	0.059
200	22	97	0.058	25	97	0.070	25	95	0.120
220	22	94	0.112	26	96	0.082	27	98	0.306
240	23	90	0.193	26	97	0.063	29	85	0.407
260	24	86	0.277	26	96	0.096	25	97	0.053
280	24	83	0.322	26	97	0.063	25	99	0.021
300	24	82	0.347	26	97	0.052	25	99	0.030
320	23	87	0.243	26	96	0.075	25	96	0.057
340	22	86	0.263	25	96	0.092	24	95	0.111
360	25	92	0.423	25	96	0.079	24	97	0.072
380	20	92	0.121	25	96	0.082	24	97	0.057
400	21	90	0.167	25	96	0.083	24	96	0.074
420	20	89	0.224	24	96	0.083	23	96	0.067
440	24	78	0.444	24	96	0.027	24	97	0.065
460	22	82	0.376	24	96	0.046	24	95	0.060
480	21	87	0.230	24	96	0.061	23	96	0.070

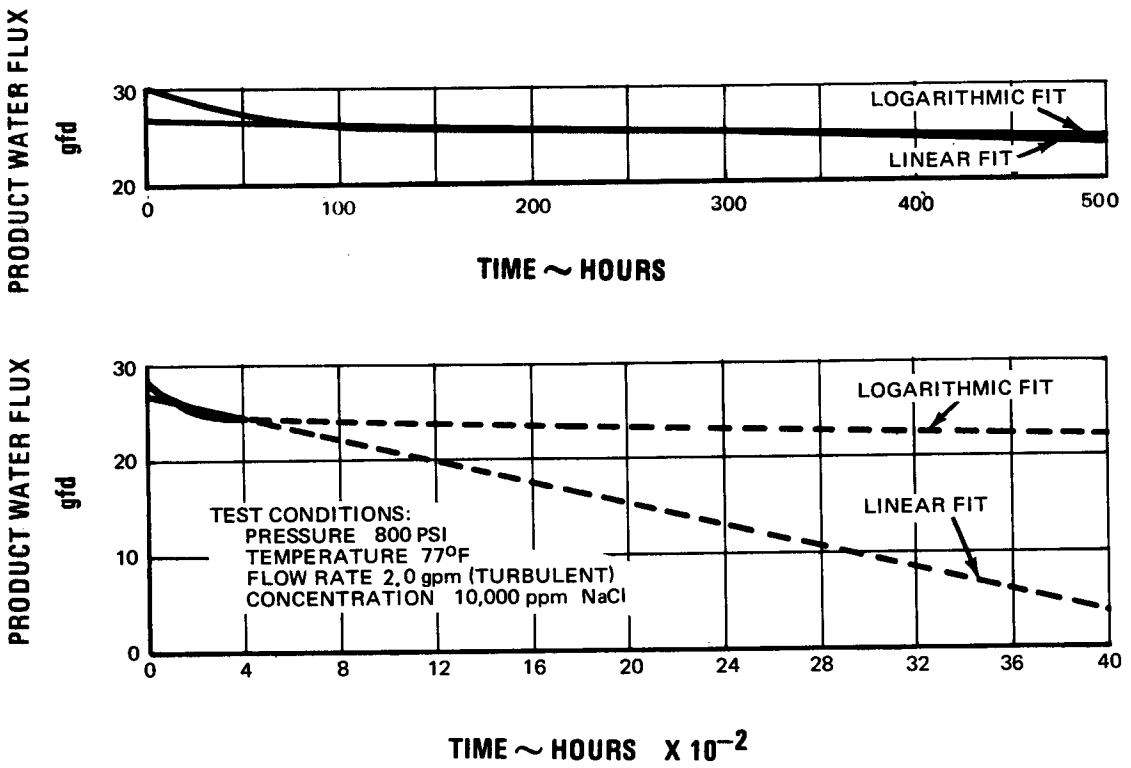

Figure 14 Preliminary Lifetime Measurements - Membrane 140B-5

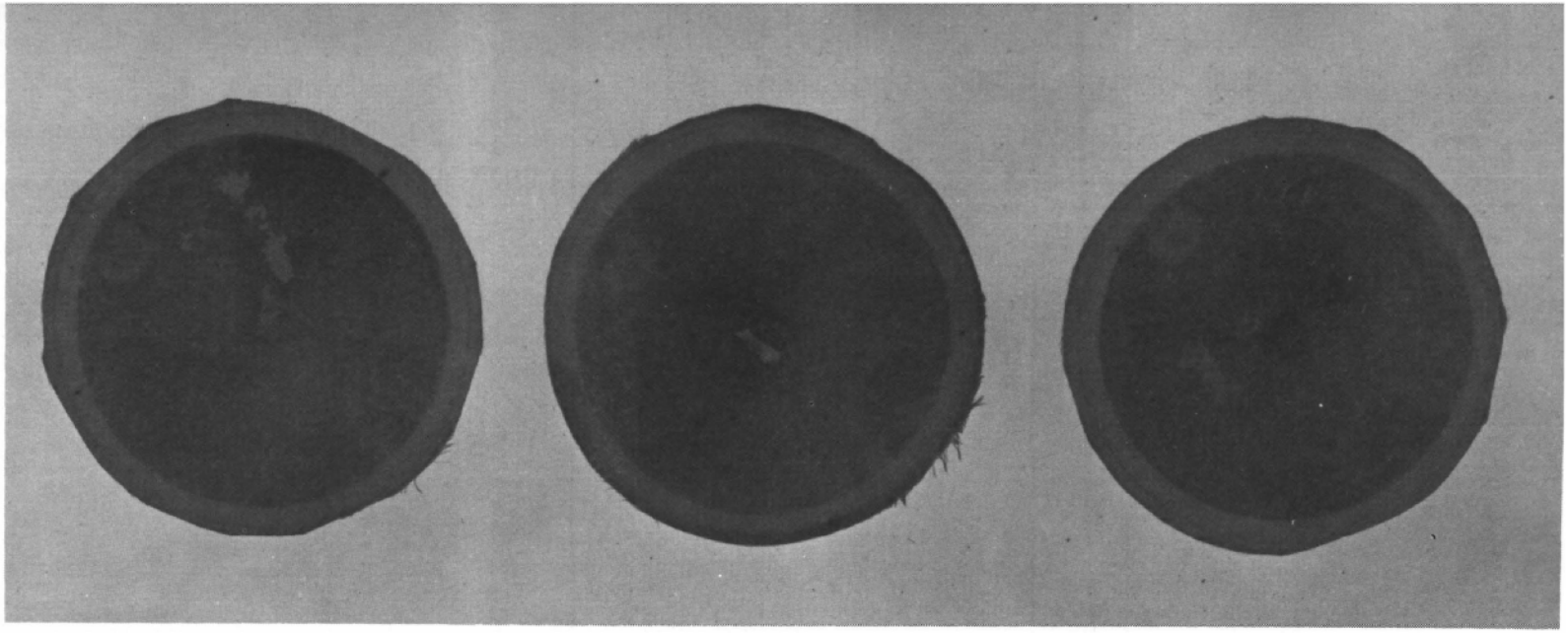

Figure 15 Photograph of Three Membranes after 489 Hours of Test

The salt rejection can be defined as follows:

$$Sr = \left[1 - \frac{C_p}{C_b} \right] 100$$

The salt rejection will still be influenced by solution pressure for a perfect membrane (no leakage) because C_p is a function of pressure since it is dependent upon j_1.

A number of membranes were tested to demonstrate the validity of these equations. The results are summarized in Figure 16 where the water permeation constant A is shown as a function of feedwater pressure, concentration and temperature. A membrane constant of 0.034 gfd/psi corresponds to a water flux of 27.2 gfd at operating conditions of 800 psi, 10,000 ppm NaCl, and 77°F. Referring to Figure 16, the water permeation constant is seen to be a function of pressure. This is caused by a change in the internal structure of the cellulose acetate as the applied pressure is increased. For the most part this change is irreversible and the water permeation constant is a function of the pressure-level history of the membrane. It is also noted that the water permeation constant is a slight function of concentration. It is now believed that this is caused by salt concentration polarization at the higher brine concentrations, but it has not been verified. The dependence of the water permeation constant on temperature was expected. The slope of the line is 0.00065 gfd/psi/°F. To convert the units of A from (gfd/psi) to (gm/cm^2 sec atm) multiply by 0.000693.

A similar family of curves can be drawn for the salt permeation constant but the data available does not yield consistent results. It is believed that for a membrane of high salt rejection, the salt permeation constant will yield curves similar to those for the water permeation constant, i.e., a function of both pressure and temperature and only slightly dependent on concentration.

A detailed discussion of the operating variables study is presented in the fifth quarterly report, PWA-3256, and the eighth quarterly report, PWA-3510.

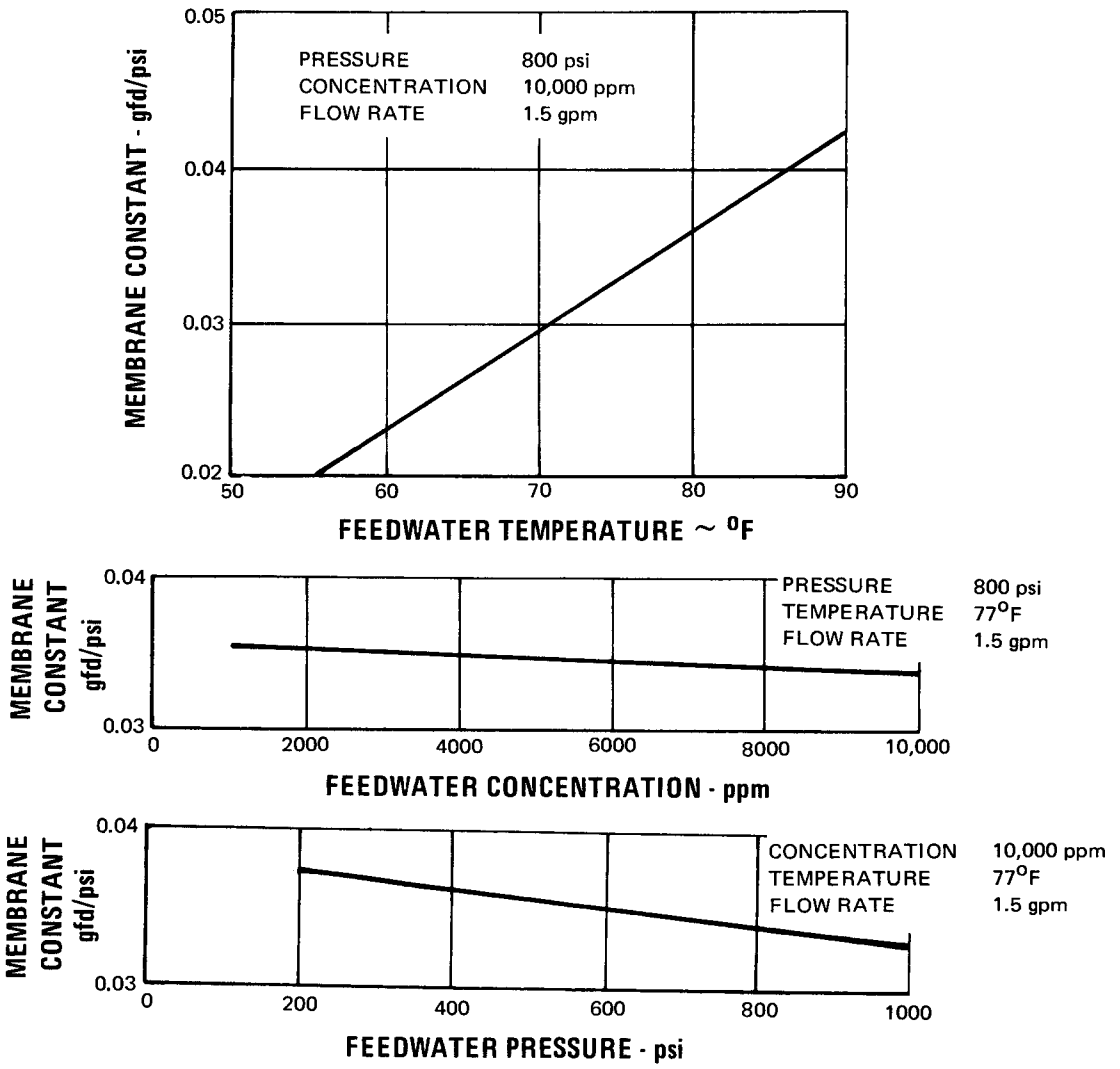

Figure 16 Water Permeation Constant as Function of Feedwater Pressure, Concentration and Temperature

V. COMPACT CARTRIDGE DEMONSTRATION

The concept of a compact cartridge investigated by Pratt & Whitney Aircraft consists of a number of composite membranes stacked between two rigid end plates and assembled on a common porous tube. This concept employs flow channels with small hydraulic diameters and feedwater turbulators to minimize the effects of concentration polarization. The design was strongly biased towards demonstrating the feasibility of the concept of a compact reverse-osmosis cartridge, and was not necessarily optimized for any given application. The cartridge size was large enough to identify and solve fabrication problems that can be expected with full-scale cartridges. This section describes the compact cartridge concept and the performance characteristics obtained. It also describes the composite membrane development program.

A. Compact Cartridges

An illustration of the compact cartridge demonstration unit is shown in Figure 17, and an exploded view of the cartridge is shown in Figure 18. The cartridge as built consisted of a number of composite membranes sandwiched between two end plates and assembled on a common porous tube. The porous tube serves as the product-water removal manifold and provides structural strength to the cartridge assembly. The composite membrane spacing is controlled by a rubber O-ring and plastic washer-spacer that is placed around the porous product-water manifold, and by a plastic frame that is placed around the periphery of the composite membrane. The rubber O-ring and spacer create a seal between the feedwater passage and the porous product-water manifold. The plastic frame, in conjunction with a tape film, separates the feedwater within the cartridge from the feedwater in the pressure vessel. Plastic screens were installed in the feedwater passage to promote mixing of the feedwater and reduce the possibility of concentration polarization. The entire assembly is held together with a tiebolt. The feedwater enters the cartridge through a series of holes in the bottom plate and flows across the composite membrane surface. At this point the feedwater is introduced into the second layer of the composite membrane stack. The concentrated feedwater is removed from the cartridge by a flexible pipe.

The composite membrane used was formed by attaching reinforced membranes to both sides of a grooved polyvinylchloride support plate. Sealing was accomplished by means of a thin polyester film, Mystic Tape No. 7300, and Pliobond cement. To prevent the membrane from deforming into the product-water grooves and causing feedwater blockage, celluloid strips were placed over the eight radial product-water removal grooves. To prevent damage to the reinforced membrane, a layer of filter paper was placed over the celluloid strips and support plate. It should be noted that the above changes were only incor-

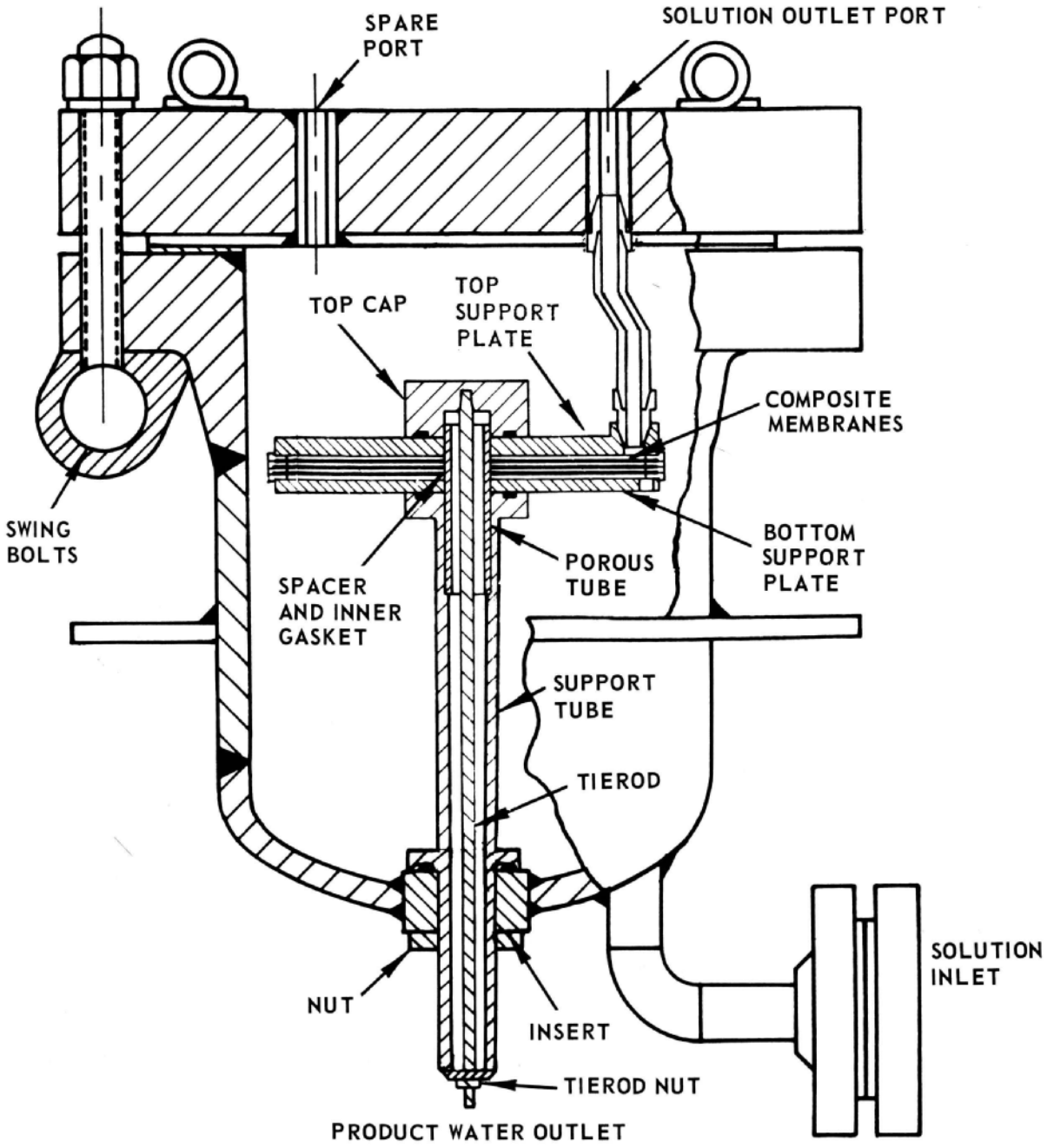

Figure 17 Reverse-Osmosis Cartridge Concept

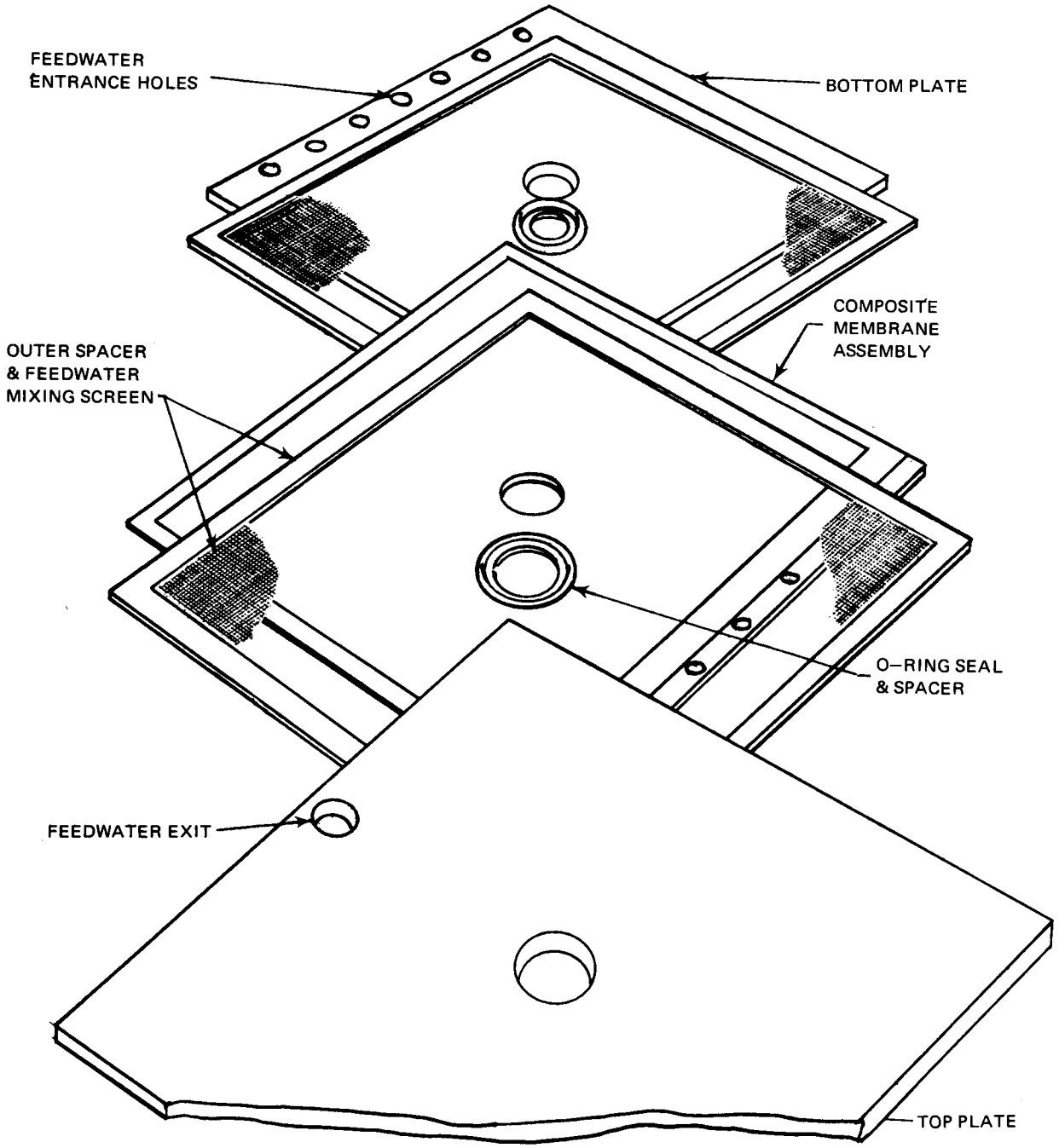

Figure 18 Exploded View of Reverse-Osmosis Cartridge

porated in order to obtain a workable composite membrane. An improvement in design of the grooved membrane support structure would eliminate the need for both the celluloid strips and the filter paper. A detailed description of the composite membrane development program is presented in Section V. B. below.

Two compact cartridges were assembled and tested. The first cartridge contained three composite membranes while the second cartridge consisted of ten composite membranes. Their average performance at 800 psi, 77°F, 1.50 gpm laminar feedwater flow rate, and 10,000 ppm NaCl feedwater concentration, was 23 gfd (55 gpd) at 93 percent salt rejection and 25 gfd (198 gpd) at 88 percent salt rejection, respectively. A design and build summary of the two compact cartridges is presented in Table 14.

The testing of the compact cartridge was performed on the reverse-osmosis test system described in Appendix 3 of this report.

1. Three-Plate Compact Cartridge

The first compact cartridge evaluated during this program consisted of 3 composite membranes with a total membrane surface area of 2.4 square feet. The cartridge was operated for 58 hours, during which time calibrations were performed with respect to feedwater pressure, temperature and flow rate. Average performance over this period at standard conditions was 23 gfd at 93 percent salt rejection. (Standard conditions are: 800 ± 10 psi, 77° ± 1°F, 1.50 ± .01 gpm and 10,000 ppm NaCl feedwater concentration).

Cartridge performance as a function of feedwater applied pressure is shown in Figure 19. Product-water flux is shown to be a linear function of applied pressure. There was a gradual reduction in salt rejection at lower applied pressures since salt transport is independent of applied pressure, while the product-water flux was directly proportional. Figure 20 shows product-water flux and salt rejection as functions of feedwater temperature. Again, a linear relationship is indicated. The slope of the product-water curve, which can be considered a temperature correction factor for Cartridge No. 1, is 0.35 gfd/°F in the range of 67 to 77°F.

A test of Cartridge No. 1 with feedwater flow rate as a variable was conducted to determine the effects of recovery factor on cartridge performance (recovery factor is the percent of the feedwater stream recovered as product-water flux). A plot of product-water flux and salt rejection as a function of feedwater flow rate is shown in Figure 21. A significant reduction in product-water flux occurred with a feedwater flow rate of 0.5 gpm (8 percent recovery) while a noticeable change in salt rejection occurred with a feedwater flow rate of 1.0 gpm (2 percent recovery).

TABLE 14

Compact Cartridge Design and Build Summary

	Design Summary	Build Summary
Composite Membrane		
Size	8.5 x 8.5 inches	8.5 x 8.5 inches
Thickness	0.050 inch	0.080 inch
Active Membrane Area	0.8 ft^2	0.8 ft^2
3-Plate Demonstration Unit		
Water Production	60	55
Packaging Density	100 to 500 ft^2/ft^3	92 ft^2/ft^3
Feedwater Pressure Loss	1 psi	30 psi
Water Production/Unit Volume	2500 to 12,500 gpd/ft^2	2110 gpd/ft^3
10-Plate Demonstration Unit		
Water Production	200 gpd	196 gpd
Packaging Density	100 to 500 ft^2/ft^3	92 ft^2/ft^3
Feedwater Pressure Loss	1 psi	35 psi
Water Production/Unit Volume	2500 to 12,500 gpd/ft^3	2250 gpd/ft^3
Cartridge Design Permits		
Variable Composite Membrane Spacing		
Variable Feedwater Path Length		
Use of Alternate Composite Membranes		
Reinforced Membrane Performance		
Product Water Flux	20 to 30 gfd	
Salt Rejection	94 to 98%	

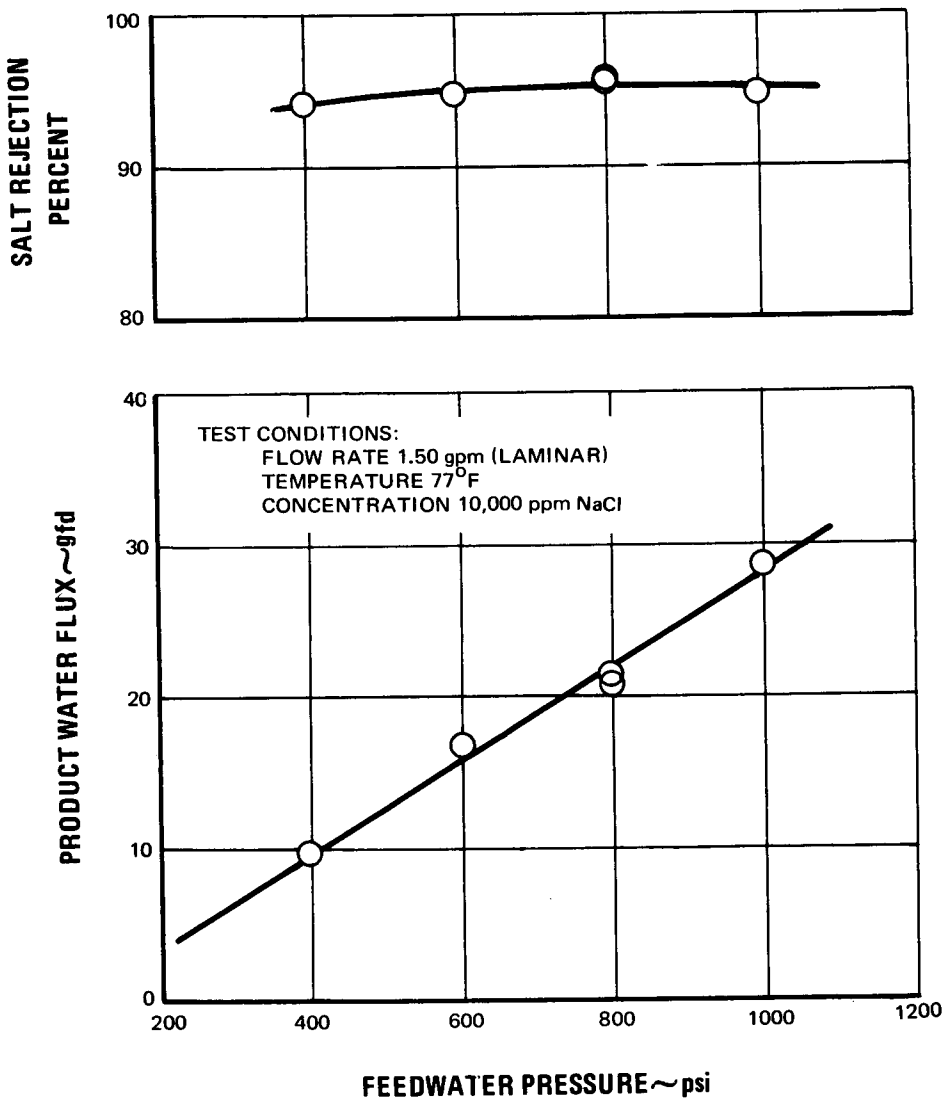

Figure 19 Performance of Compact Cartridge No. 1 vs Feedwater Pressure

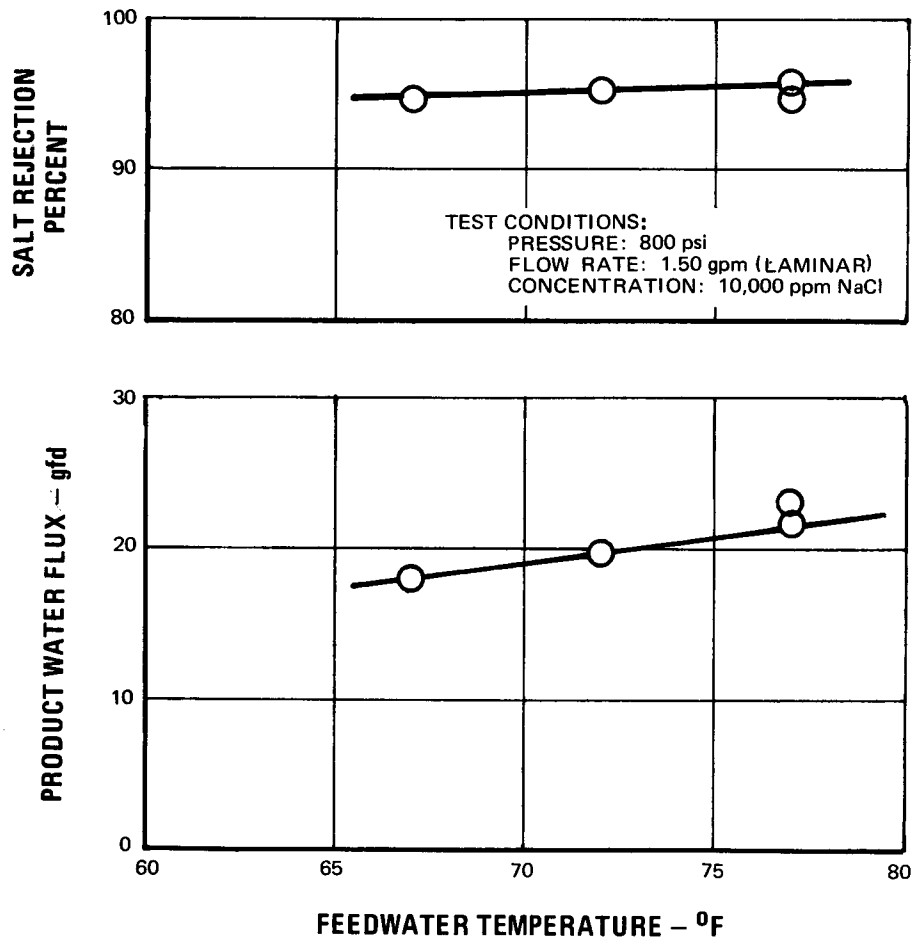

Figure 20 Performance of Compact Cartridge No. 1 vs Feedwater Temperature

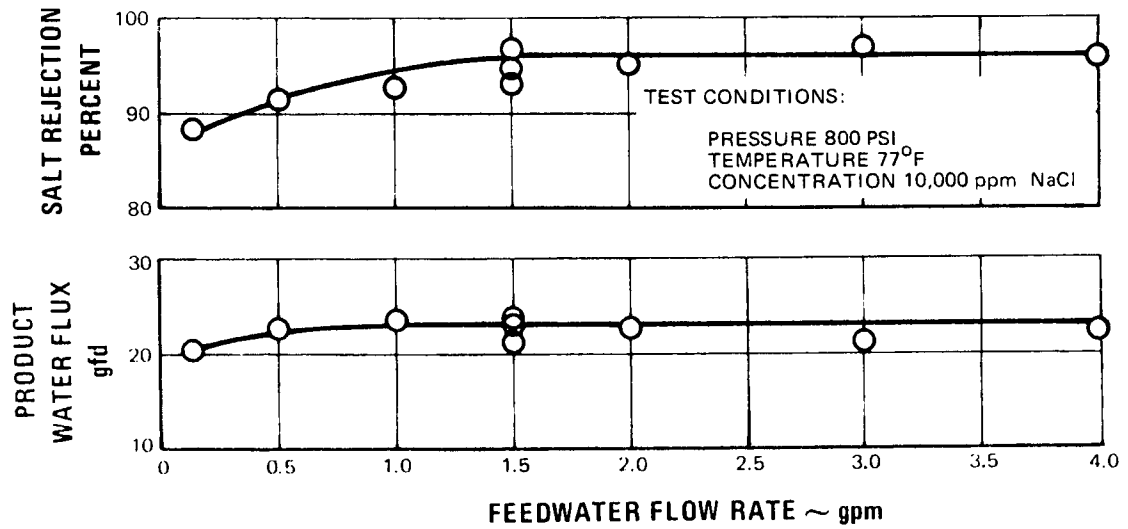

Figure 21 Performance of Compact Cartridge No. 1 vs Feedwater Flow Rate

Cartridge performance as a function of operating time is shown in Figure 22. The initially-high product-water flux and erratic salt rejection during the first ten hours of operation can possibly be attributed to a leak in the composite-membrane tape seal that was discovered during post-test inspection of the cartridge. It is believed that this leak became sealed during continued operation.

Theoretical values for the product-water flux and salt rejection of Cartridge No. 1 as functions of feedwater flow rate and applied pressure are presented in Figures 23 and 24. These curves were calculated using an analysis based on the method of Brian[4] for predicting concentration polarization. The curve marked "zero polarization" disregards the effect of concentration polarization but takes into account the increase in bulk concentration down the channel. The curve marked "predicted polarization" takes into account the effect of concentration polarization for laminar flow, neglecting the presence of turbulators. The experimental data for Cartridge No. 1 are also plotted on this curve. As

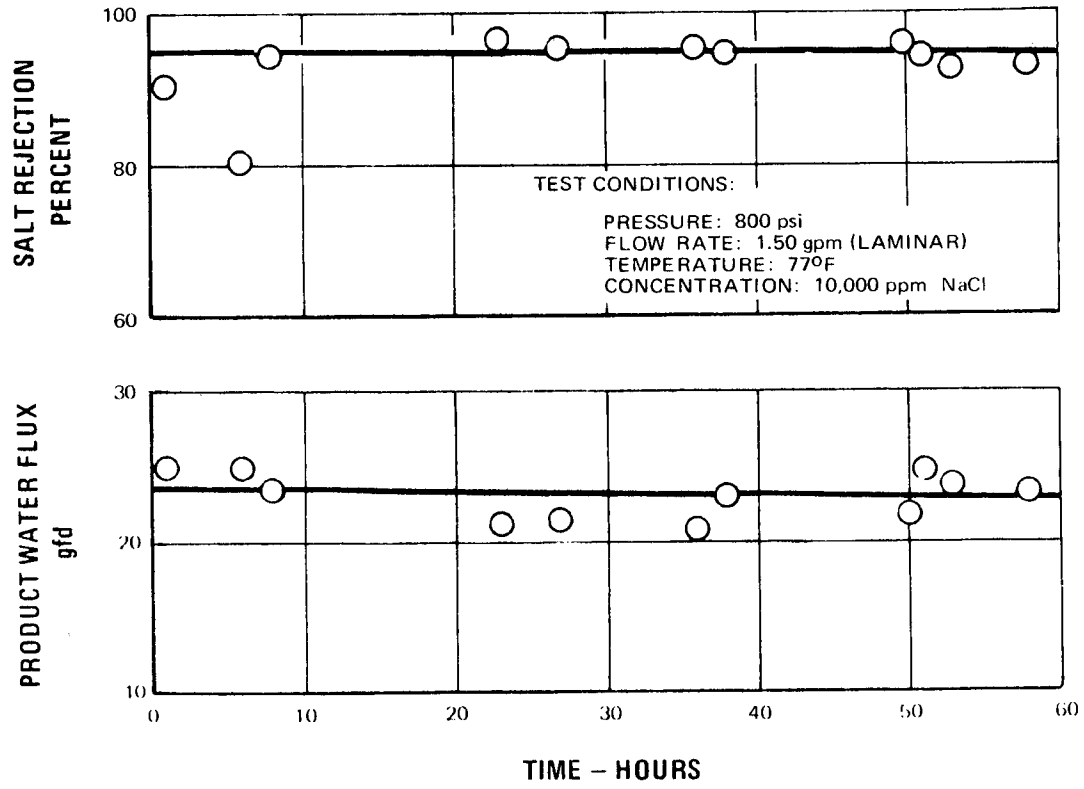

Figure 22 Performance of Compact Cartridge No. 1 vs Operating Time

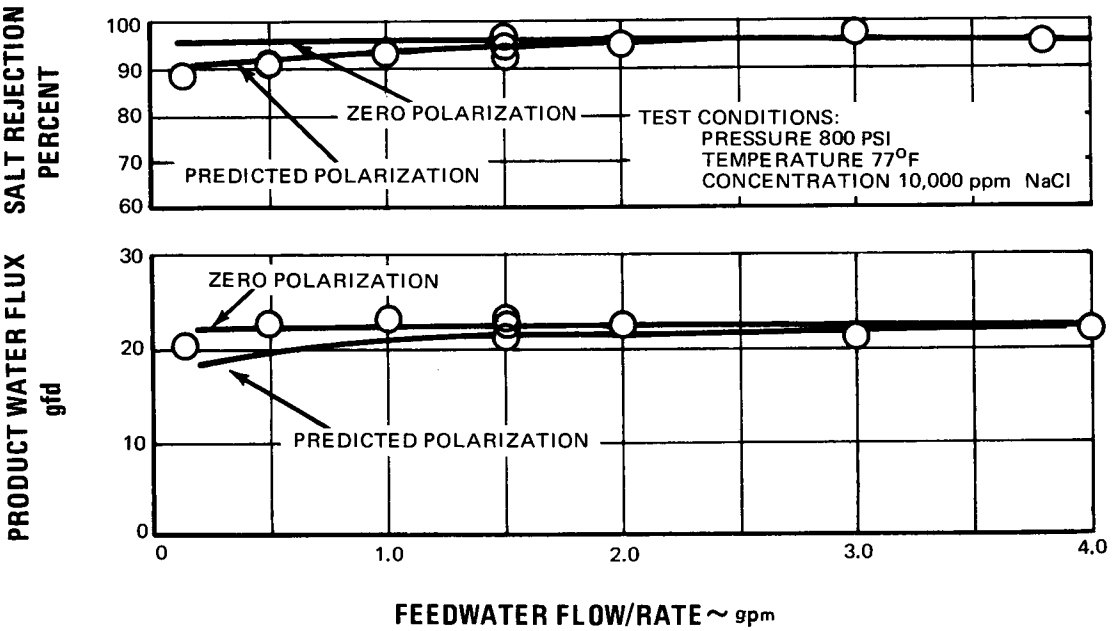

Figure 23 Performance of Compact Cartridge No. 1 vs Feedwater Flow Rate

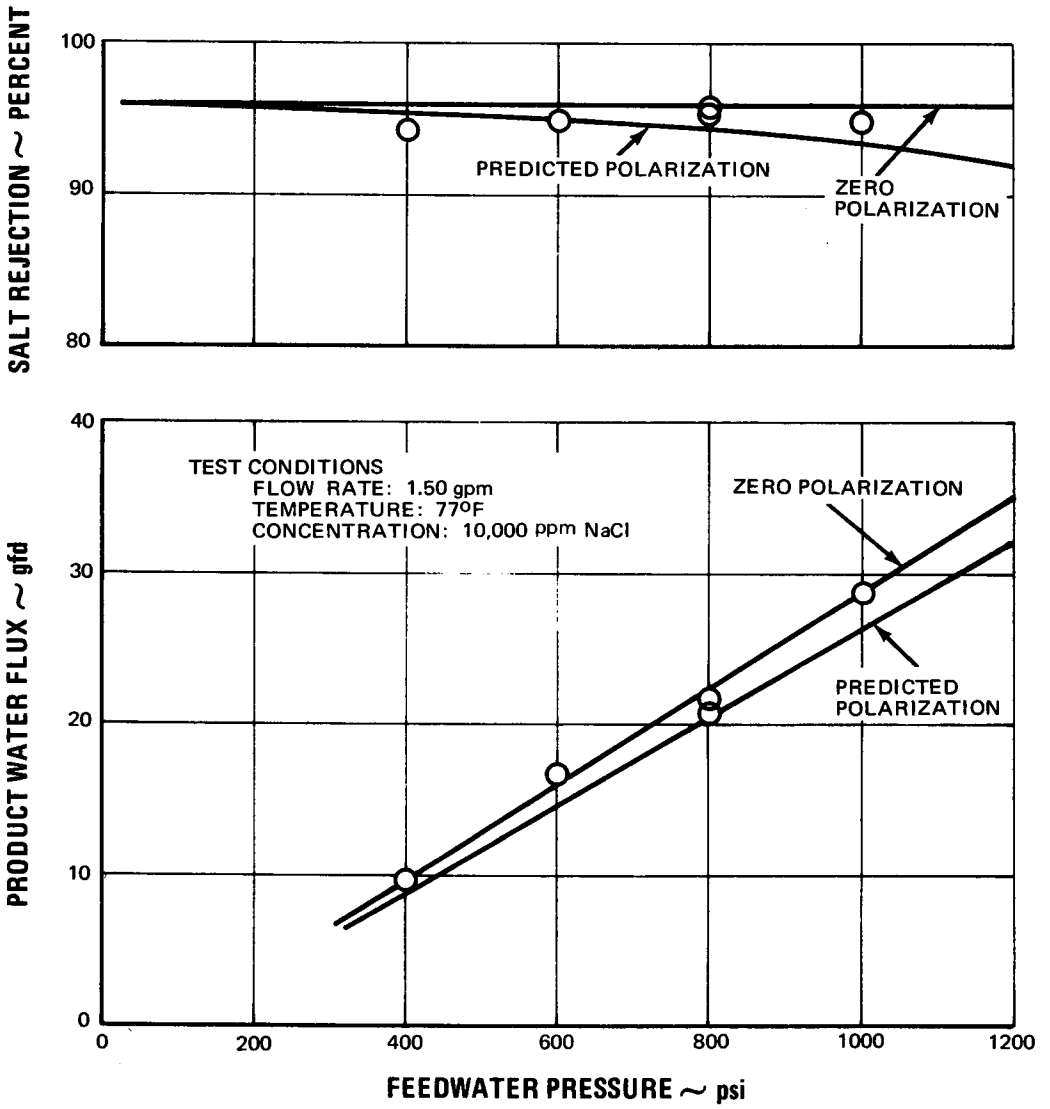

Figure 24 Performance of Compact Cartridge No. 1 vs Feedwater Pressure

can be seen, the data is in excellent agreement with the prediction. Also, the experimental data points fall very close to the zero-polarization case, indicating success of the compact cartridge in minmizing polarization effects. It is within the limits of experimental accuracy and there is a slight degradation with time, as shown in Figure 22.

The analysis predicted average product-water flux, product-water concentration and brine pressure loss for the cartridge, taking into account the following effects:

1) Axial variation of product-water flux caused by,
   a) The axial increase in the effective osmotic pressure of the brine at the membrane surface caused by the combined interactions of:
      1) the axial increase in brine bulk concentration due to product-water removal,
      2) the effect of polarization which results from the back diffusion of rejected salt from the membrane surface to the bulk of the brine stream as predicted by Brian, and
   b) Axial decrease in brine pressure caused by fluid friction.

2) Brine pressure losses due to entrance and exit effects.

3) Membrane salt rejections less than 100 percent.

To facilitate calculations the analysis was programmed on a high-speed digital computer. A detailed description of the method used to predict the cartridge performance is presented in Section VI below. These calculations were based on an open channel without feedwater turbulators or product-water collection manifold. The latter factors should make the predicted polarization curves slightly pessimistic. The experimentally-observed average membrane constant and salt rejection at feedwater flow rates in excess of 2.0 gpm were considered characteristic of the membranes and used as input for these calculations. A feedwater inlet concentration of 10,000 ppm NaCl was also used as input data and all salt rejections were calculated with respect to this concentration (negligibly different from salt rejections based on the average of inlet and exit bulk concentrations up to approximately 30 percent recovery).

Wall concentration as a function of channel length is shown in Figure 25, together with the average bulk concentration. It was assumed that the feedwater solution is completely mixed as it passes through the seven 1/4-inch solution passage holes from one feedwater channel to the next. Concentration polarization is more severe in the first and fourth channels since these channels have one impervious wall (top and bottom plates). This circumstance leads to a higher feedwater concentration adjacent to the membrane surface. It should

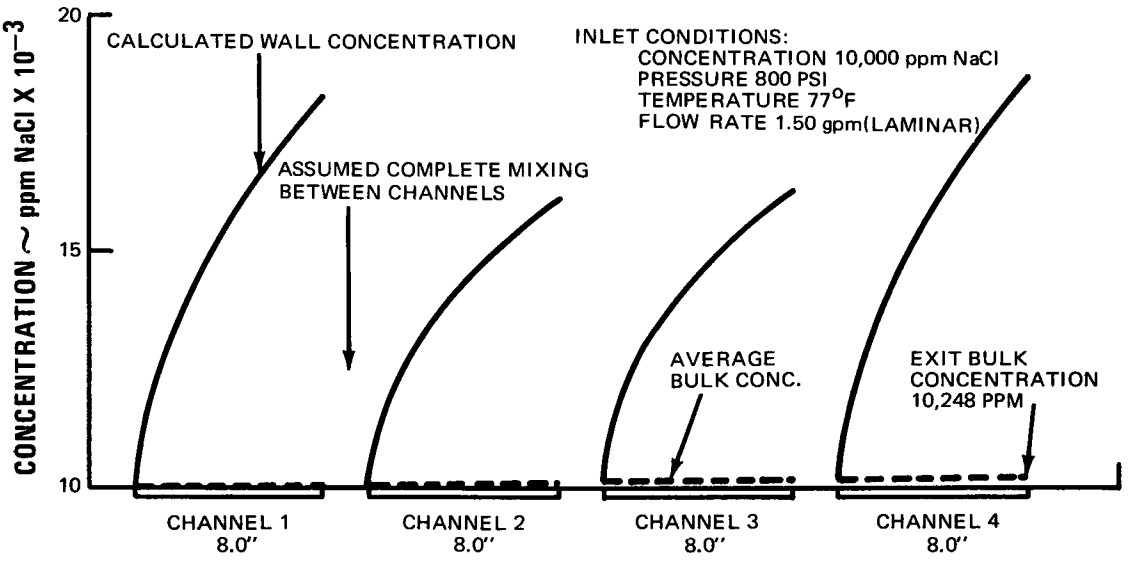

Figure 25 Calculated Wall Concentration vs Channel Length

be noted that this effect occurs in only two channels, regardless of the number of composite membranes in the cartridge, so that it would become negligible in large cartridges.

Cartridge No. 1 was disassembled and inspected at the completion of testing. In general, the cartridge was in very good condition. All O-rings appeared to seal effectively. The composite membrane tape and Pliobond seals were intact except for the center composite membrane where one tape joint failed and resulted in a relatively small leak (estimated from a discoloration noted under the reinforced membrane). This leak was previously mentioned in regard to the initially-poor cartridge performance. There was no apparent damage to the composite membrane surfaces from the feedwater turbulators. A rust-colored film had been deposited on all membrane surfaces.

2. Ten-Plate Compact Cartridge

The second compact cartridge to be tested (No. 2-1) consisted of ten composite membranes with a total active membrane area of 8.0 square feet. This cartridge was assembled in a manner similar to Cartridge No. 1. Cartridge No. 2-1 was tested for 90 hours with an average performance of 24 gfd (193 gpd) at 89 percent salt rejection at the standard conditions previously mentioned. The cartridge was disassembled, a badly pinholed composite membrane removed, and assembled with a new composite membrane. This cartridge, No. 2-2, was operated for an additional 75 hours with an average performance of 25 gfd (203 gpd) at 86 percent salt rejection.

Compact Cartridge No. 2-1 was calibrated with respect to feedwater flow rate and pressure. Membrane performance is shown in Figures 26 and 27 as a function of feedwater flow rate and applied pressure, together with the predicted performance values calculated in the same manner as those for Cartridge No. 1. These predicted performance values were based on an average membrane constant and salt rejection obtained from the experimental data at turbulent feedwater conditions. During the feedwater flow calibration, Figure 26, a shift in the cartridge salt-rejection characteristics occurred at the feedwater flow rates below the 1.5 gpm data points. The downward shift in the salt rejection and the slight increase in the product-water flux indicates leakage of the

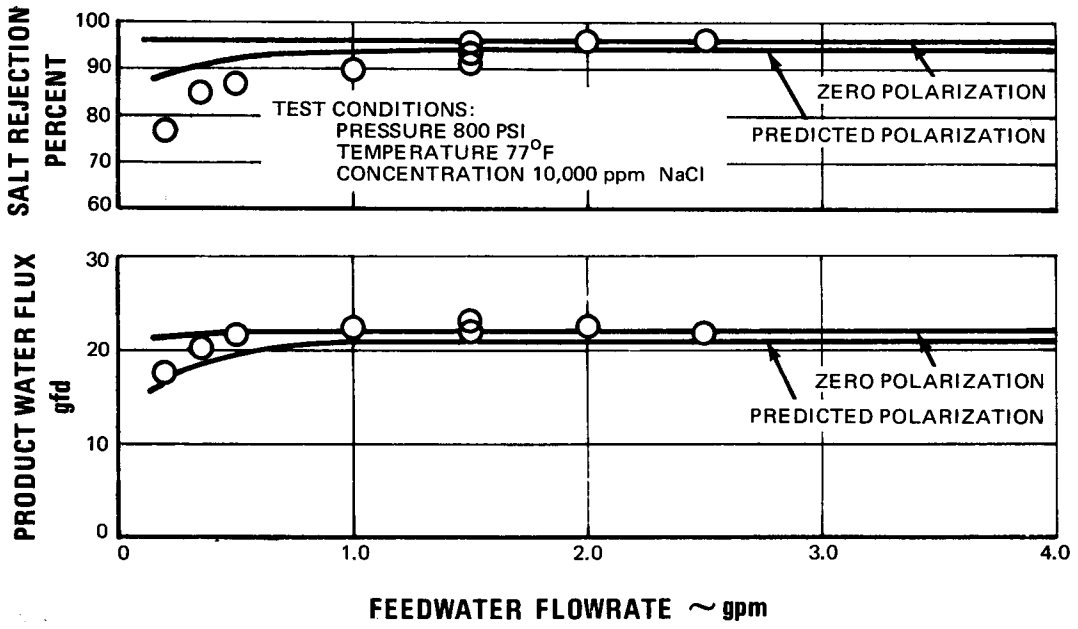

Figure 26 Performance of Compact Cartridge No. 2-1 vs Feedwater Flow Rate

feedwater into the product-water stream, as opposed to concentration polarization. Concentration polarization would have caused a decrease in both salt rejection and product-water flux. Feedwater leakage is verified by a plot of reduced product-water flux versus feedwater flow rate, as shown in Figure 28. This plot does not show a performance shift, implying that the diffusive flux remained unchanged. The feedwater pressure calibration, Figure 27, was performed subsequent to the flow rate calibration. The product-water flux is shown to be a linear function of the applied pressure. The low salt rejection is attributed to leakage through imperfections in the membrane surface. A plot of feedwater leakage into the product-water stream during the feedwater pressure calibration is shown in Figure 29. The initially-high leak rate at 800 psi is probably the result of membrane relaxation during the interval between the

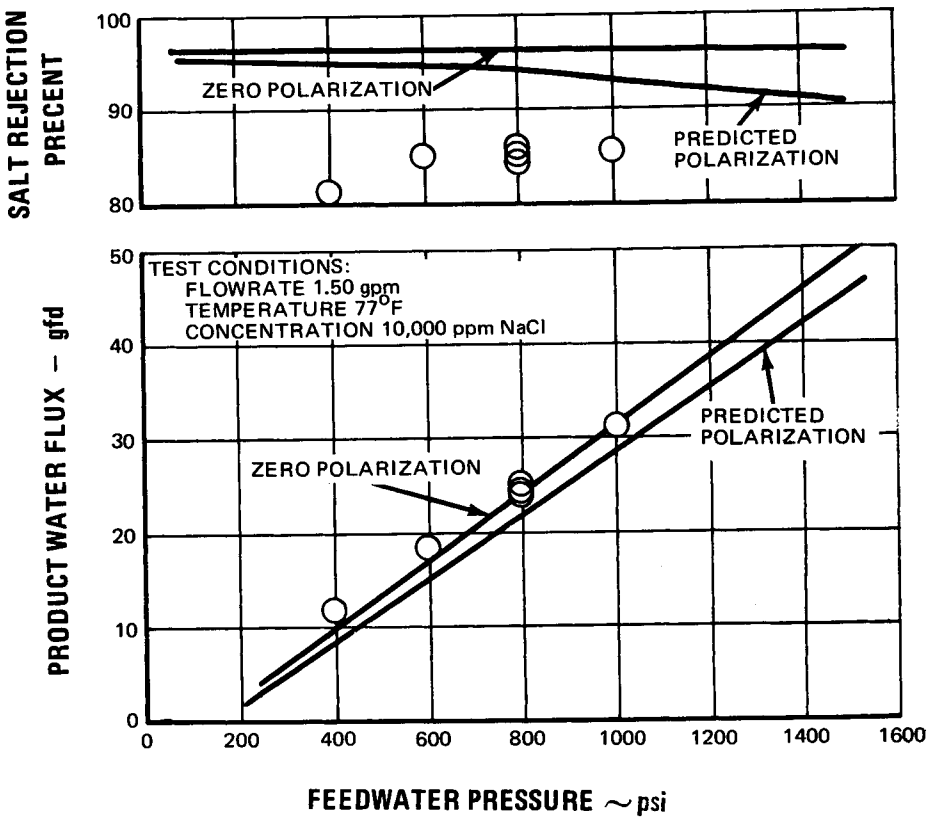

Figure 27 Performance of Compact Cartridge No. 2-1 vs Feedwater Pressure

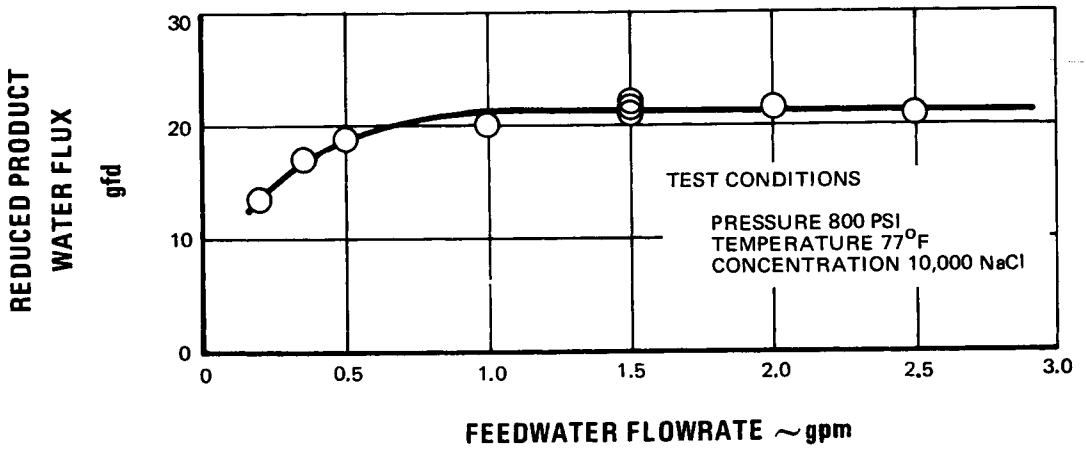

Figure 28 Reduced Product-Water Flux vs Feedwater Flow Rate - Compact Cartridge No. 2-1

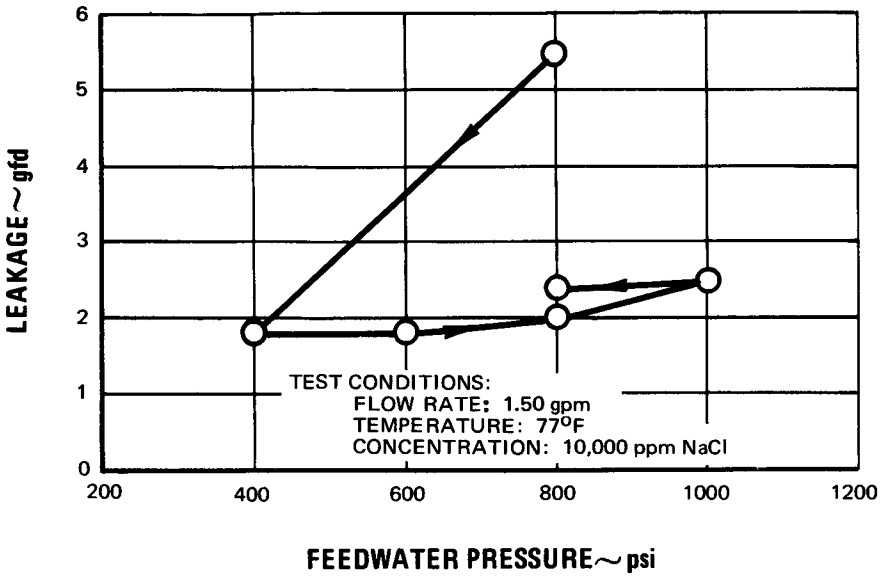

Figure 29 Leakage vs Feedwater Pressure - Compact Cartridge No. 2-1

feedwater flow rate and pressure calibrations. A recovery rate of approximately 50 percent was obtained with the cartridge. Compact Cartridge No. 2-1 is shown partially assembled in Figure 30 and installed in a pressure vessel in Figure 31.

Compact Cartridge No. 2-1 was disassembled and inspected. All of the composite membranes were found to be somewhat pinholed, and one composite, No. 178A, was found to be particularly badly pinholed. This membrane was removed and replaced with Composite No. 175B. The cartridge was then reassembled as Compact Cartridge No. 2-2.

A feedwater concentration and pressure calibration was performed on Cartridge No. 2-2, and is shown in Figure 32. This data did not reveal any significant performance improvement. As there was no improvement in the cartridge salt rejection level, the test was terminated. Cartridge No. 2-2 was disassembled and individual composite membranes were inspected. Every composite membrane in the cartridge had become pinholed to some extent, ranging from 5 or 6 up to 30 pinholes per composite per side. Further, in almost all cases there was a significant discoloration in the filter-paper underlay beneath the site of the pinhole, indicating a leak through pores in the membrane surface large enough to account for the reduced salt rejection level, rather than through the tape and O-ring seals. A composite membrane after test is shown in Figure 33.

Post-test examination of this cartridge showed that, 1) the composite membrane seals withstood the combined effect of pressure and flow rate, 2) there was no

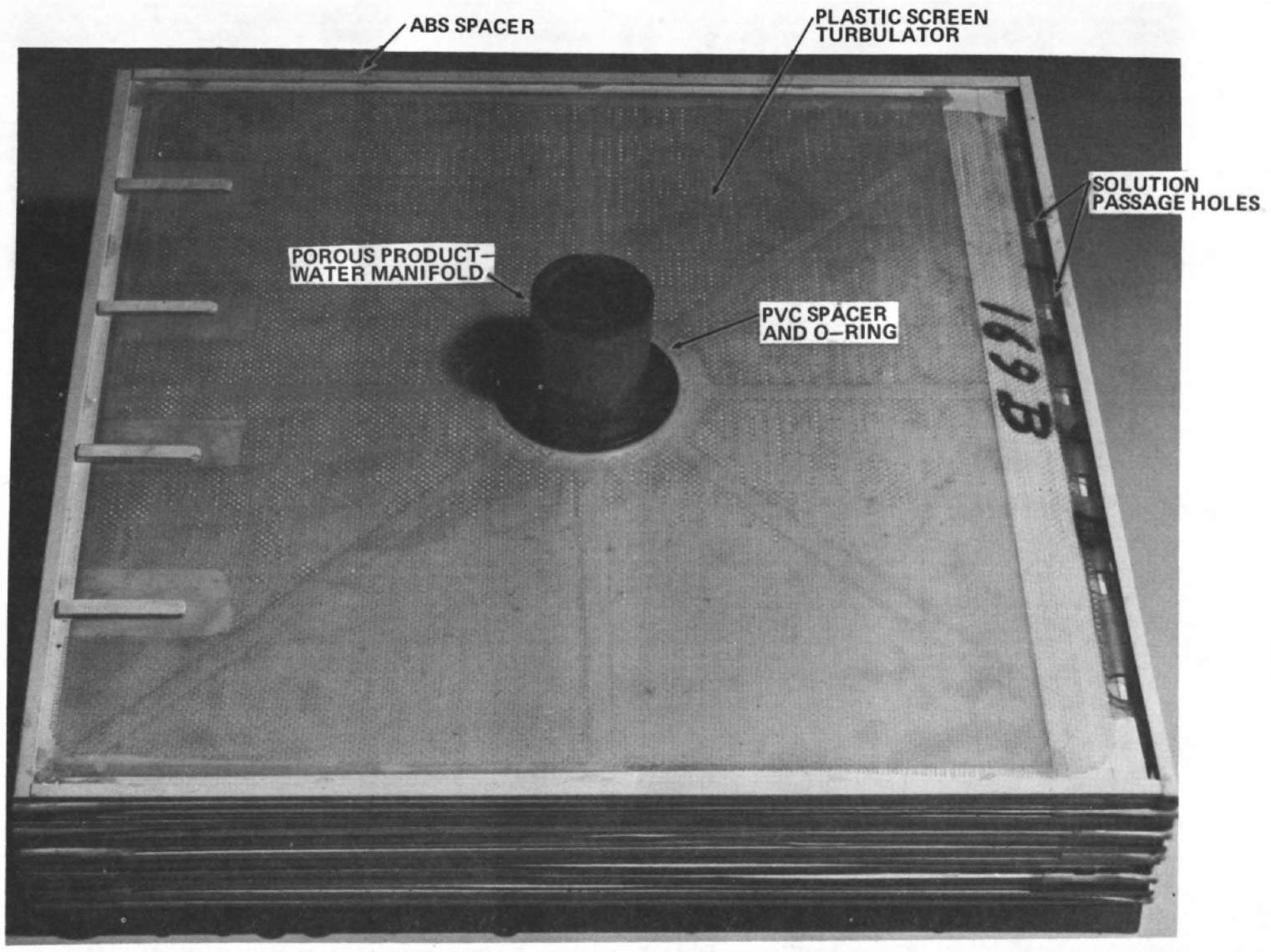

Figure 30 Reverse-Osmosis Cartridge Partially Assembled XP-88771

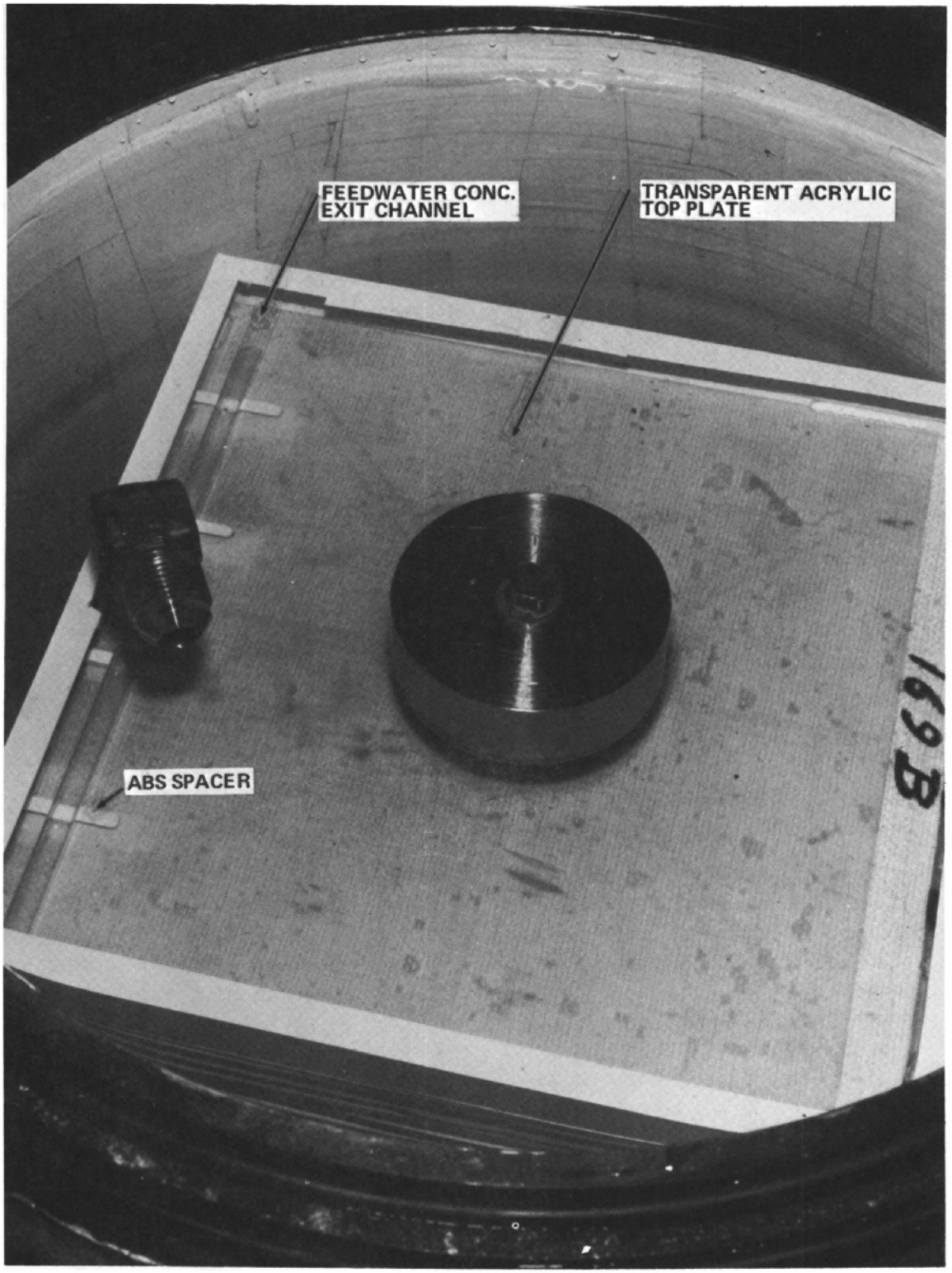

Figure 31 Assembly of Compact Reverse-Osmosis Cartridge and Pressure Vessel XP-88775

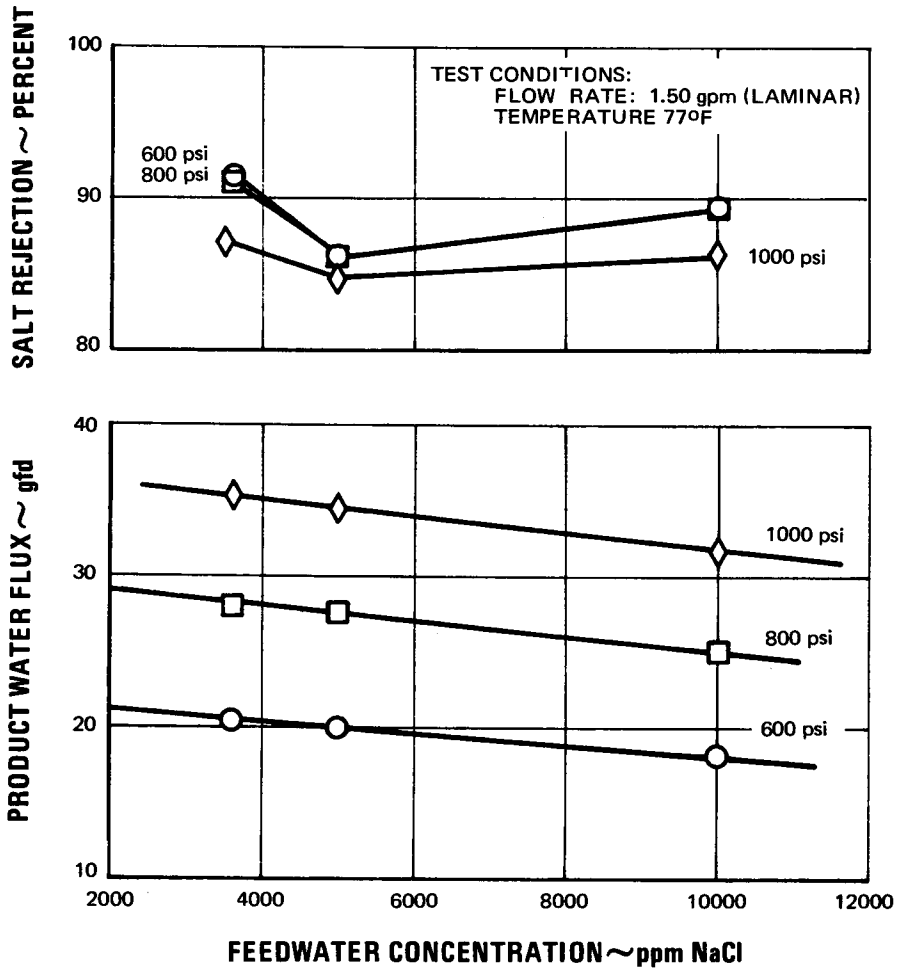

Figure 32 Performance vs Feedwater Concentration - Compact Cartridge No. 2-2

visible damage to the membrane surface from the plastic screen turbulator, 3) the turbulators did not provide nucleation for precipitates, and 4) the cartridge tape shroud had not suffered any apparent damage. Compact Cartridge No. 2-1 was disassembled after 91 hours at test conditions. Then it was reassembled with only a single composite membrane being changed, yet it achieved nearly pre-teardown performance.

The test program performed on Cartridge No. 2 as a function of operating time is presented in Figure 34. The cartridge was exposed to 15 pressure cycles during a seventeen-day period. The points shown on this figure represent the average performance taken over a stabilized time period. The shaded points represent data obtained at the standard conditions of 800 psi feedwater pressure, 77°F temperature, 1.5 gpm laminar flow rate and 10,000 ppm NaCl feedwater solution. At these conditions, the cartridge initially produced 24 gfd with a salt rejection of 94 percent. The level of performance shifted to 25 gfd at 86 percent after 22 hours of operation, and remained at that level for an additional 143 hours. This indicates that the pore leakage did not increase with time and that the effect of concentration polarization was negligible.

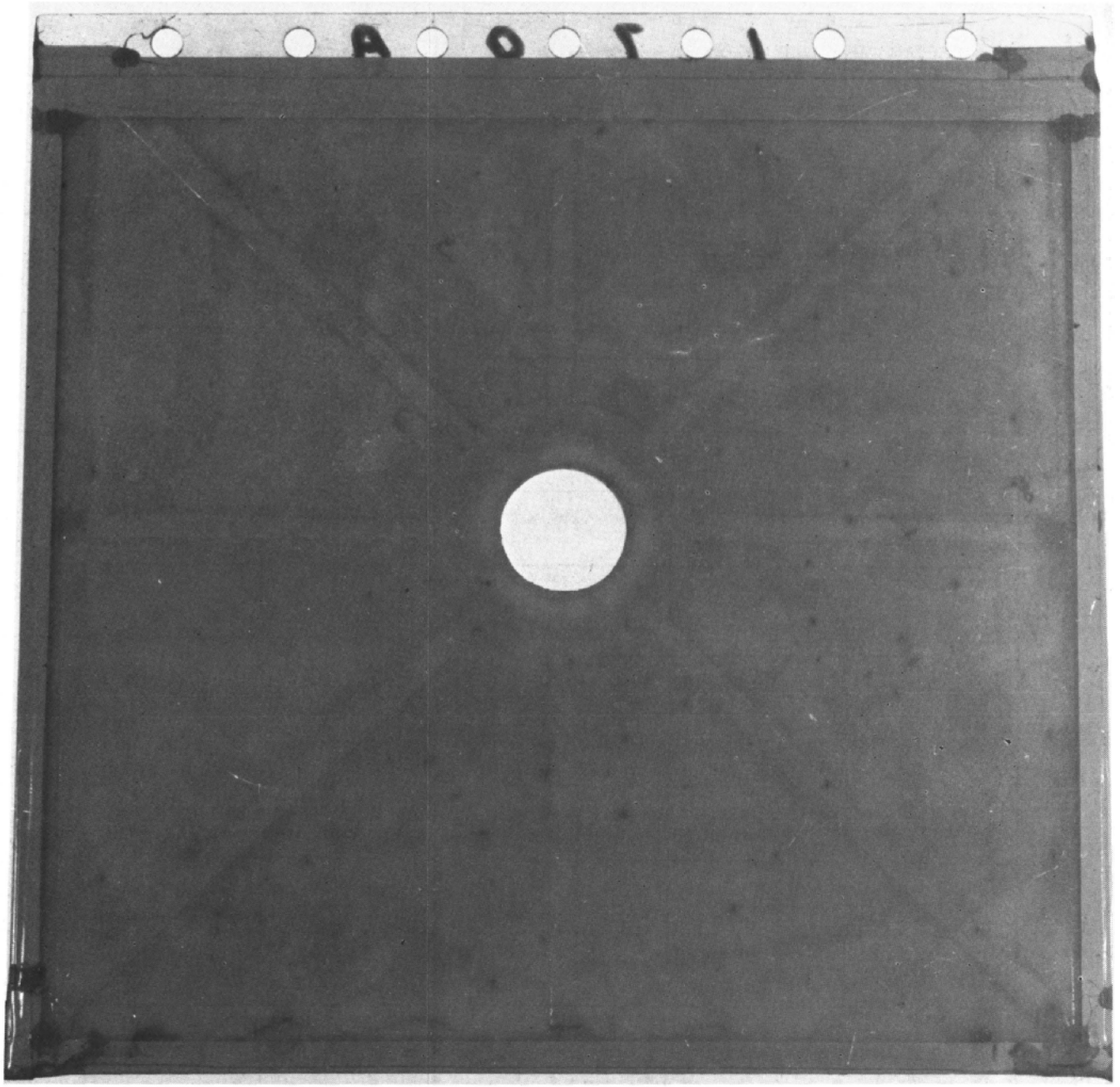

Figure 33 Typical Composite Membrane after Test XP-88846

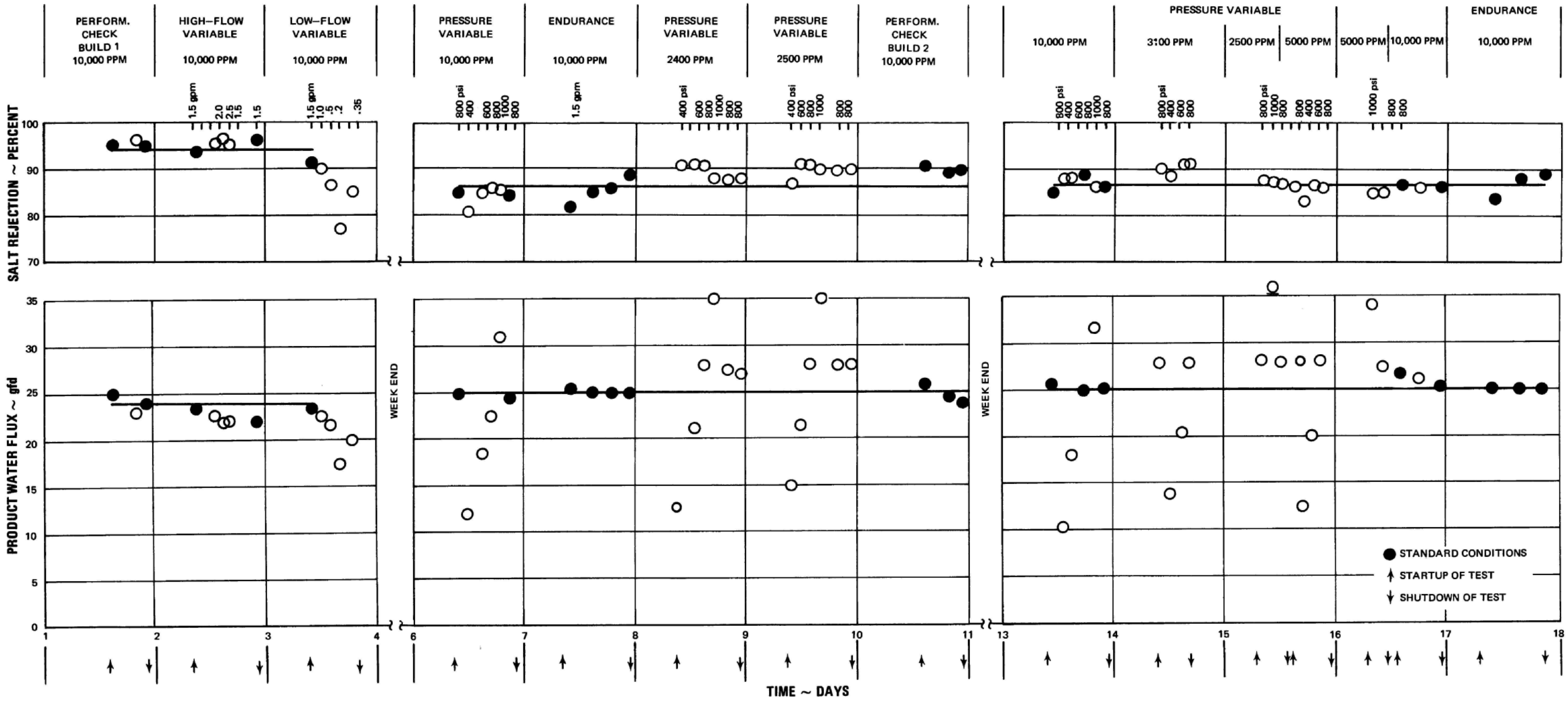

Figure 34 Performance as Function of Operating Time - Compact Cartridge No. 2

B. Composite Membrane Development

The composite membrane is the active element of the compact cartridge. It provides the semipermeable surface through which the reverse-osmosis process takes place, and passes the product water to a central manifold. As a consequence the composite membranes make up the bulk of a compact cartridge. For example, a typical compact cartridge will contain over 200 of these composite membranes arranged in a stack, properly sealed, structurally supported and manifolded to permit removal of the product water. A typical plant of one million gallons per day capacity will require approximately 25 compact cartridges. The large number of composite membranes required for a single plant indicates that if the reverse-osmosis process becomes established it will be necessary to manufacture composite membranes on a volume basis and at low cost.

Since the manufacturing of a composite membrane is not an established technology, a need exists to develop the necessary techniques for the manufacturing of composite membranes. Three types of composite membranes were investigated during the contractual time period, 1) a rigid composite membrane, 2) a flexible composite membrane, and 3) a direct-cast composite membrane. In the first and second methods a reinforced membrane, which was previously cast and treated in a separate operation, was sealed to a grooved PVC support plate and laminated plastic screen respectively, with a pressure-sensitive polyester film. In the third method the membrane was cast directly onto the surface of a reinforcing material that had been previously attached to a support material. The major effort to develop a composite membrane was directed towards the use of a grooved membrane-support plate. Studies indicated that the reinforced membranes could bridge grooves up to 12 mils wide without physical damage. The laminated screen concept proved too difficult to form and support, and was discontinued. The primary problem associated with the direct-cast process is the casting of a uniform membrane film directly onto the surface of the porous support material. A poorly-formed membrane may result due to solution penetration into the porous support material, difficulty in casting a uniform film, membrane shrinkage during the cold-bath and hot-bath processing, and possible distortion of the support material.

The composite membrane developed for this program was formed by attaching reinforced membranes to the upper and lower surfaces of a grooved plastic plate. A pattern of circular grooves 6 mils wide and radial grooves 10 mils wide was molded into the plastic surface as shown in Figure 35. The circular grooves were spaced 12 mils between centers and were 6 mils deep. Polyvinylchloride plastic was chosen for the initial specimens. The reinforced membranes were attached to the plastic with a tape or cement. The radial grooves transport the water that passes through the membrane to the central hole which contains the porous product-water manifold. Seven 1/4-inch diameter holes permitted passage to the next plate. The thickness of the plastic plate was 30 mils and it was 8.5 inches square.

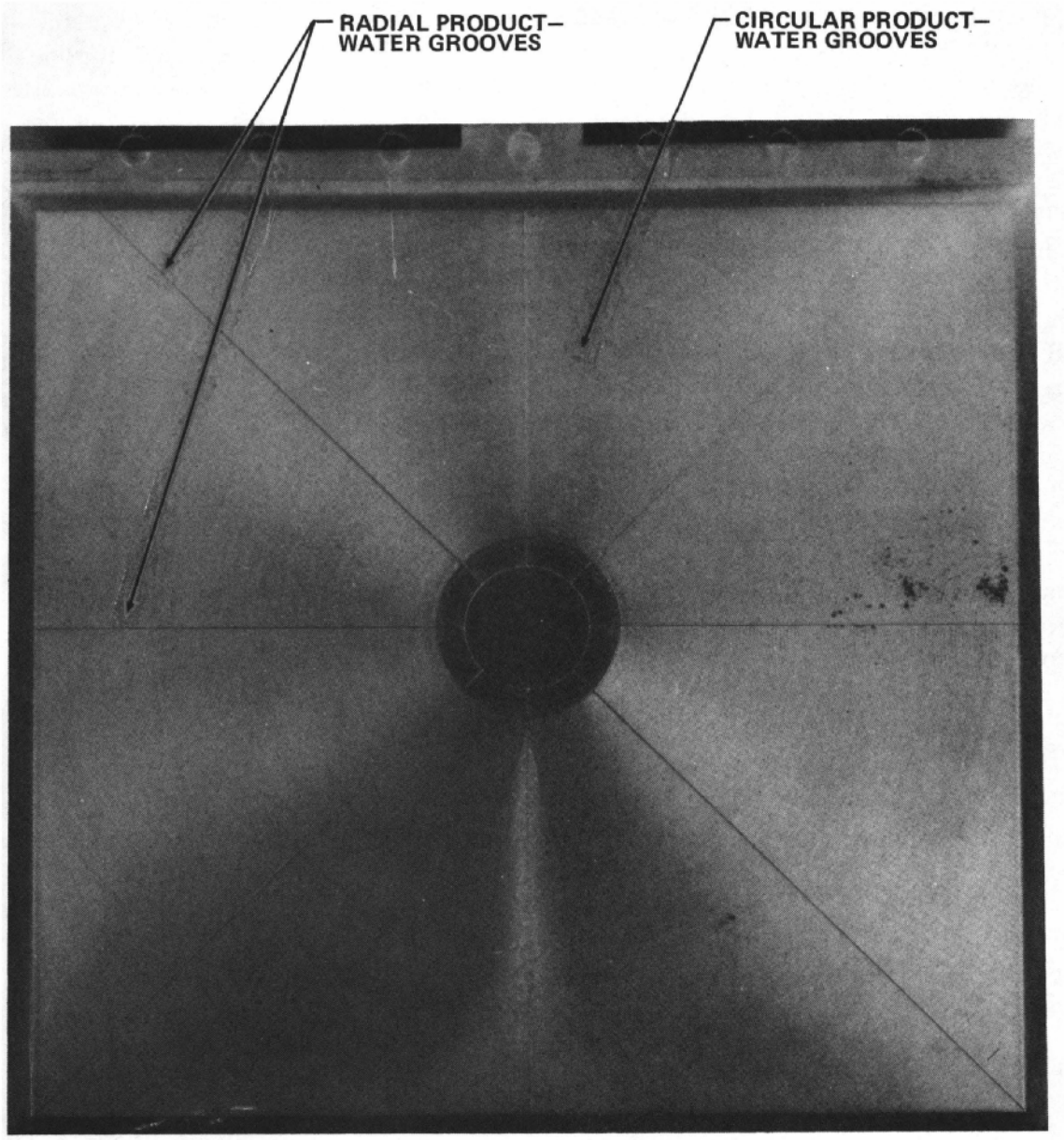

Figure 35 Composite Membrane Support Plate XP-84967

The composite membrane was made in the following way. Two pieces of reinforced membrane were cut into two pieces 8.5 x 7.75 inches and a 1.0 inch central hole was cut out of each. The 8.5-inch dimension was the width of the support plate and the 7.75-inch dimension the distance from the bottom edge to the step in the edge containing the brine-passage holes. The membranes were attached, one at a time, to the zero-loss support material, using 1/2-inch wide Mystic Tape 7300. Three edges of the composite were taped before taping the second membrane to the opposite side. First, the edge opposite the brine-passage holes was taped. Approximately 1/4 inch of the tape width was attached to the membrane and the remaining 1/4 inch was folded over and attached to the support plate. The other two edges were taped in a similar manner. The whole process was repeated for the second side. The last edge of both reinforced membranes (the edge along the brine-passage holes) was taped with one continuous piece of tape wrapped completely around the composite. At each corner, a drop of Pliobond was applied to seal the tape overlap. Figure 36 shows a typical composite membrane after fabrication.

Although a PVC zero-loss support material was used, several alternates exist. Composite membranes have been formed on two layers of 40-mesh 0.010-inch thick stainless-steel screen. Similarly, plastic screen could be employed.

During the initial development phase of the composite membranes it became evident that membrane deformation was occurring in the area of the circular and radial grooves for product-water removal. This resulted in a partial blockage of the grooves. Previous studies had shown that reinforced membranes can bridge gaps up to 12 mils wide and 10 mils deep without physical damage to the membrane. Membrane deformation was expected, however, and inspection of the membrane support plate revealed that the depth of the grooves was only about 4 mils while its design depth was 6 mils. The deformation of the membrane into the radial grooves for product-water removal resulted in a feedwater leak path between the reinforced membrane and the inner O-ring spacer gasket and into the product-water collection manifold. The membrane deformation and leakage problem was resolved by placing an impervious celluloid material 7 mils thick over the radial grooves for product-water removal. This material was cut into the shape of a washer of 1 inch inside diameter and 2 inches outside diameter with eight projections 1/8 inch wide by 4 inches long. The washer eliminated the feedwater leak between the membrane and inner O-ring spacer gasket, while the long projections prevented the membrane from deforming into the radial product-removal grooves. A second change was an underlay of Whatman No. 50 filter paper to support the membrane over the circular product-water removal grooves.

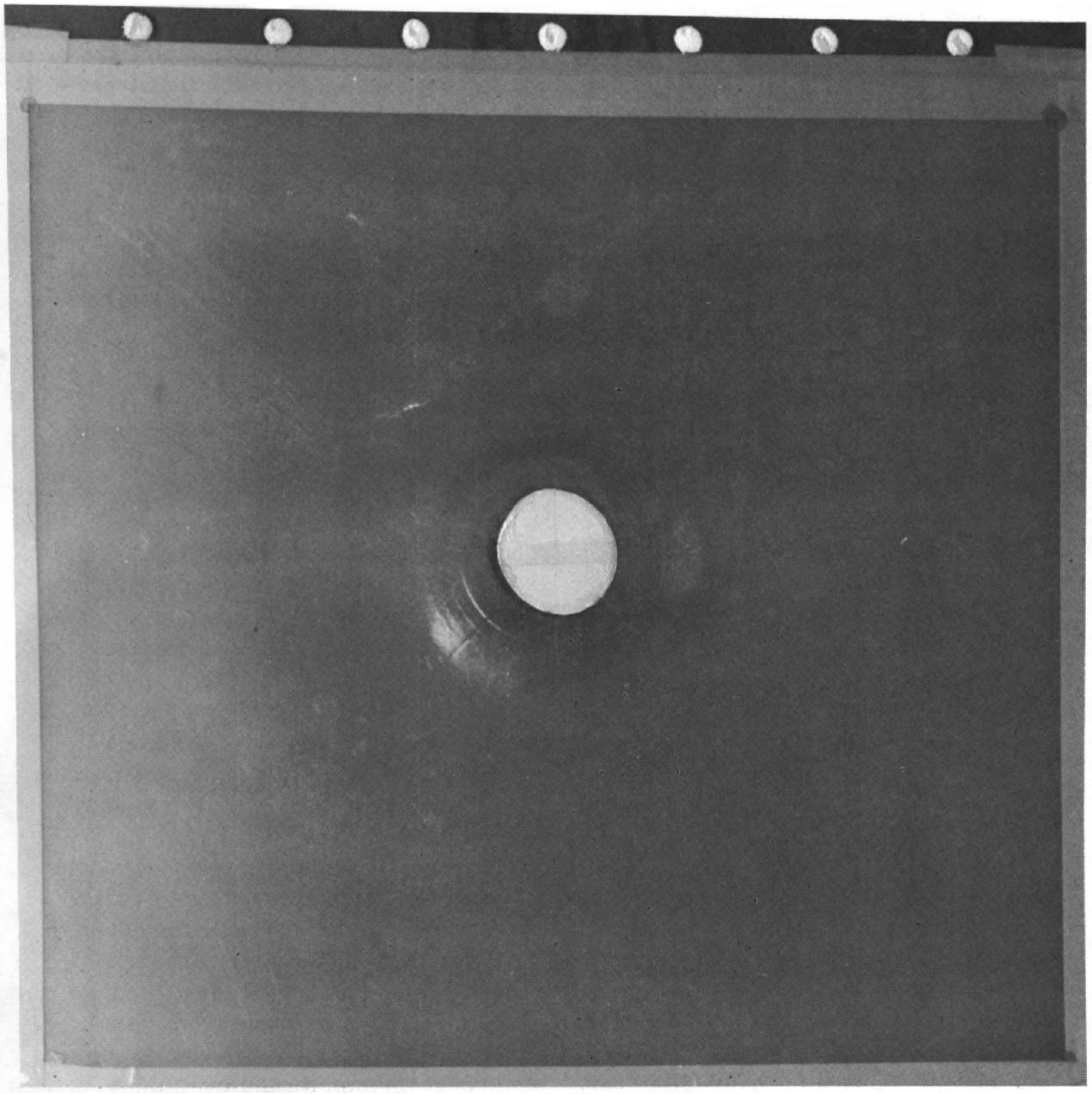

Figure 36 Composite Membrane Assembly XP-84968

The above changes were incorporated as a temporary measure in order to obtain a workable composite membrane. Future membrane support plates should contain deeper circular and radial grooves for product-water removal. Also, the number of radial grooves should be increased with a corresponding decrease in their width. This would tend to eliminate leakage between the inner O-ring seal spacer and reinforced membrane.

Thirty-one composite membranes were assembled and evaluated. Table 15 presents the composite membrane performance data and unique construction details when evaluated at the conditions of 800 psi applied pressure, 77°F feedwater temperature, 10,000 ppm NaCl feedwater concentration, and a 1.5 gpm feedwater flow rate (laminar - 1.2 ft/sec, Reynolds number - 1000). The feedwater flow rate of 1.2 ft/sec was calculated on the basis of an open channel 8.5 inches wide by 0.050 inch high.

C. Composite Membrane Seal Development

Before a composite membrane could be fabricated it became necessary to find a means of sealing the reinforced membrane to the membrane support plate. The seal must form a water-tight bond between reinforced membranes or between a reinforced membrane and its support. The seal program consisted of three parallel efforts, 1) the development of a tape seal, 2) the development of a liquid-adhesive seal, and 3) the development of a direct-cast composite membrane. The direct-cast composite membrane is attractive as it would eliminate the need for a tape or adhesive seal, but relies on the cast solution to form its own seal during the membrane-formation process.

The first approach to forming a seal for a composite membrane was to tape a reinforced membrane to a plastic material. Fifteen tapes were obtained which had a water-impervious film, pressure-sensitive adhesive and chemical stability in water. The properties of these tapes are listed in Table 16. Nine pressure-sensitive adhesive tapes were used to attach reinforced membranes to PVC. Two methods of application were used. In one case, a damp membrane was attached to dry PVC; in the other case the membranes were attached to the PVC while submerged in water. The membranes taped to the plastic were left in a 10,000 ppm aqueous solution of NaCl for six days. The results are summarized in Table 17. Mystic Tape No. 7300, a polyester pressure-sensitive film 1 mil thick with a 1.5-mil silicone adhesive, was selected for further studies. A lap joint was unavoidable, therefore a liquid adhesive, Goodyear Rubber Pliobond cement, was used to maintain a water-tight seal. The ability of this type of seal to withstand long periods at operating conditions and its applicability to composite membrane fabrication was examined by constructing and evaluating a composite membrane.

TABLE 15

Performance and Construction Details of Composite Membranes

Composite Membrane No.	Performance GFD	% S.R.	Construction Details	Remarks
148A	23	0	PVC supp't plate	Unsatisfactory Performance
148B	15	46	PVC supp't plate	" "
150A	15	70	Brass washer at product water exit	" "
152A	19	58	Brass washer at product water	" "
153A	20	74	Celluloid support over supp't plate	" "
157A	12	83	Celluloid support and Whatman No. 1 filter paper	" "
151A	13	91	Brass washer at product water exit	" "
160B	34	31	Plastic screen over support plate	" "
161A	27	55	Plastic screen over support plate	" "
164A	11	80	Celluloid washer and Whatman No. 50 filter paper	" "
167A	35	54	100 mesh nickel screen and celluloid washer	" "
159A	23	90	Celluloid support; Whatman No. 50 filter paper and feedwater turbulators	Acceptable Performance - Not Used
168A	28	76	100 mesh nickel screen and turbulator	Unsatisfactory Performance
163B	17	89	Celluloid support; Whatman No. 50 filter paper and feedwater turbulators	" "
169A	27	87	" " " "	Acceptable Performance - Not Used
169B	24	92	" " " "	Selected for Cartridge No. 2
170B	30	70	" " " "	Unsatisfactory Performance
170A	25	84	" " " "	Selected for Cartridge No. 1
171A	29	78	" " " "	Unsatisfactory Performance
174A	27	83	" " " "	Selected for Cartridge No. 1
173B	26	84	Celluloid support; Whatman No. 50 filter paper and feedwater turbulators	Selected for Cartridge No. 1
174B	27	91	" " " "	Selected for Cartridge No. 2
176B	26	88	" " " "	Selected for Cartridge No. 2
179A	25	93	" " " "	" "
179B	29	88	" " " "	" "
180A	29	90	" " " "	" "
181A	28	91	" " " "	" "
181B	28	91	" " " "	" "
175B	30	81	" " " "	Selected to replace Comp. No. 178A in Cartridge No. 2 - Build 2
178A	30	89	" " " "	Selected for Cartridge No. 2
178B	28	88	" " " "	" "

TABLE 16

Properties of Sealing Tapes

Manufacturer	Manufacturer's Designation	P&WA Designation	Film Material & Thickness (mils)	Adhesive Type & Thickness (mils)	Total Thickness (mils)	Moisture Rate
Behr Manning Co.	Bear Tape No. 197	PMC 4124	saturated flat rope paper	rubber base adhesive	7	----
3M Co.	Scotch No. 898	PMC 4133-E	viscose reinforced cellulose acetate	rubber resin	7	----
3M Co.	Scotch No. 470	PMC 4134	vinyl plastic	synthetic rubber	6	3.0 gm/in^2/24 hr
Sherman Paper Products	C-50 Correflex	PMC 4140-B	flat Kraft backing	synthetic rubber	9	N.A.
Plymouth Rubber Co.	Slipknot No. 10	PMC 4142	pigmented plastic	cyclohexanone solvent adhesive	10	N.A.
3M Co.	Scotch No. 400	PMC 4143	treated paper tissue (2)	crude rubber (3)	15	N.A.
Mystic Tape Div. Borden Chem Co.	Mystik No. 7300	PMC 4188	Mylar polyester (1)	silicone adhesive (1.5)	2.5	N.A.
3M Co.	Scotch No. 425	PMC 4224	soft aluminum foil (3)	synthetic rubber (2)	5	0.1 gm/100 in^2/24 hr
3M Co.	Scotch No. 472	PMC 4237	vinyl plastic	pigmented rubber blend	10	2.0 gm/100 in^2/24 hr
3M Co.	Scotch No. 481	PMC 4239	pigmented plastic	rubber blend	9	0.4 gm/100 in^2/24 hr
3M Co.	Scotch No. 74	PMC 4243	polyester film	thermal-setting adhesive	1	N.A.
3M Co.	Scotch No. 471	None	pigmented vinyl plastic	synthetic rubber	5	2.0 gm/100 in^2/24 hr
Mystik Tape Div.	Mystik No. 7503	None	Teflon (3)	silicone (3)	6	N.A.
3M Co.	Scotch No. 33	None	vinyl plastic	silicone	7	N.A.
Conn. Hard Rubber	Temp-R-Tape	None	Teflon (3)	silicone (3)	6	N.A.

N.A. - Information not available

TABLE 17

Initial Tape Screening Results

Tape	Dry Application		Wet Application		Selected for Operational Evaluation	Comments
	Adhesion to Membrane	Adhesion to PVC	Adhesion to Membrane	Adhesion to PVC		
Scotch No. 470	good	good	moderate	moderate	yes	
Mystik No. 7300	good	good	good	good	yes	
Scotch No. 472	moderate	moderate	moderate	moderate	no	adhesive discolored cellulose-acetate membrane and caused separation of nylon backing
Scotch No. 481	moderate	moderate	poor	moderate	no	adhesive reacted with PVC, resulting in a soft spongy interface
Scotch No. 74	good	moderate	good	moderate	yes	
Scotch No. 471	good	good	good	good	yes	
Mystik No. 7503	poor	moderate	poor	moderate	no	very little adhesion between tape and cellulose acetate
Scotch No. 33	moderate	moderate	poor	moderate	no	adhesive caused cellulose acetate to separate from nylon backing
Temp-R-Tape Type T	good	good	good	moderate	yes	

Test Conditions: 144 hours
static
ambient pressure
77°F
solution, 10,000 ppm NaCl

The second approach in forming a composite membrane seal was to use a liquid adhesive to attach a reinforced membrane to a PVC support. Five adhesives were obtained for membrane attachment and sealing studies. Table 18 lists the adhesives and their manufacturers.

TABLE 18

Membrane-to-PVC Adhesives

Loctite 404	Loctite Corporation
Epoxy 907	Miller-Stephenson Chemical Company
Pliobond	Goodyear Rubber Company
Silicone DC-92-018	Dow Corning
Polypoxy 7050, 7055	Pettit Paint Company

Membrane-to-PVC composites were formed and evaluated. The performance obtained is presented in Table 19.

TABLE 19

Performance of Membrane-to-PVC Composites

Adhesive	Number of Samples	Product-Water Flux, gfd	Salt Rejection, %
Pliobond	5	31	66
Epoxy 907	4	42	61
DC-92-018	6	29	57
Polypoxy	3	-	70

Loctite 404 cement was considered unsatisfactory because it penetrated the reinforced membrane to such a degree that a satisfactory seal could not be obtained. A series of multiple applications of this cement, or an additive to the cement to increase adhesive viscosity, possible could have eliminated this problem. Visual examination of these specimens shows that the seals remained in contact and that the adhesive-to-membrane and the adhesive-to-PVC contact surfaces were continuous. It is assumed that the feedwater penetrated the seal in the area of the membrane porous gel. Further evaluation of adhesive seals was discontinued in favor of the tape-cement seal.

The third approach to the development of a composite membrane was to attach a nylon reinforcing material to both sides of a support material, and to cast a membrane directly onto these surfaces. This approach is particularly attractive since it eliminates the membrane-to-support material seal. The support material could consist of a grooved support plate or a metal or plastic screen. Both of these material types demonstrated that they are acceptable membrane-support materials with respect to their hydrodynamic characteristics under load. Two direct-cast techniques were considered, a "dip cast" and a "double cast". The dip-cast technique consisted of dipping a nylon-wrapped membrane-support plate in a membrane cast solution and withdrawing it at a uniform rate. Rollers or straight-edge surfaces removed the excess cast solution from the composite, leaving the desired membrane film thickness. After allowing sufficient time for solution evaporation, the composite would be given the standard cold-bath and hot-bath treatments. The double-cast technique consisted of casting on one side of a nylon-wrapped support plate, cold-bath treating, casting the second side and again cold-bath treating the membrane. This process forms a water-tight bond around the edges of the composite, due to the solvating of the first membrane by the second cast solution. The double-cast method was selected as the more workable of the two direct-cast techniques, since existing cast equipment could be used.

Eight double casts were made with partial success. A membrane of high quality was cast over the central region of each composite, but excessive membrane buildup was present at the edges of the composite. These composites were not evaluated as the membrane buildup resulted in a poor seal for the composite membrane. Additional work would be required to develop a workable direct-cast technique.

In view of the fact that satisfactory composites have been formed by the use of a tape-cement seal, the adhesive seal effort and the direct-cast effort were discontinued.

A detailed description of the adhesive and direct-cast techniques was presented in the sixth and seventh quarterly reports, PWA-3322 and PWA-3376.

VI. SYSTEM PREDICTION STUDIES

An analysis was performed to develop a method for theoretical prediction of the performance of a compact reverse-osmosis cartridge. The cartridge model configuration consists of flat rectangular composite membranes. The analysis consisted of two parts. The first predicted product-water flux, product-water concentration and brine pressure loss for these cartridges, taking into account the following effects:

1) Axial variation of product-water flux caused by:

   A) The axial increase in the effective osmotic pressure of the brine at the membrane surface caused by the combined interactions of:

      1) the axial increase in brine bulk concentration due to product-water removal,

      2) the effects of polarization resulting from the finite rate of back diffusion of rejected salt at the membrane surface into the bulk of the brine stream, as predicted by Brian[4], and

      3) axial decrease in brine pressure caused by fluid friction.

2) Brine pressure losses due to entrance and exit effects.

3) Membrane salt rejections less than 100 per cent.

To facilitate calculations the analysis was programmed on a high-speed digital computer. This information was then used in the second part to calculate the energy required per unit of product and the number of stages to obtain product water with less than 500 ppm of solids.

It was found that for both brackish and sea water the composite spacing should be minimized. Also relatively high salt rejections are required by both brackish and sea water; in general, values greater than 95 percent are required. Lastly, most efficient operation can be obtained by minimizing the number of stages required, even though this requires higher salt rejection or lower recovery rates.

A. Cartridge Configurations

Two compact cartridge configurations were considered for analysis and are illustrated in Figures 37 and 38. The scheme shown in Figure 37 represents a series of single-pass cartridges where the brine flows once through each cartridge with

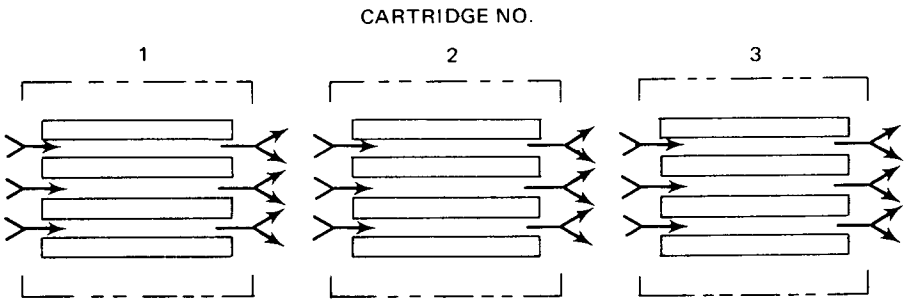

Figure 37 Single-Pass Cartridge Configuration

a mixing chamber between them. This arrangement is of the type that might be used in large-scale commercial applications.

In the cartridge shown in Figure 38 the brine makes many passes before leaving the cartridge. This arrangement makes it possible to achieve a long flow path in a small volume. It is, therefore, particularly useful for laboratory testing. Pratt & Whitney Aircraft employed this configuration for the cartridge tests presented elsewhere in this report.

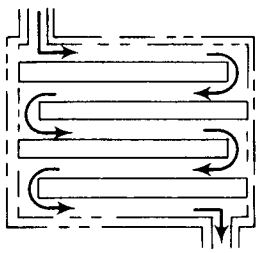

Figure 38 Multipass Cartridge Configuration

For both configurations the flow path of the brine can be considered to consist of a series of equal-length channels with brine mixing between the channels, as shown in Figure 39. Each channel is formed between a pair of flat parallel reverse-osmosis membranes which remove purified product water from the brine at a varying flux rate. This flux rate depends upon the local hydrostatic pressure of the brine and the local osmotic pressure of the brine at the membrane surface.

In the analysis it was assumed that fully-developed laminar flow was maintained in each channel and that product water was removed at equal rates by the membranes on each side of the channel.

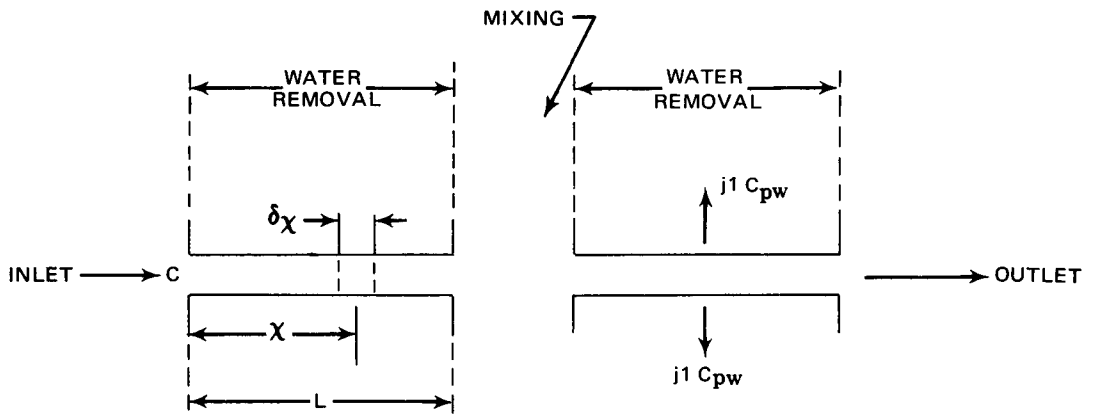

Figure 39 Cartridge Simulation Model

B. Description of Analysis

A finite-difference procedure was used in which each channel was divided into a specified number of equal-length increments. Mass balance, product-water flux, brine pressure loss, and concentration polarization calculations were made for each successive increment in the direction of flow to determine the axial variation of the following parameters for each channel in the series.

Figure 39 illustrates the geometry of a channel and the ways it is broken up into increments for analysis. It defines the channel length, incremental length and distance, product-water flux removal and concentration, and the feedwater inlet and outlet concentration. In addition, contraction and expansion pressure losses were determined for the flow of brine into and out of each channel in the series.

The flow of salt solution through an incremental length of cartridge is illustrated in Figure 40 where the feed brine is seen to flow between the two flat membrane surfaces, and the purified product water flows through the membranes in a direction perpendicular to the brine flow. The flow of brine, product water and salt across the boundaries of each increment can be determined by using the following steady-state equations.

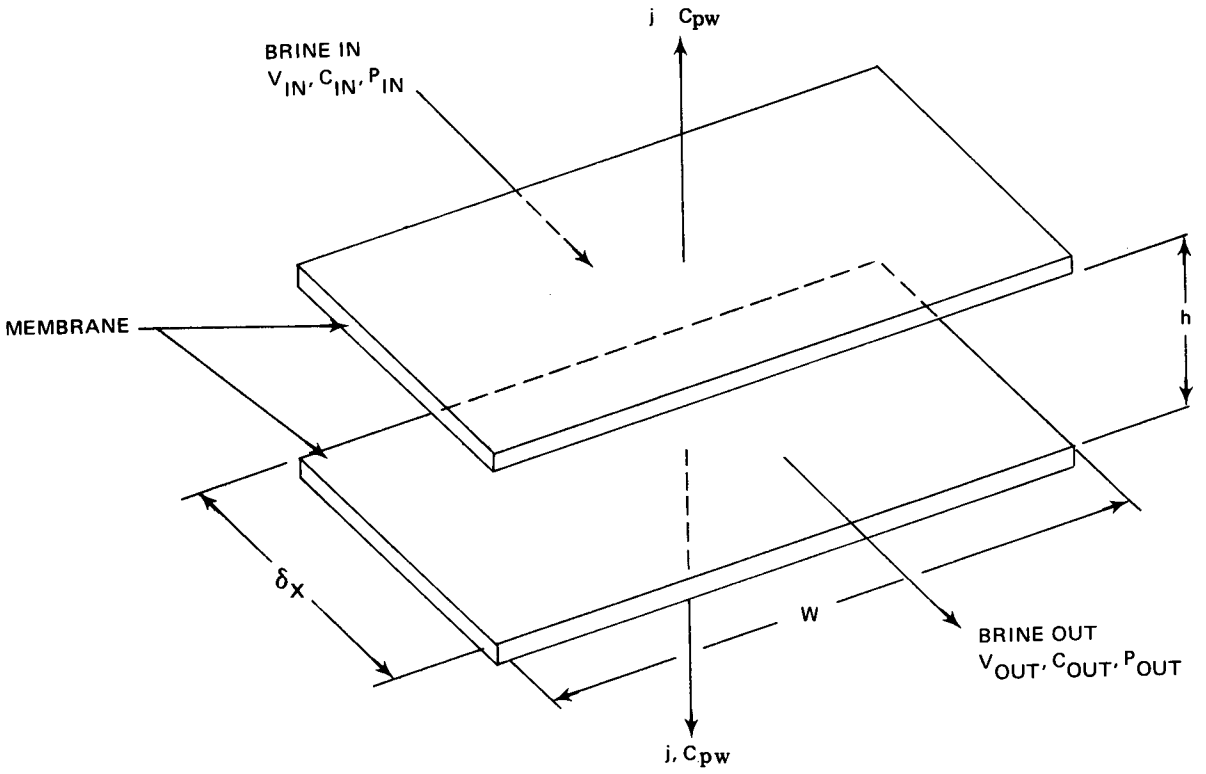

Figure 40 Channel Increment

$$\rho_{in} V_{in} (hW) - \rho_{out} V_{out} (hW) = 2j \rho_{pw} (W \delta_x) \quad (1)$$

$$C_{in} \rho_{in} V_{in} (hW) - C_{out} \rho_{out} V_{out} (hW) = 2 C_{pwj} \rho_{pw} (W \delta_x) \quad (2)$$

where

$$C_{pw} = (1-S_r) C_w \quad (3)$$

The terms on the left side of Equation (1) represent the difference between the mass flow rate of the brine entering the increment and the mass flow rate of brine leaving the increment, while the term on the right represents the mass flow rate of the product water passing across the membrane surfaces. Similarly the terms on the left side of Equation (2) represent the difference between the mass flow rates of salt dissolved in the brine which enter and leave the increment, while the terms on the right represent the mass flow rate of the salt dissolved in the product water which is not rejected and passes through the membrane surface. To simplify the analysis it was assumed that

$$\rho_{in} = \rho_{pw} = \rho_{out} = \text{Constant} \tag{4}$$

Equation (3) relates the concentration of the brine at the membrane surface, C_w, and the membrane salt rejection, Sr, to the product water concentration C_{pw}.

The product-water flux across the membrane surface of each increment was obtained from the following familiar equation

$$j = A\,(\bar{P} - \pi_w + \pi_{pw}) \tag{5}$$

Where the brine pressure was taken as the average pressure for the increment

$$\bar{P} = \frac{P_{in} + P_{out}}{2} \tag{6}$$

Equation (5) was based on the assumption that the pressure of the product water is zero.

The axial pressure drop of the brine flow through an increment was calculated from the following relation which assumes fully developed laminar flow

$$P_{in} - P_{out} = 12\,\mu\,\frac{\delta x}{h}\,\bar{V} \tag{7}$$

where

$$\bar{V} = \frac{V_{in} + V_{out}}{2} \tag{8}$$

The osmotic pressure of the brine at the membrane surface and the osmotic pressure of the product water were calculated using the relation

$$\pi = 0.0217\,(C)^{0.931} \tag{9}$$

which was fitted to osmotic pressure data obtained from Reference 5 for temperatures between 70° and 100°F.

Polarization effects were calculated from the following equation which relates the average bulk concentration of the increment $\bar{C}$ to the brine concentration at the membrane surface C_w

$$C_w = \bar{C}[\Gamma + 1.0] \tag{10}$$

where

$$\bar{C} = \frac{C_{in} + C_{out}}{2} \tag{11}$$

The factor Γ was calculated using the following relations from Reference 6.

$$\Gamma = 1.536 (\xi)^{1/3} \tag{12a}$$

$$\Gamma = \xi + 5 \left[1 - \exp (-\sqrt{\xi/3}) \right] \tag{12b}$$

$$\Gamma = \frac{1}{3 \alpha^2} \tag{12c}$$

where

$$\xi = \frac{\bar{j} x}{3 V_o h \alpha^2} \tag{13}$$

and

$$\alpha = \frac{Ds}{\bar{j} h} \tag{14}$$

Equation (12a) was used in the initial entry region of the channel (i.e., $\xi < 0.02$). Equation (12c) was used far downstream in the channel where the concentration profile approaches an asymptotic value. Equation (12b) was used in the intermediate region where the other two equations did not apply. A plot of Γ as a function of ξ and α for variable water flux across the membrane with complete salt rejection is shown in Figure 41.

Equations (13) and (14) require knowledge of the average product-water flux of the channel, $\bar{j}$. This necessitated the use of an iterative procedure as discussed below.

The analysis, as programmed on the computer, required the following primary variables as known inputs:

1) Inlet pressure of brine, P_o
2) Inlet concentration of brine, C_o
3) Inlet velocity of brine, V_o
4) Height of the flow channels, h
5) Length of a flow channel, L
6) Number of channels in series, N_{cis}
7) Membrane constant, A
8) Membrane salt rejection, Sr

With this information the computer calculated the following results:

1) For the series of channels as a whole
   a) Average product-water flux
   b) Average product-water concentration
   c) Fractional water recovery
   d) Brine pressure loss from the entrance of the first channel to the exit of the last channel

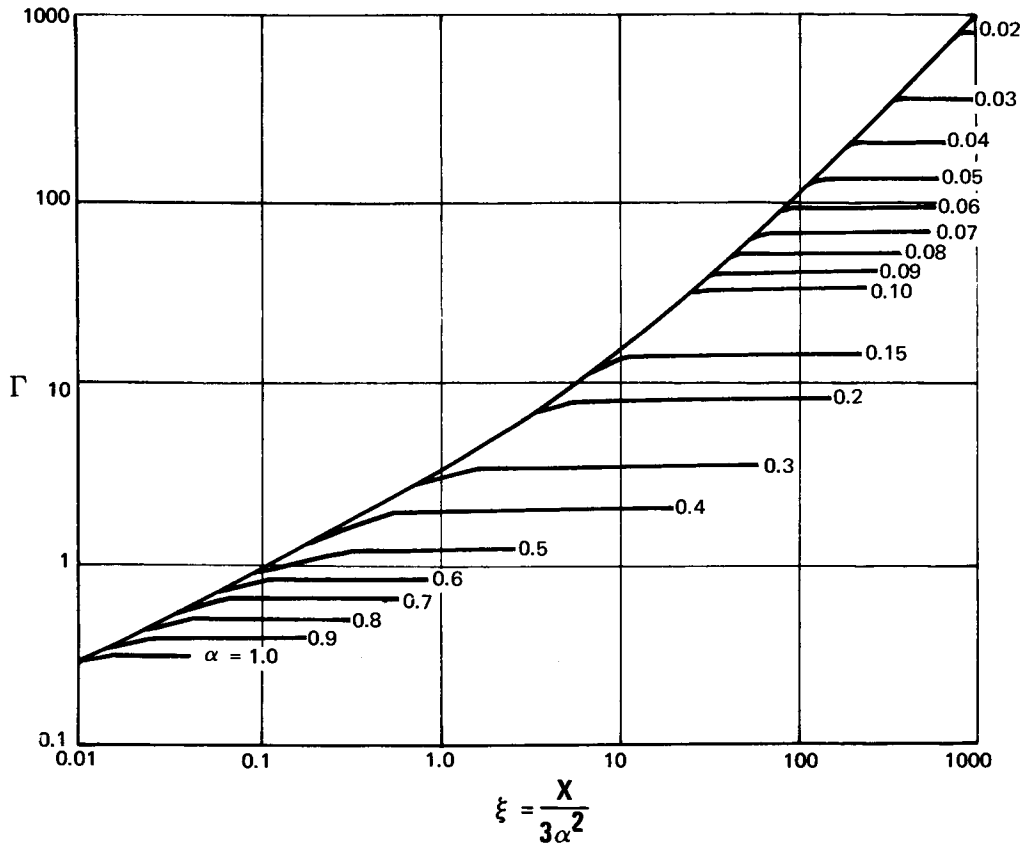

Figure 41 Polarization as Function of Configuration and Membrane Characteristics

2) For each individual cartridge
   a) Average product-water flux
   b) Average product-water concentration
   c) Fractional water recovery
   d) Brine pressure loss
   e) Axial variation of product-water flux
   f) Axial variation of product-water concentration
   g) Axial variation of brine concentration at the membrane surface

In obtaining these results the computer followed the step-by-step procedure which is outlined below:

1) From the channel height and the brine inlet velocity the contraction pressure loss was calculated for the feed brine entering the first channel in the series using the equations of Reference 7.

2) An average product-water flux was then assumed for the channel. This value was used in the calculation of the polarization effects for all increments in the channel.

3) The calculation proceeded increment-by-increment along the channel in the direction of the brine flow. For each increment the computer solved Equations (1) through (14) simultaneously by an iterative technique. Following this procedure the computer generated axial profiles for the variables listed below:

   a) Brine pressure
   b) Bulk concentration of the brine
   c) Concentration of the brine at the membrane surface
   d) Product-water flux
   e) Product-water concentration

4) When the end of the channel was reached, average values were calculated for the product-water flux and the product-water concentration.

5) The calculated value of the average product-water flux was compared with the assumed value.

6) If the two values of product-water flux agreed within a specified tolerance, the calculation proceeded. If not, a new average flux was assumed and Steps 3), 4), and 5) were repeated until agreement was achieved between two successive iterations.

7) After the program had converged on average flux, the expansion pressure loss of the brine at the exit to the channel was calculated, using the equations of Reference 7.

8) The fractional recovery and total brine pressure loss were then calculated for the first channel.

9) Steps 1) through 8) were repeated successively for the remaining channels in the series.

10) After the calculations were completed for all channels, the values were calculated for the following parameters, considering the series of channels as a whole.

   a) Average product-water flux
   b) Average product-water concentration
   c) Overall brine pressure loss
   d) Overall fractional recovery

C. Cartridge Performance Analysis

Before a comprehensive analysis of the cartridge performance could be performed, it was necessary to select the parameters that would influence the cartridge performance. The parameters selected for this study and their levels are given in Table 20.

TABLE 20

Cartridge Parameters and Their Levels

	Brackish Water	Sea Water
applied pressure, psi	400, 800, 1200	1000, 1300, 1600
recovery factor, %	50, 75, 90	30, 50, 70
channel height, in.	0.02, 0.04, 0.06	0.02, 0.04, 0.06
salt rejection, %	90, 95, 99	99, 99.3, 99.5
inlet brine concentration, ppm	1500	35,000
inlet velocity, ft/sec	0.2	0.2
channel width, in.	12.0	12.0
channels in series	4	4

The parameters which have the greatest influence on the performance characteristics of the cartridge are; 1) applied pressure, 2) recovery factor, 3) channel height, and 4) salt rejection. The levels of these parameters were selected to provide performance characteristics at conditions above and below those conditions specified by the Office of Saline Water as being standard. The increased pressure level for the sea water case is to overcome the increased osmotic pressure of sea water. Also, the recovery factor is lower and the salt rejection higher for the sea water cases. This was done in an effort to decrease concentration polarization and obtain a product water containing less than 500 ppm of sodium chloride.

D. Results and Conclusions

The results of the analysis are given in terms of average product-water flux, $\bar{J}$, the average ideal product-water flux, $\bar{J}_{id}$, product water concentration, C_p, and the ratio of average to ideal product-water flux. The significance of these variables is detailed below:

$\bar{J}_{id}$ The average product-water flux of a membrane with a fully-mixed brine stream, i.e., ignoring the effects of concentration polarization and feed brine pressure loss.

$\bar{J}$ The average product-water flux for membranes without full mixing and considering concentration polarization.

C_p The product-water concentration. It is important that this be kept as low as possible.

$\bar{J}/\bar{J}_{id}$ A measure of the effectiveness of the brine flow channel in minimizing polarization and brine pressure loss effects. This variable is a normalized flux relative to the best that can be achieved in a fully mixed stream. Therefore it gives a measure of the effect of concentration polarization and brine pressure loss.

Tables 21 and 22 give the values of $\bar{J}$, $\bar{J}_{id}$, C_p, and $\bar{J}/\bar{J}_{id}$ calculated in this study for brackish water and sea water, respectively. For convenience, the results are summarized in Figures 42-46. Figure 42 shows the effect of pressure on

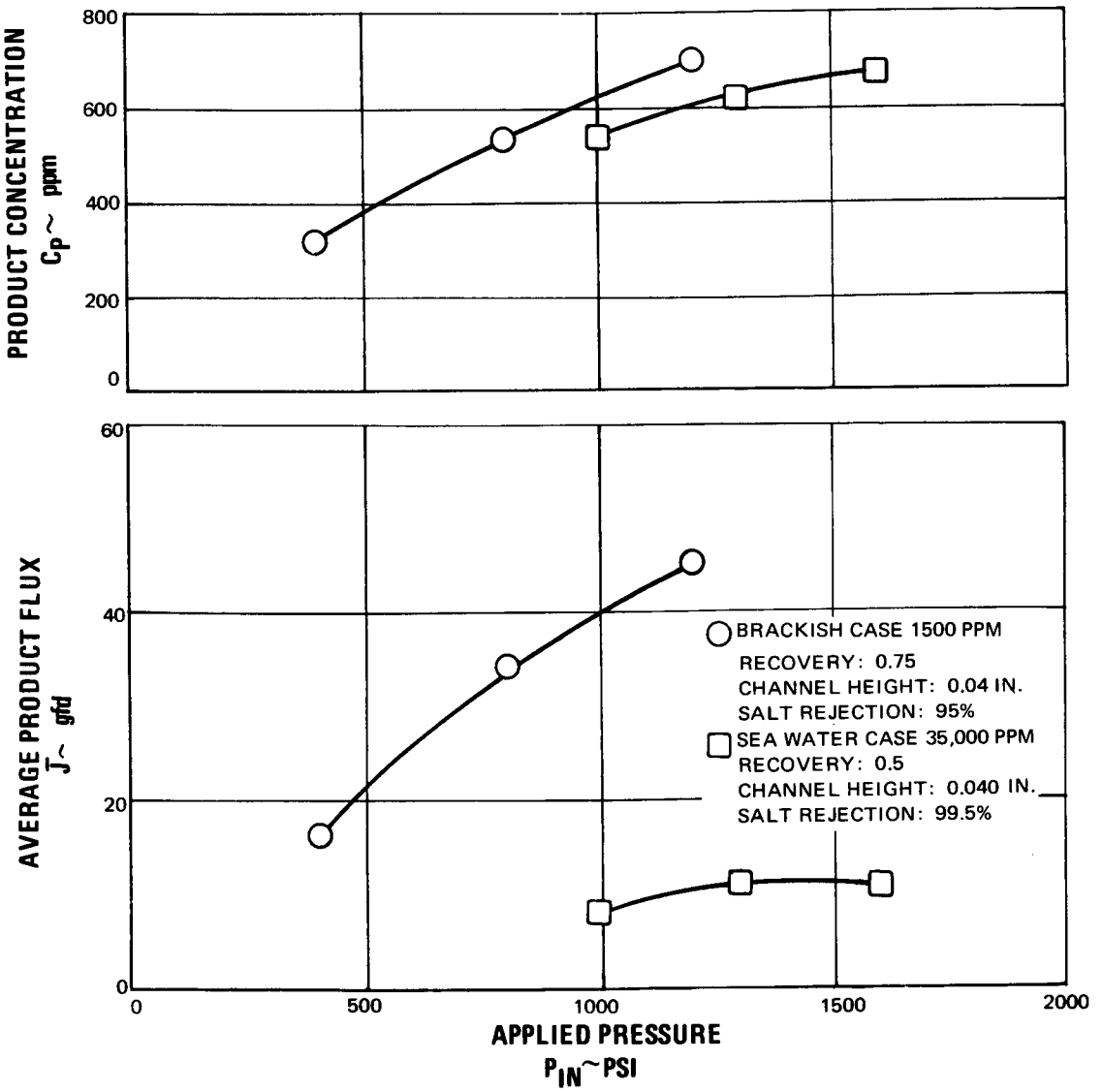

Figure 42 Comparison of Standard Brackish and Sea Water Cases

TABLE 21

Cartridge Performance Values as Functions of Channel Height, Salt Rejection and Recovery Factor
(Brackish Water - 1500 ppm NaCl)

	Channel Height, mils	Salt Rejection, %	50% Recovery Pressure Levels, psi 400	800	1200	75% Recovery Pressure Levels, psi 400	800	1200	90% Recovery Pressure Levels, psi 400	800	1200
Average Flux $\bar{J}$, gfd	20	90	23.1	47.8	61.7	22.4	46.3	60.6	21.9	45.4	59.1
		95	18.1	37.4	48.7	17.6	36.0	47.3	17.0	35.2	46.3
		99	12.2	25.0	32.4	11.9	24.4	31.6	11.5	23.8	31.2
	40	90	22.2	45.8	60.3	21.0	43.9	58.4	20.0	42.2	57.3
		95	17.5	36.0	47.0	16.5	34.2	44.8	14.6	32.0	43.3
		99	11.8	24.4	31.8	11.3	23.1	30.4	10.7	22.0	28.8
	60	90	21.4	44.1	58.3	20.0	42.2	56.5	18.5	41.2	56.6
		95	16.9	34.8	45.5	15.5	32.5	42.9	14.2	29.8	40.8
		99	11.5	23.8	30.9	10.7	22.1	29.1	9.9	20.2	26.9
Ideal Flux $\bar{J}_{id}$, gfd	20	90	23.9	49.4	64.1	23.4	48.9	63.7	22.7	48.1	63.0
		95	18.6	38.5	49.9	18.2	38.1	49.6	17.6	37.5	49.0
		99	12.3	25.5	33.1	12.1	25.3	32.9	11.6	24.8	32.5
	40	90	49.4	49.4	64.1	23.4	48.9	63.7	22.7	48.1	63.0
		95	38.5	38.5	49.9	18.2	38.1	49.6	17.6	37.1	49.0
		99	25.5	25.5	33.1	12.1	25.3	32.9	11.6	24.8	32.5
	60	90	49.4	49.4	64.1	23.4	48.9	63.7	22.7	48.1	63.0
		95	38.5	38.5	49.9	18.2	38.1	49.6	17.6	37.5	49.0
		99	25.5	25.5	33.1	12.1	25.3	32.9	11.6	24.8	32.5

TABLE 21 (Cont'd)

Cartridge Performance Values as Functions of Channel Height, Salt Rejection and Recovery Factor
Brackish Water - 1500 ppm

	Channel Height mils	Salt Rejection %	50% Recovery Pressure Levels 400	800	1200	75% Recovery Pressure Levels 400	800	1200	90% Recovery Pressure Levels 400	800	1200
Product Conc. Cp, ppm	20	90	344	472	676	449	700	883	530	848	1159
		95	155	218	251	203	356	405	255	422	521
		99	26	36	44	34	53	70	44	68	84
	40	90	494	794	950	673	1104	1313	821	1362	
		95	216	355	448	307	527	694	385	698	851
		99	36	55	67	50	88	111	63	116	156
	60	90	617	1073	1339	830	1391		1015		
		95	276	479	632	397	690	917	492	876	1119
		99	45	72	94	65	117	152	83	156	204
RATIO $\bar{J}/\bar{J}_{id}$	20	90	0.907	0.965	0.962	0.957	0.948	0.951	0.965	0.944	0.938
		95	0.970	0.973	0.975	0.966	0.943	0.955	0.966	0.940	0.944
		99	0.979	0.986	0.979	0.985	0.966	0.963	0.985	0.960	0.960
	40	90	0.927	0.925	0.940	0.895	0.898	0.917	0.879	0.876	0.910
		95	0.934	0.938	0.941	0.906	0.897	0.904	0.884	0.855	0.882
		99	0.953	0.956	0.959	0.938	0.916	0.925	0.922	0.885	0.886
	60	90	0.893	0.893	0.909	0.851	0.862	0.888	0.817	0.856	0.898
		95	0.902	0.905	0.910	0.851	0.852	0.866	0.809	0.795	0.831
		99	0.930	0.931	0.935	0.890	0.874	0.886	0.853	0.812	0.827

TABLE 22

Cartridge Performance Values as Functions of Channel Height, Salt Rejection and Recovery Factor
(Sea Water - 35,000 ppm NaCl)

	Channel Height mils	Salt Rejection %	30% Recovery Pressure Levels, psi 1000	1300	1600	50% Recovery Pressure Levels, psi 1000	1300	1600	70 % Recovery Pressure Levels, psi 1000	1300	1600
Average Flux $\bar{J}$, gfd	20	99	14.1	18.4	16.1	12.1	15.9	14.7	5.0	12.4	12.5
		99.3	13.7	17.8	15.6	11.6	15.5	14.3	5.0	11.8	12.3
		99.5	13.3	16.8	15.0	11.4	14.8	13.6	4.6	11.7	11.7
	40	99	10.7	14.5	13.7	8.4	11.2	11.4	3.5	8.3	9.3
		99.3	10.5	13.9	13.1	8.3	11.0	11.1	3.3	8.0	9.0
		99.5	10.1	13.6	12.8	8.1	10.7	10.8	3.1	7.9	8.8
	60	99	8.7	12.7	12.0	6.4	10.3	9.3	2.6	5.9	7.2
		99.3	8.5	12.4	11.6	6.3	9.2	9.1	2.4	5.8	7.1
		99.5	8.3	11.5	11.2	6.2	8.3	8.8	2.3	5.7	7.0
Ideal Flux $\bar{J}_{id}$, gfd	20	99	18.3	23.1	18.6	16.2	21.3	17.6	12.6	18.3	15.8
		99.3	17.6	22.0	17.8	15.5	20.3	16.8	12.1	17.4	15.0
		99.5	16.8	21.1	17.0	14.8	19.4	16.0	11.5	16.7	14.3
	40	99	18.3	23.1	18.6	16.2	21.3	17.5	12.6	18.3	15.8
		99.3	17.6	22.0	17.8	15.5	20.3	16.8	12.1	17.4	15.0
		99.5	16.8	21.1	17.0	14.8	19.4	16.0	17.5	16.7	4.3
	60	99	18.3	23.1	18.7	16.2	21.3	17.6	12.6	16.3	16.3
		99.3	17.6	22.0	17.8	15.6	20.2	16.8	11.2	15.6	15.5
		99.5	16.8	21.1	17.0	14.8	19.4	16.0	10.6	14.9	14.8

TABLE 22 (Cont.)

Cartridge Performance Values as Functions of Channel Height, Salt Rejection and Recovery Factor
(Sea Water - 35,000 ppm NaCl)

	Channel Height mils	Salt Rejection %	30% Recovery Pressure Levels, psi 1000	1300	1600	50% Recovery Pressure Levels, psi 1000	1300	1600	70% Recovery Pressure Levels, psi 1000	1300	1600
Average Flux $\bar{J}$, gfd	20	99	558	600	595	614	692	671	676	782	776
		99.3	413	442	430	459	508	491	505	581	586
		99.5	271	300	280	301	339	326	332	382	375
	40	99	649	731	729	720	838	857	754	919	962
		99.3	482	546	544	536	620	635	561	684	714
		99.5	320	359	354	354	411	417	370	452	469
	60	99	687	798	819	757	841	944	782	954	1061
		99.3	512	594	607	565	645	701	579	713	789
		99.5	340	391	400	375	435	464	382	472	521
Ideal Flux $\bar{J}_{id}$, gfd	20	99	0.767	0.798	0.865	0.748	0.747	0.831	0.397	0.677	0.793
		99.3	0.779	0.811	0.874	0.745	0.766	0.852	0.413	0.678	0.816
		99.5	0.793	0.798	0.885	0.765	0.762	0.852	0.404	0.700	0.818
	40	99	0.582	0.629	0.735	0.521	0.524	0.651	0.275	0.454	0.592
		99.3	0.596	0.632	0.738	0.531	0.542	0.662	0.274	0.462	0.600
		99.5	0.602	0.645	0.753	0.544	0.552	0.674	0.270	0.473	0.616
	60	99	0.507	0.550	0.645	0.393	0.483	0.529	0.209	0.363	0.444
		99.3	0.515	0.566	0.653	0.404	0.452	0.542	0.217	0.371	0.458
		99.5	0.524	0.544	0.663	0.417	0.429	0.552	0.215	0.383	0.470

performance. Note that higher pressure levels are necessary for sea-water operation, with the attendant increase in energy requirements. Also it is seen that flux levels are lower for sea water than for brackish water. This is caused by a combination of concentration polarization and decreased membrane constant at the higher salt rejection and higher pressures required for sea-water desalination. It is for this reason that there does not appear to be any advantage in going to pressures higher than 1200-1400 psi, even for sea water. It also shows the difficulty in desalting sea water in a single-stage system as the product-water salt concentration is greater than the 500 ppm maximum established by OSW.

Figure 43 shows performance as a function of channel height for brackish and

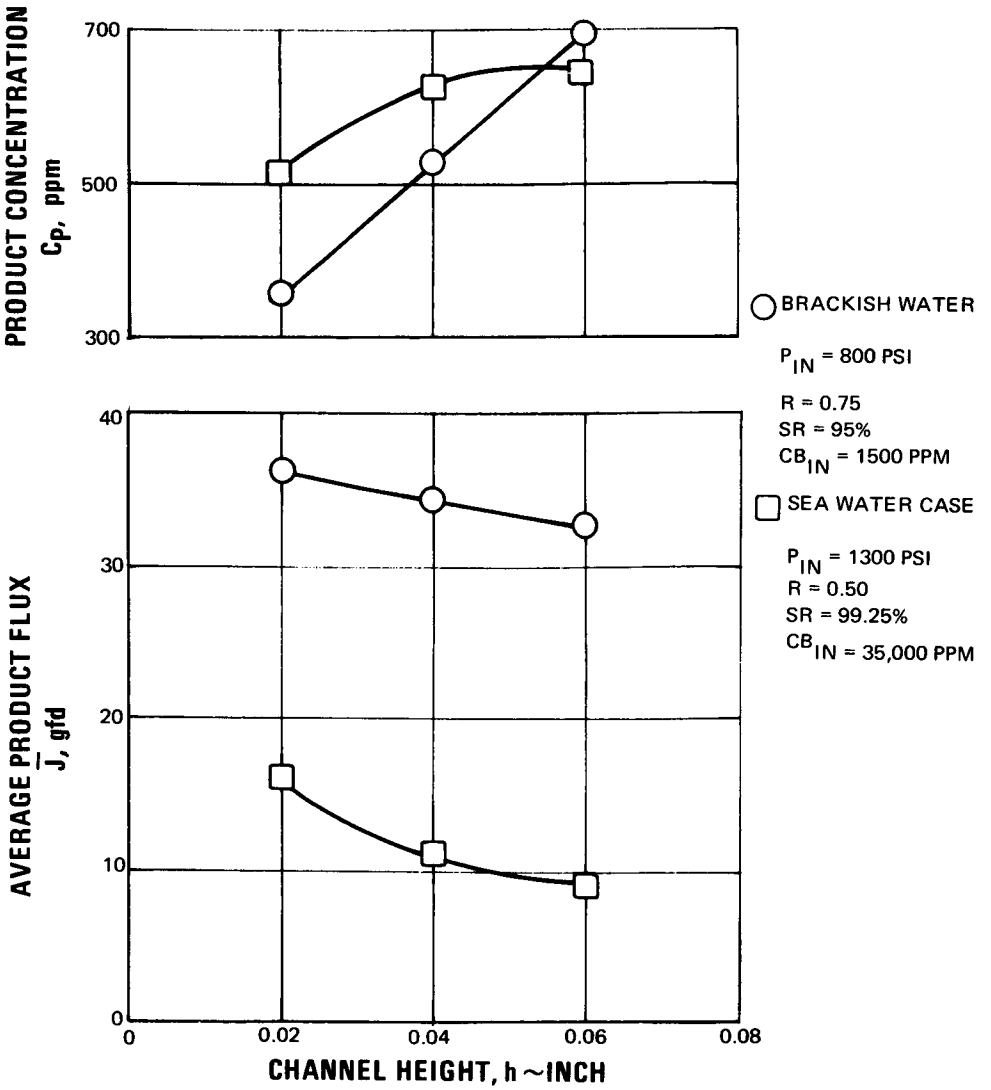

Figure 43 Performance as Function of Channel Height for Brackish and Sea Water

sea-water cases. It shows that an increase in channel height in both cases decreases the product-water flux and increases the product-water concentration. This can be understood by referring to Figure 44 which shows the ratio of membrane performance and gives a direct measure of the amount of concentration polarization present and the membrane efficiency. Polarization causes an approximate 15 percent decrease in membrane usage at 0.06 inch for brackish water and about 55 percent decrease for sea water. Therefore, the channel height should be minimized to decrease polarization. This is also desirable to increase the packing density of the cartridge. The calculation showed that the hydraulic pressure drop even at 0.02 inch is less than 5 psi and is therefore essentially negligible.

Figures 45 and 46 show the effect of recovery on performance. Figure 45 shows that an increase of the recovery causes a decrease in product-water flux and an increase in product-water concentration. This is caused by a combination of higher bulk brine concentration and increased concentration polarization at higher recoveries. The degree of concentration polarization can be seen in Figure 46. At even quite high recoveries, concentration polarization does not decrease the flux rate for brackish water more than 15 percent, while for sea water even at a low recovery rate, concentration polarization decreases the flux by 40 to 50 percent. These results indicate that the compact cartridge is suitable for desalting brackish water but that sea water is a much more difficult problem.

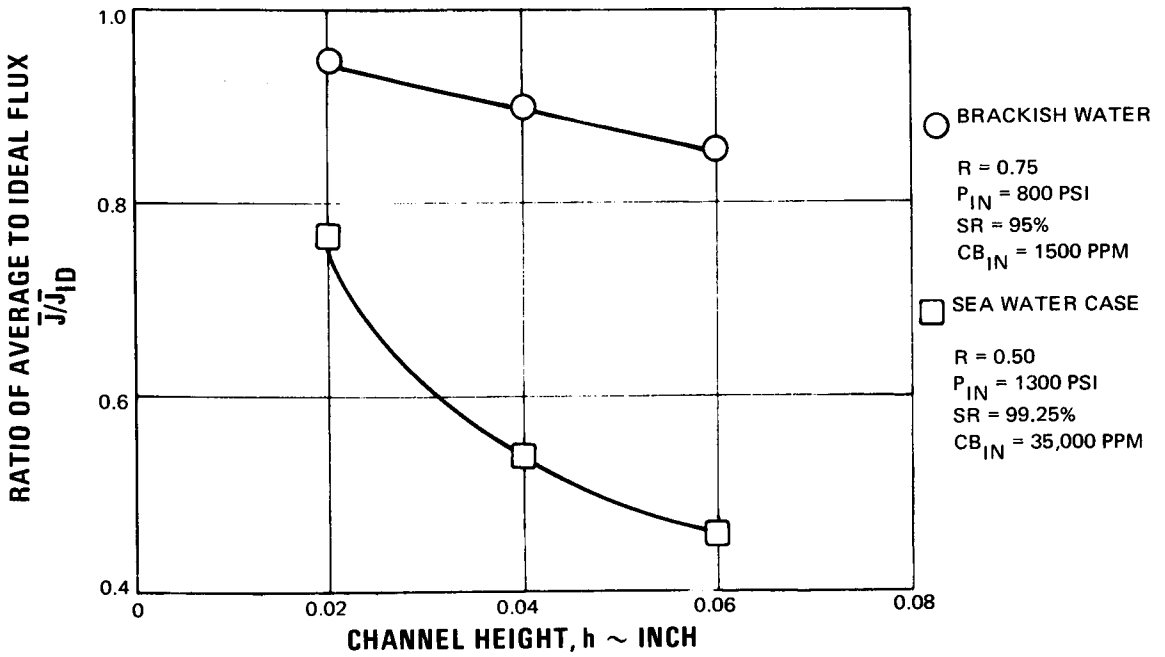

Figure 44 Ratio of Membrane Performances as Function of Channel Height

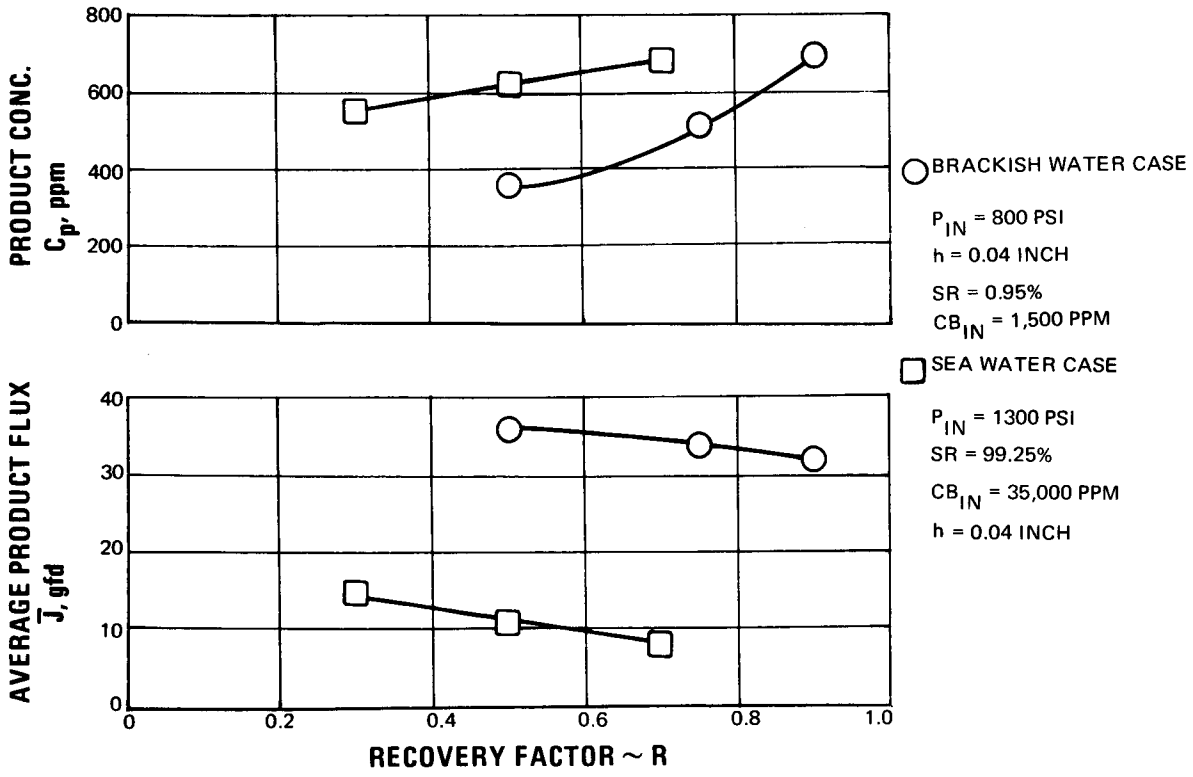

Figure 45 Performance as Function of Recovery for Brackish and Sea Water

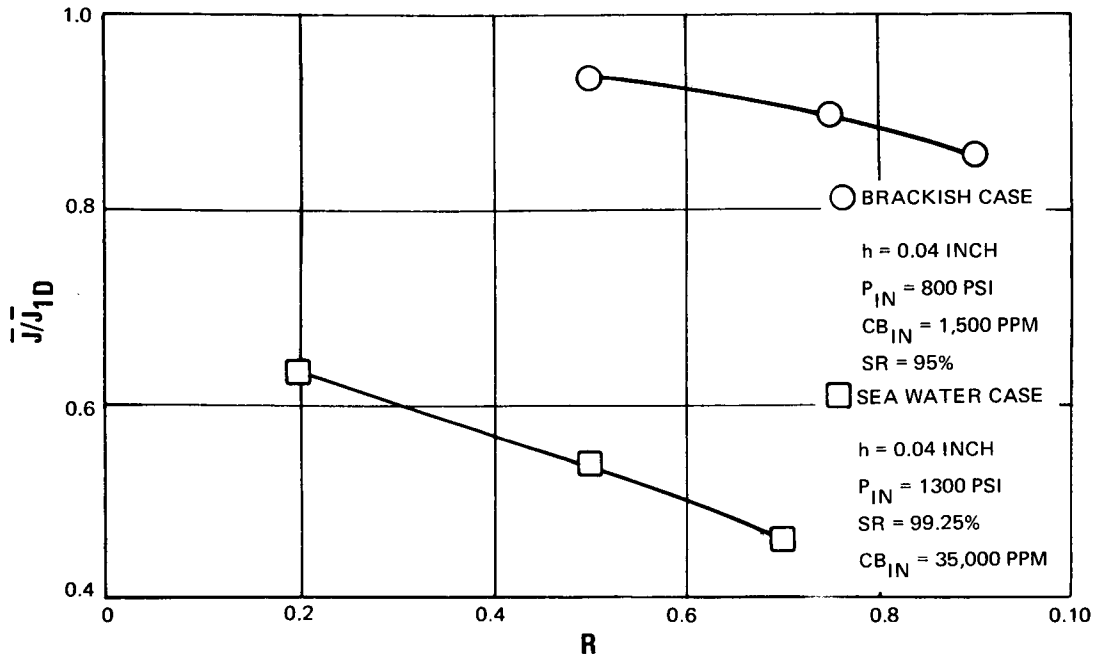

Figure 46 Ratio of Average to Ideal Flux as Function of Recovery

The results of this part of the analysis can be summarized as follows: 1) pressure levels greater than 1000-1200 psi do not appear to offer any advantages, 2) the channel spacing should be minimized consistent with good design, and 3) the compact cartridge is suitable for use with brackish water and only a small amount of concentration polarization occurs.

E. Analysis of Staging

The staging arrangement considered in this analysis is illustrated in Figure 47. It will be noted that the outlet brine of each stage is recirculated to the input of the preceding stage. The outlet brine of the first stage is discharged through a recovery turbine. In addition, this analysis was based on the following assumptions:

1) The method outlined in the preceding section could be applied to each stage
2) Salt rejection - membrane constant characteristics as shown in Figure 48
3) Packing density (membrane surface area/volume) = 250 ft^{-1}
4) Product-water concentration - 500 ppm
5) Product-water quantity - 1,000,000 gpd
6) Pump efficiency - 75 percent
7) Recovery turbine efficiency = 60 percent

The method of analysis was to determine the inlet concentration and flow rate of each stage with the equation:

$$F_{in} = F_p + F_o$$

$$C_{in} = \frac{F_p C_p + F_o C_o}{F_{in}}$$

Where F = flow rate, gpm

C = concentration, ppm

and the subscripts indicate:

in = inlet conditions of stage

p = product of previous stage or feed

o = outlet of following stage

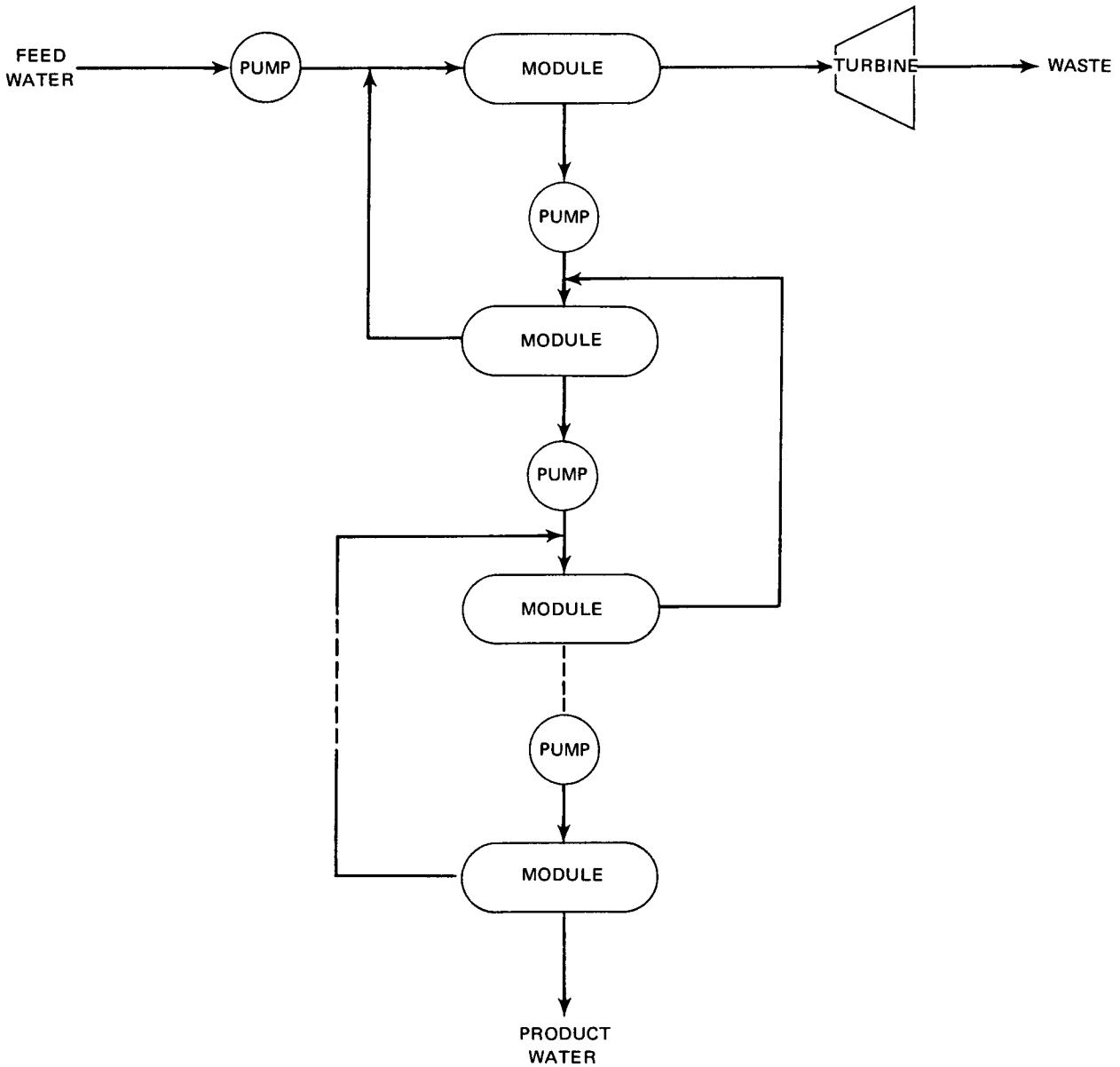

Figure 47 Staging Arrangement

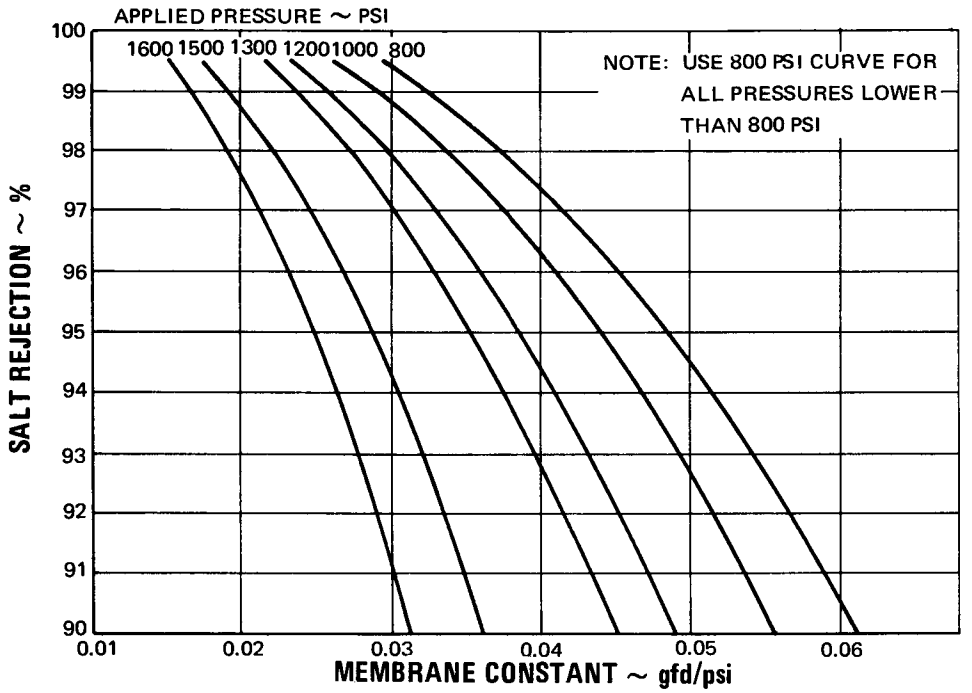

Figure 48 Membrane Performance Map

The outlet and product concentrations and recovery factor were calculated using the method of the preceding section. An iterative procedure was used, and for convenience, was programmed on a high-speed digital computer. The computer program calculated the energy requirements and surface area needed for a one million gallon per day plant.

The results from this analysis are given in Table 23. This table is divided into three parts. The upper portion is for membranes with 99 percent salt rejection. These membranes will require only a single-stage system. The middle portion of the table gives the results for membranes with 95 percent salt rejection. For low recoveries a single stage can be used but higher recoveries will require a multistage system. The lower portion of the table gives the results for membranes with 90 percent rejection. For the most part these membranes will require multistage systems.

Particular attention is given to the column labelled "Energy Requirement for Product with 500 ppm" and the column labelled "Surface Area Required". In each case it can be seen that the energy requirements decrease with increasing recovery but increase with the number of stages required. Also, it can be seen that the surface area required for a one million gallon per day plant decreases as the salt rejection and recovery levels are decreased. In order to

TABLE 23

Cartridge Staging Summary

Total Stages	Recovery	Salt Rejection, %	Inlet Pressure, psig	Feed Water, gpm	Inlet Concentration, gpm	Product Water, gpm	Product Concentration, gpm	Average Product-Water Flux gfd	Average Product-Water Flux per Stages, gfd	Energy Required, kw-hr/kgal	Energy Required for 500 ppm Product, kw-hr/kgal	Surface area Required for MGPD sq ft	Volume, cu ft
1	0.207	99	800	3357	1500	695	35	24.3		24.03	16.40	41,190	164.8
1	0.508	99	800	1368	1500	695	60	23.4		11.86	8.24	42,660	170.6
1	0.669	99	800	1039	1500	695	80	22.8		9.84	6.93	43,950	175.8
1	0.948	99	800	733	1500	695	137	20.1		7.97	5.85	49,750	199.0
1	0.196	95	800	3546	1500	695	218	36.2		12.19	19.65	27,590	110.4
1	0.509	95	800	1365	1500	695	384	34.6		11.84	10.61	28,890	115.6
1	0.673	95	800	1033	1500	695	501	33.4		9.80	9.80	29,900	119.6
2	0.890	95	800	781	1500	695	448	14.9	31.4	16.85	16.02	67,550	270.2
1	0.201	90	800	3458	1500	695	502	45.7		24.50	24.50	21,900	87.6
2	0.210	90	800	3301	1500	695	340	13.1	45.7	43.02	37.09	77,190	308.8
2	0.333	90	800	2085	1500	695	470	15.0	44.9	31.71	30.79	67,140	268.6
4	0.516	90	800	1347	1500	695	490	7.3	44.1	51.40	50.89	139,860	559.4

optimize a system it would be desirable to have the lowest energy requirements and the smallest membrane surface area possible. This can be achieved by selecting a membrane with the lowest acceptable salt rejection and with the highest possible recovery, provided that neither causes an increase in the number of stages required. Of the cases given, the one that is most nearly optimum is a membrane of 95 percent salt rejection operating in a single stage at 820 psi with a 66 percent recovery. This condition gives an energy requirement of 9.8 kw hr/kgal and requires 29,900 sq ft of membrane area.

In view of good plant design the following trade-off must also be considered: an increase in the operating pressure will result in a reduction in the membrane surface area required to produce a given amount of water. There will be a corresponding reduction in the cartridge volume. However, the cost savings in having a smaller cartridge will be eventually offset by the higher cost of the pumping equipment, added power requirements and an increase in the pressure vessel size, due to the higher operating pressures. The need for a complete system analysis is apparent before optimized desalting systems can be placed in operation.

VII. DESIGN CONFIGURATION STUDIES

A design study of possible configurations for a compact reverse-osmosis desalting cartridge was conducted. Three basic concepts were chosen for consideration, plate-and-frame, tubular, and spiral. The designs were compared with respect to packaging density, water production per volume, concentration polarization and energy requirements. The tubular and the circular plate-and-frame configurations were selected for a more comprehensive study. Preliminary design layouts of these configurations have been prepared. These designs were then compared with respect to water production, hydraulic pressure drop, concentration polarization and packaging density. The results of the study showed that a circular plate-and-frame design, with turbulators to reduce concentration polarization, offers the best promise for a compact desalting cartridge with high packaging density, low energy consumption, and ease of fabrication.

A. Preliminary Design Concepts

Six designs were chosen as being representative of possible concepts for a compact disposable reverse-osmosis cartridge. The designs selected for consideration included two plate-and-frame configurations, two tubular, and two spiral. Emphasis was placed on configurations that would readily lend themselves to reinforced membranes. The six designs selected for evaluation are illustrated in Figures 49 through 54. A brief description of each design follows.

Figure 49 and 50 illustrate the two plate-and-frame concepts considered. The rectangular plate-and-frame concept is shown in Figure 49. This design consists of a number of composite membranes assembled into a compact reverse-osmosis matrix and fitted with manifolds to collect the product water. It is similar to the compact-cartridge demonstration unit evaluated during this contract. It has the advantage of being easily adapted to various laboratory configurations as well as having flow dynamics that can be calculated. Any number of these cartridges can be stacked in a pressure vessel so that the feedwater flows axially through the passages created by the composite membranes which are parallel to the axis of the pressure vessel. The product water flows through the composite membrane support material to a porous support tube and is removed through a water collection manifold. The circular plate-and-frame concept is illustrated in Figure 50. In this design the feedwater flows radially inward to a central tube where it is redirected through another assembly or discarded as waste. The product water is collected in a manner similar to the rectangular plate-and-frame concept. This design has the disadvantage of not lending itself easily to theoretical analysis but makes more effective use of the available pressure vessel volume. Both design concepts would incorporate mechanical mixing devices in the feedwater stream to reduce the effects of concentration polarization. These

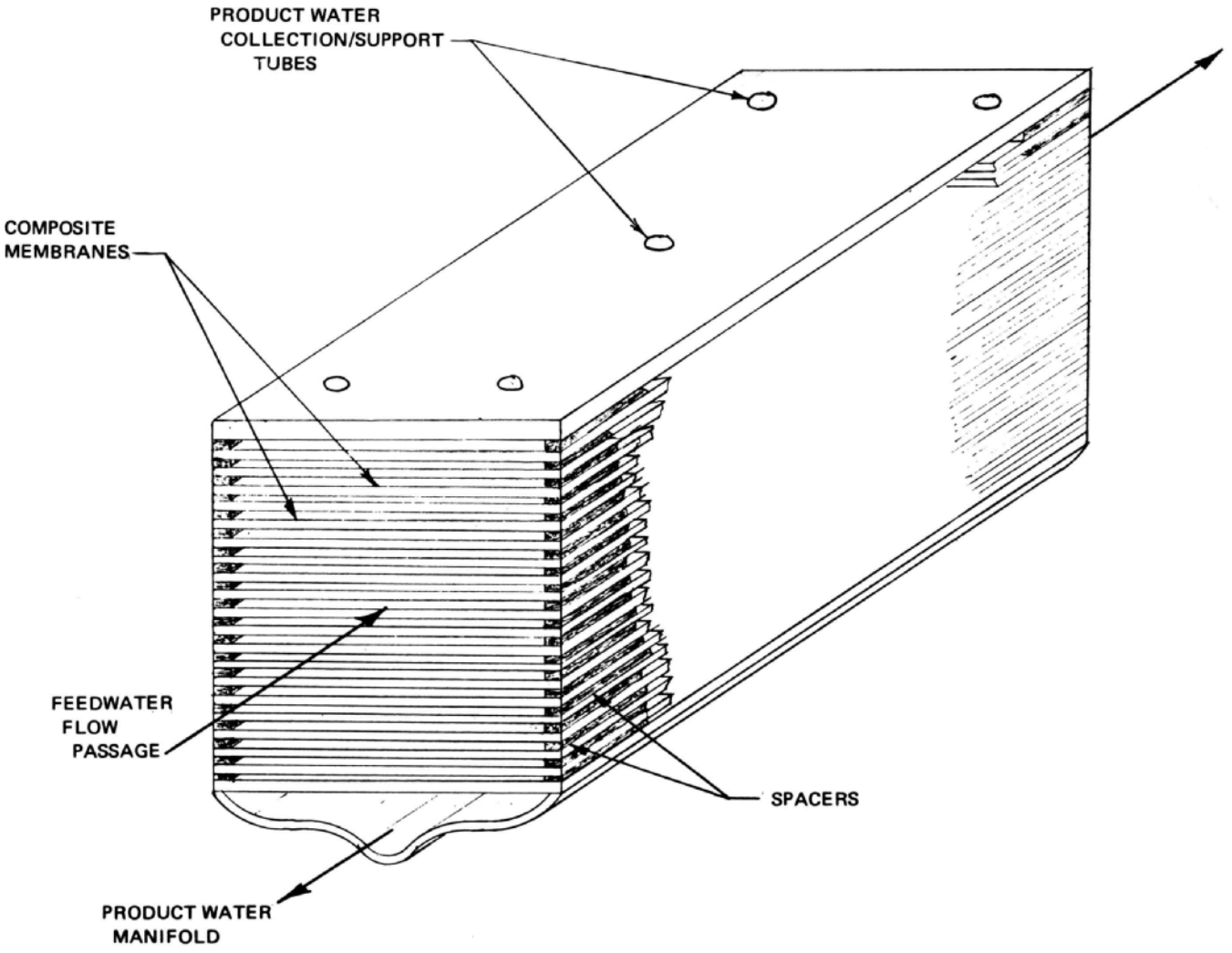

Figure 49 Rectangular Plate-and-Frame Concept

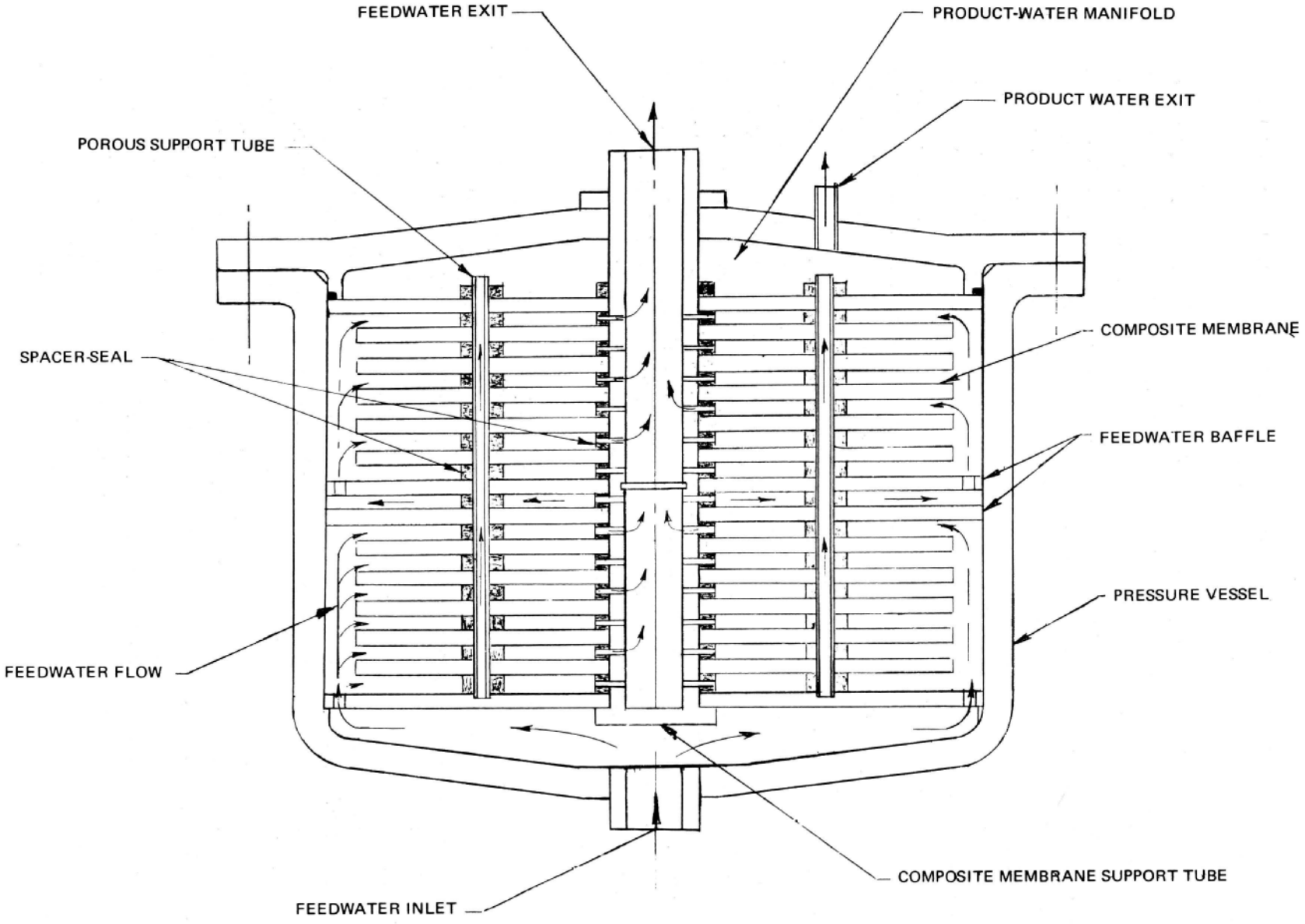

Figure 50 Circular Plate-and-Frame Concept

devices would be integrated with the composite membrane spacers and would help to maintain the feedwater flow geometry.

The two tubular concepts are illustrated in Figures 51 and 52. Figure 51 illustrates a tubular design with the reinforced membranes supported on the internal surface of the support tube. This design has the advantage of not needing an additional pressure vessel as the support tube performs this task. The tube could be formed from a completely porous structure having the desired structural requirement or from a tube containing internal grooves (rifling) for the removal of the product water. This design permits using turbulent feedwater flow without a severe increase in the energy requirements for pumping. Operating with a turbulent feedwater will reduce or minimize the effects of concentration polarization. The design also lends itself to easy replacement of a tubular element that has deteriorated beyond its usefulness. The main disadvantage of this design is the low packaging density, which requires a larger volume as compared with the compact plate-and-frame concept. Figure 52 illustrates a tubular concept with the reinforced membranes external to the support tube. A pressure vessel is needed to contain the feedwater. The product water passes through the membrane and down the length of the support tube where it is removed through a product-water collection manifold. A potting material supports the tubular element and forms a seal between the product water and feedwater. The packaging density of this concept is extremely low and does not easily lend itself to reinforced membranes. Also, it does not have the advantage of turbulent feedwater flow as in the previous mentioned tubular design. It does however lend itself to a hollow fiber design.

The spiral design concepts are illustrated in Figures 53 and 54. Figure 53 shows an involute design where the feed solution flows between the coiled composite membranes. In this illustration the product water is removed through a central tube. Figure 54 shows a spiral design where the feedwater enters on the outside of the spiral, flows radially inward, and is withdrawn from the central tube. The product water is withdrawn from the composite membrane assembly edges. The spiral designs have the highest packaging density of the configurations investigated. Also, the reinforced membranes lend themselves to a design of this type as they have demonstrated sufficient flexural strength to withstand the coiling requirements associated with this concept. A few disadvantages of the spiral concept are that it would be necessary to develop, 1) a flexible seal in the area of the feedwater inlet and outlet and the product-water exit, 2) a flexible membrane-support material of high water permeability, and 3) a feedwater mixer (turbulator) to minimize the effects of concentration polarization. Selection of this material is very critical as membrane contact against this material during operation may cause membrane failure, hence premature failure of a desalting cartridge. Other uses for the feedwater mixers are to maintain a uniform feedwater flow channel and to maintain uniform feedwater flow throughout the cartridge. The three basic design

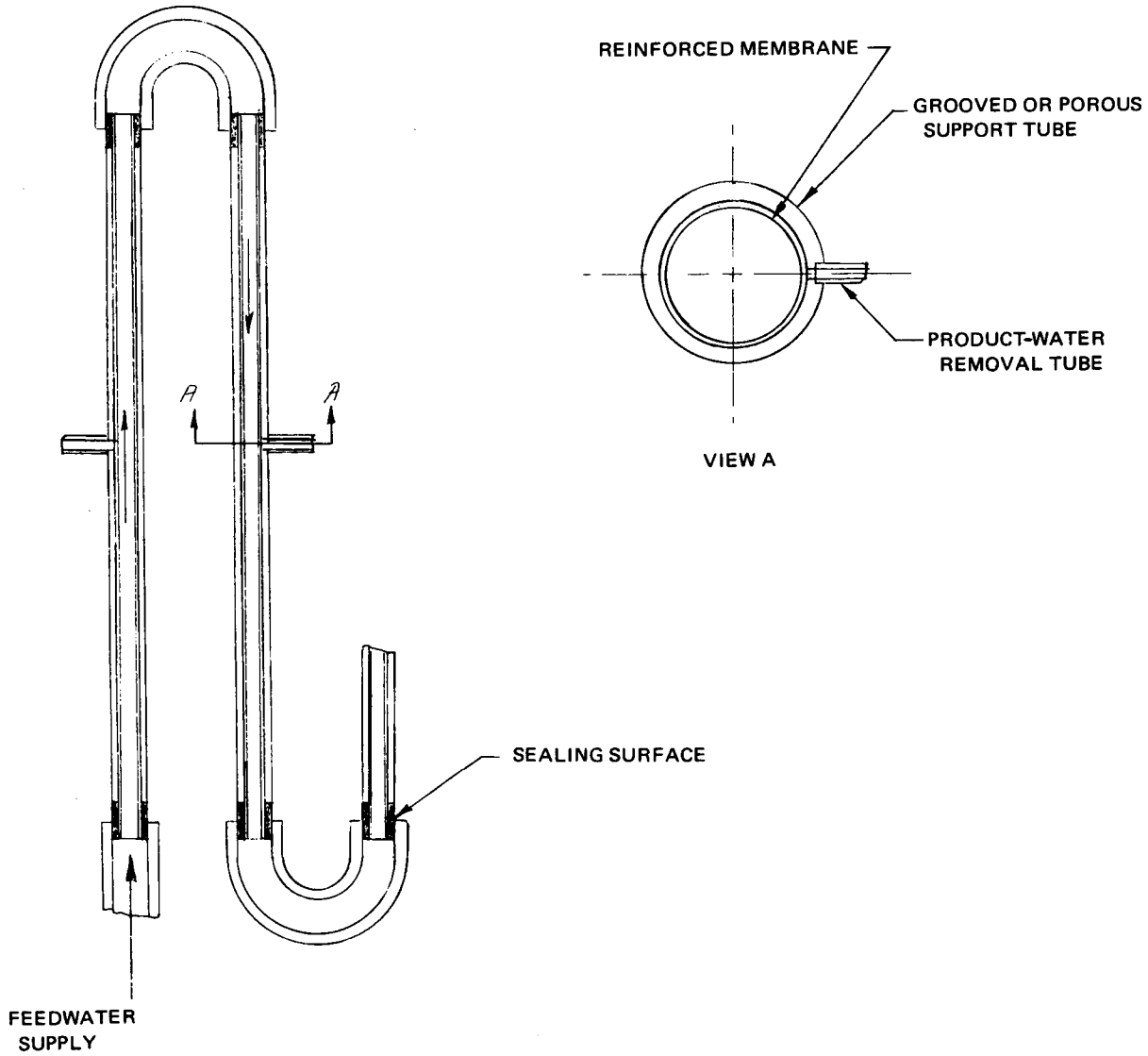

Figure 51 Tubular Concept

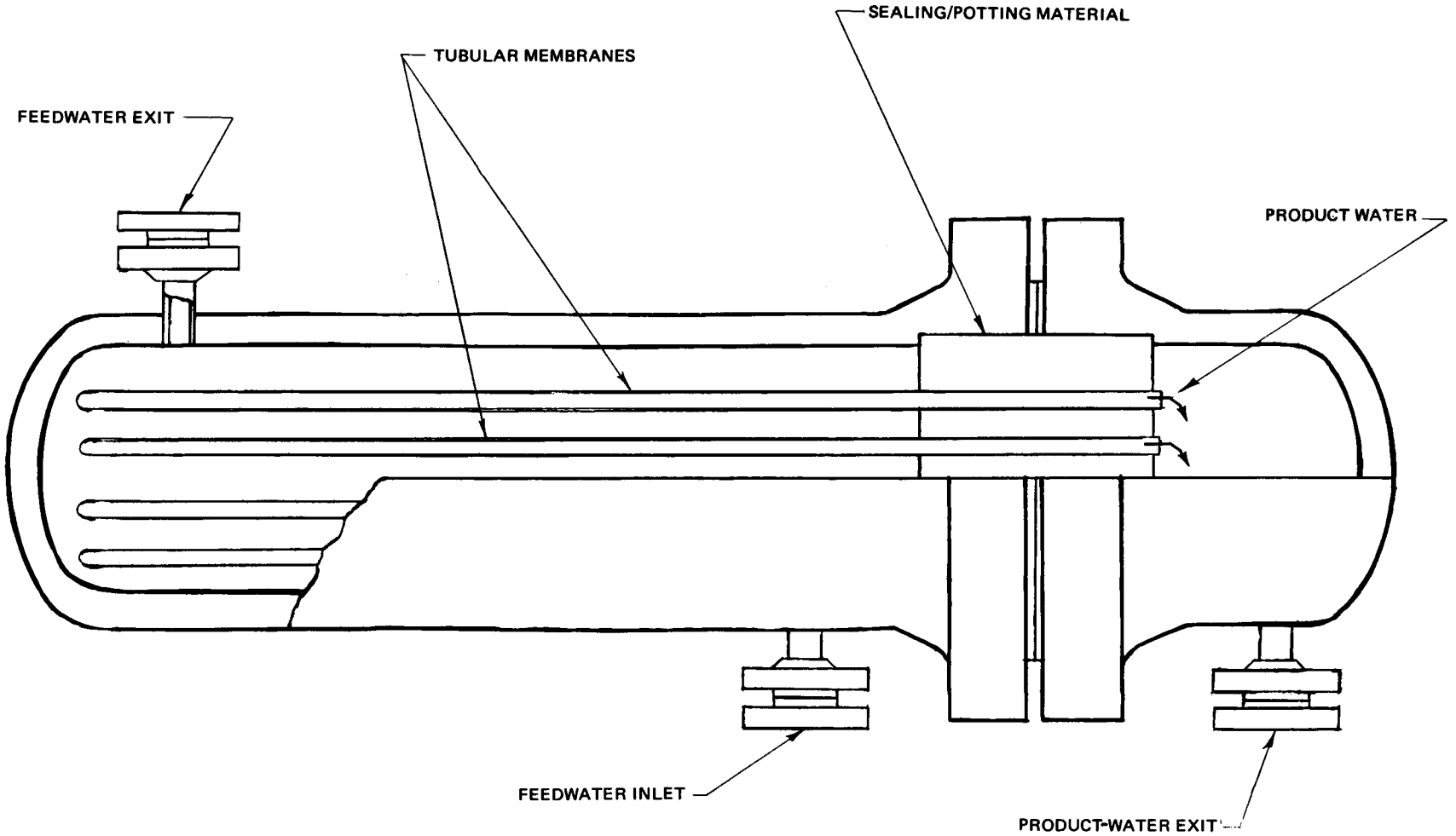

Figure 52 Tubular Concept

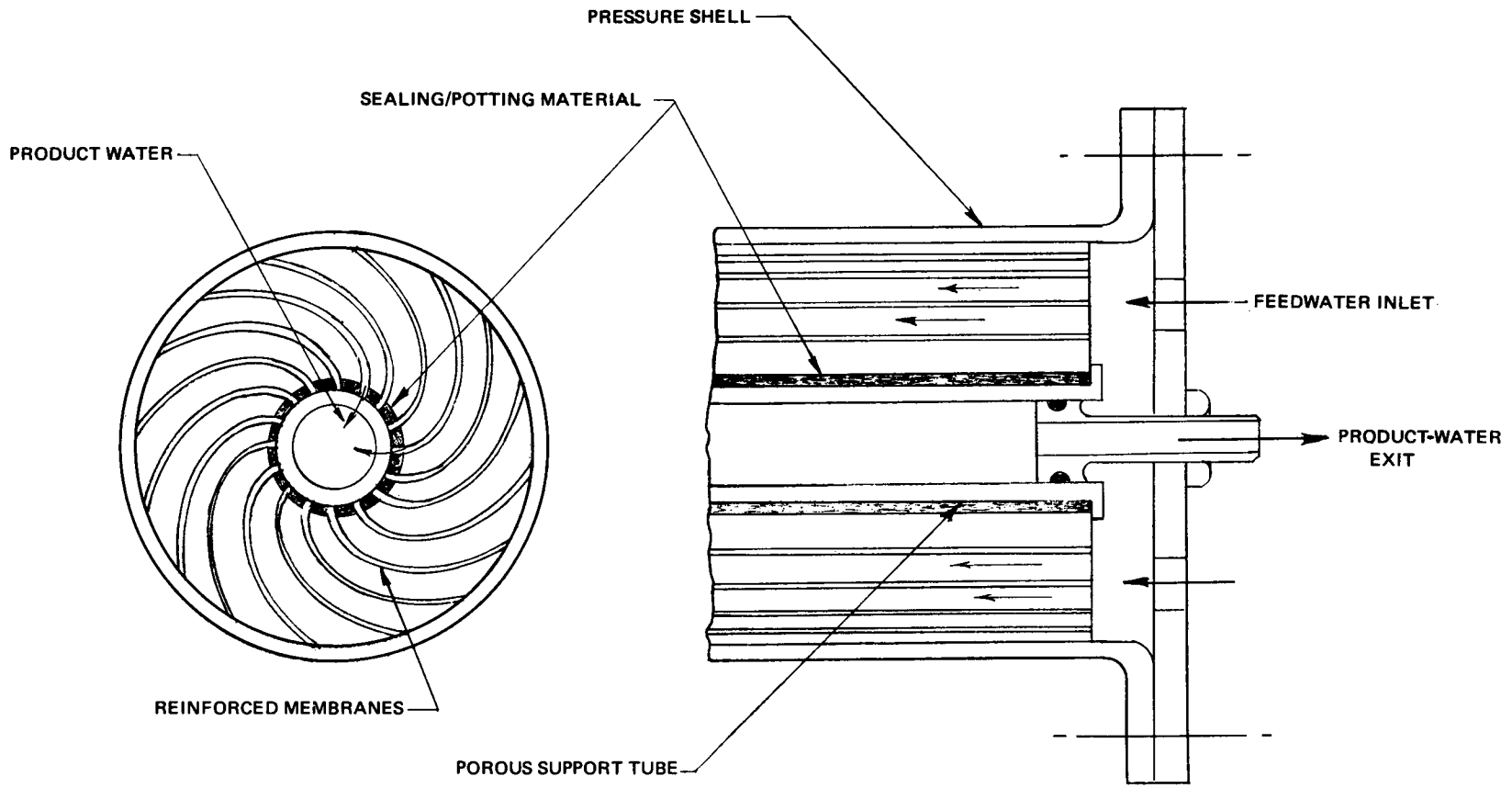

Figure 53 Involute Concept

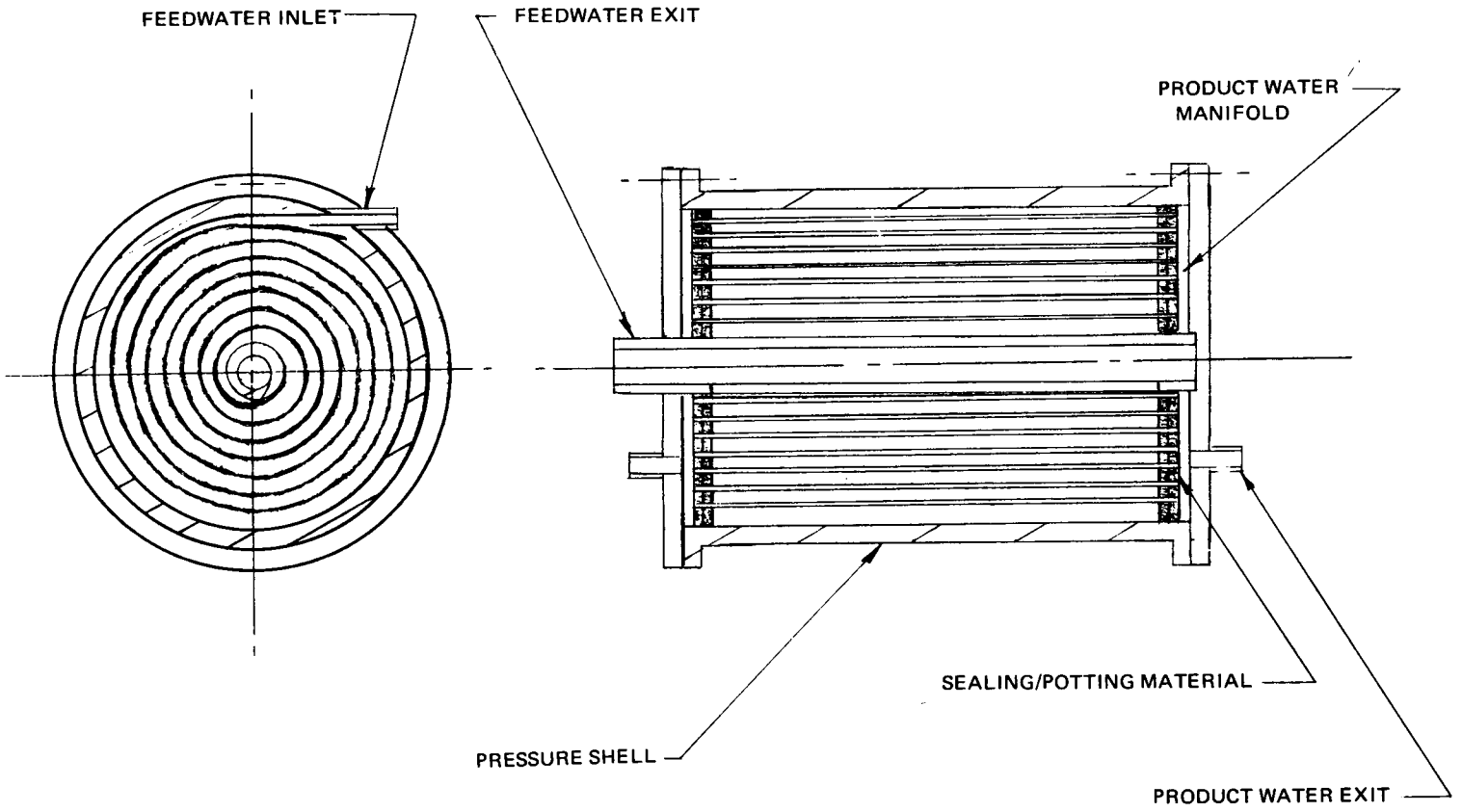

Figure 54 Spiral Concept

configurations were compared and evaluated with respect to packaging density, concentration polarization, energy requirements and water production per volume.

The average packaging density of each desalination cartridge and module was calculated. A cartridge is defined as a composite membrane arrangement properly secured and sealed in a set configuration. A module consists of at least one cartridge installed within a pressure vessel fitted with the necessary hardware. The pressure vessel is normally a permanent item in a desalination system while the cartridge is removable and expendable.

The packaging densities for the cartridge designs and their respective modules were calculated. A cartridge volume of 9.5 cubic feet was selected for study with a composite membrane center-to-center spacing of 0.080 inch. The spiral and the plate-and-frame designs have the highest cartridge packaging densities with 300 and 295 ft^2/ft^3 respectively. The tubular designs have the lowest cartridge packaging densities with 270 ft^2/ft^3 assuming a tube diameter of 0.080 inch. This value is rather unrealistic since a center-to-center spacing of 0.080 inch requires small tubes obtainable only with hollow fibers. Hollow fibers were not considered in this study as they do not lend themselves to reinforced membranes. A tube diameter of 0.250 inch is more realistic than the 0.080 inch tubes. A cartridge of 0.250-inch tubes gives a packaging density of 88 ft^2/ft^3, only one-third that of the other designs. The packaging densities were then calculated on the basis of a module of 13 cubic feet volume that contained cartridges requiring 9.5 cubic feet of volume. The following packaging densities were obtained:

	Packaging Density, ft^2/ft^3
spiral design	220
circular plate-and-frame design	215
rectangular plate-and-frame design	140
tubular design	88

The module packaging density takes into consideration a certain percentage of unusable pressure vessel volume, including provisions for internal cartridge supports and feedwater inlet and exit and product-water removal plumbing. Packaging density as a function of composite membrane spacing for the spiral, plate-and-frame and tubular design concepts is presented in Figures 55 and 56. The spacing for the plate-and-frame and spiral designs is the center-to-center distance between the composite membranes; for the tubular designs the spacing is the center-to-center distance between adjacent tubes. The spiral design concept has the highest packaging density as it makes more effective use of the available pressure vessel volume. Figure 57 presents the relative merits of the design concepts evaluated and shows water production as a function of module volume. The circular plate-and-frame and spiral designs give considerably more product water for a given module volume. This study disregarded the possible effects due to concentration polarization.

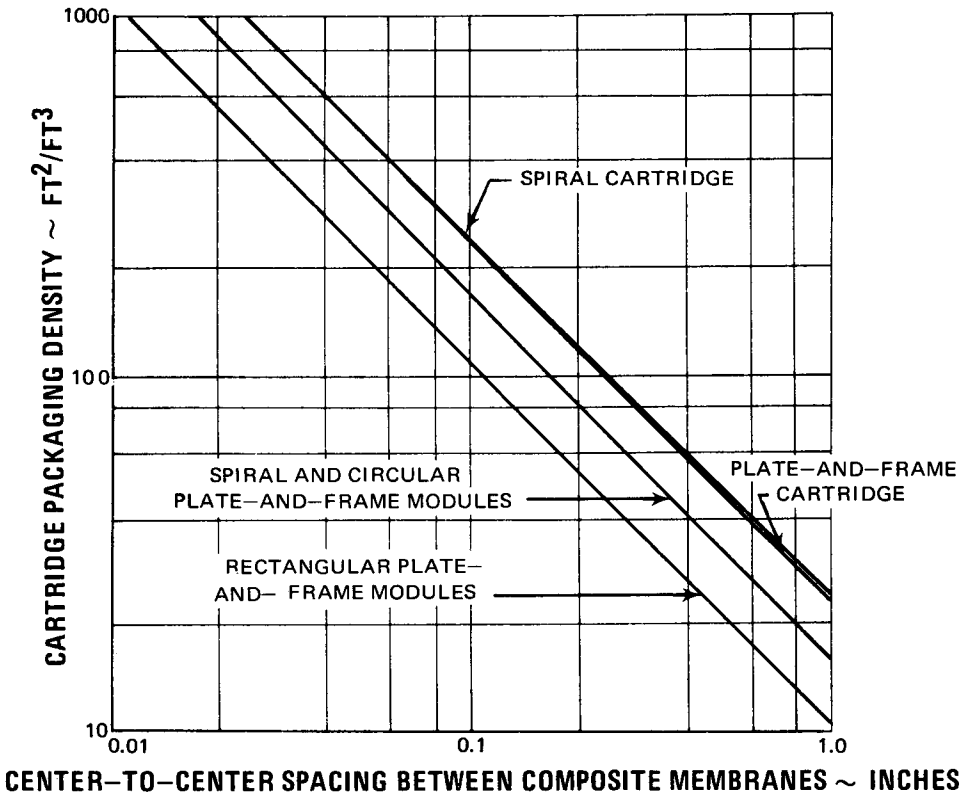

Figure 55 Packaging Density as Function of Composite Membrane Spacing for Spiral and Plate-and-Frame Configurations

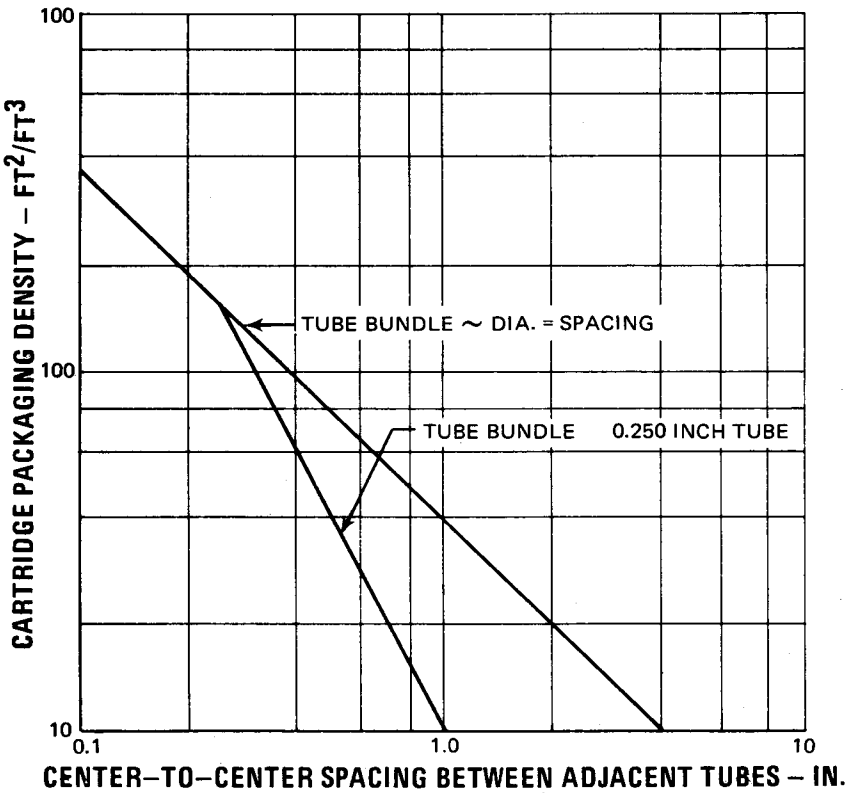

Figure 56 Packaging Density as Function of Tube Spacing for Tubular Configurations

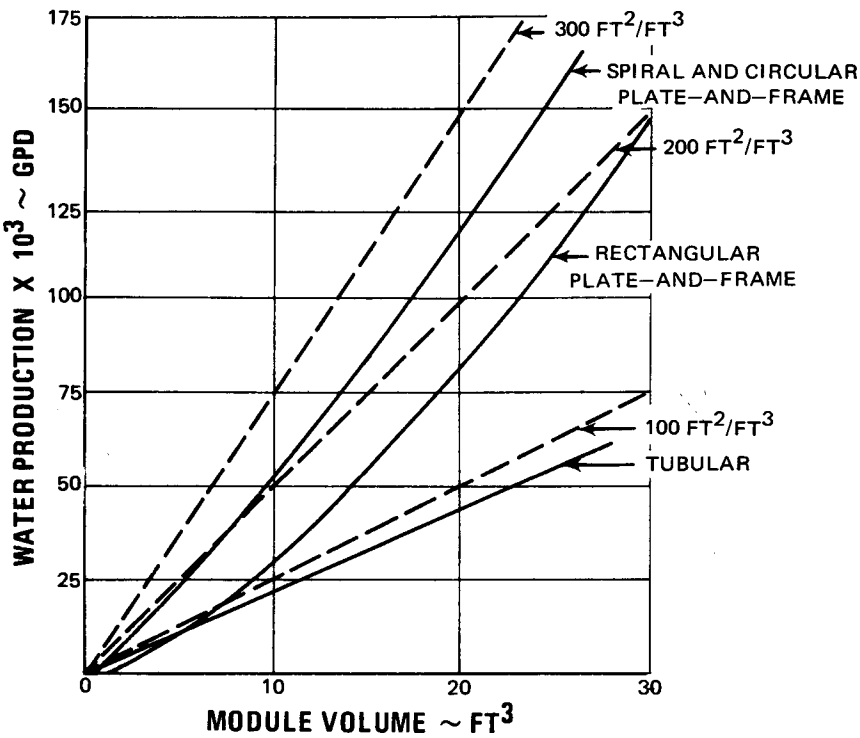

Figure 57 Water Production vs Volume for Modules of Various Configurations

Another method of comparing different design concepts is to estimate the amount of concentration polarization present and the possibility of reducing it to an acceptable level. The amount of concentration polarization determines to a large degree the amount of energy required to desalt a given amount of solution, so that the concentration polarization should be reduced to as low a level as possible. This can be done in two ways. First, turbulent flow can be used to increase the mixing of the bulk of the liquid and the boundary layer. If laminar flow must be used, as in plate-and-frame designs, feedwater mixers must be used to mix the bulk and boundary layer. Secondly, an additive may be used to increase the diffusion of the salt in solution. At Pratt & Whitney Aircraft, feedwater mixers have been found to be an effective means of reducing concentration polarization to an acceptable level in plate-and-frame designs. The effects of a feedwater additive were not evaluated experimentally. It appears that tubular designs will not require turbulators and that turbulent flow can be used. This is an advantage for the tubular designs which may counter the disadvantage of low packing density. However, this must be substantiated by a detailed system study.

An additional consideration for evaluating a given design must be the amount of effort required to develop it to a production level. Of the designs considered, the tubular concepts would probably require the least amount of development, and the spiral concepts the most. Since the spiral and the circular plate-and-frame concepts are comparable with respect to packing density and concentration polarization, the circular plate and frame was chosen for additional studies as less development would be required.

B. Design Analysis

The design configuration studies performed indicate that the circular plate-and-frame design concept is the best compromise between packaging density and energy requirements, assuming that concentration polarization can be kept to an acceptable level. This may be accomplished with the use of feedwater mixers. An alternate choice appears to be the tubular concept with the reinforced membranes installed on the inside of a support tube.

Layouts of a preliminary circular plate-and-frame cartridge configuration are shown in Figures 58 and 59. Figure 58 shows a longitudinal section of the pressure vessel containing two compact cartridges. The feed enters the vessel at one end and enters the cartridge at the outer edge of the composite plates. The feed then flows radially inward between the composite to a center collecting channel where it flows out of the pressure vessel. Product water passes through the membrane and is channeled to porous collection tubes. These tubes are shown as emptying directly out of the pressure vessel. An alternate design for product-water collection tubes using perforated tubes is also shown. It will be noted that the product-water collection tubes also serve as tierods to maintain

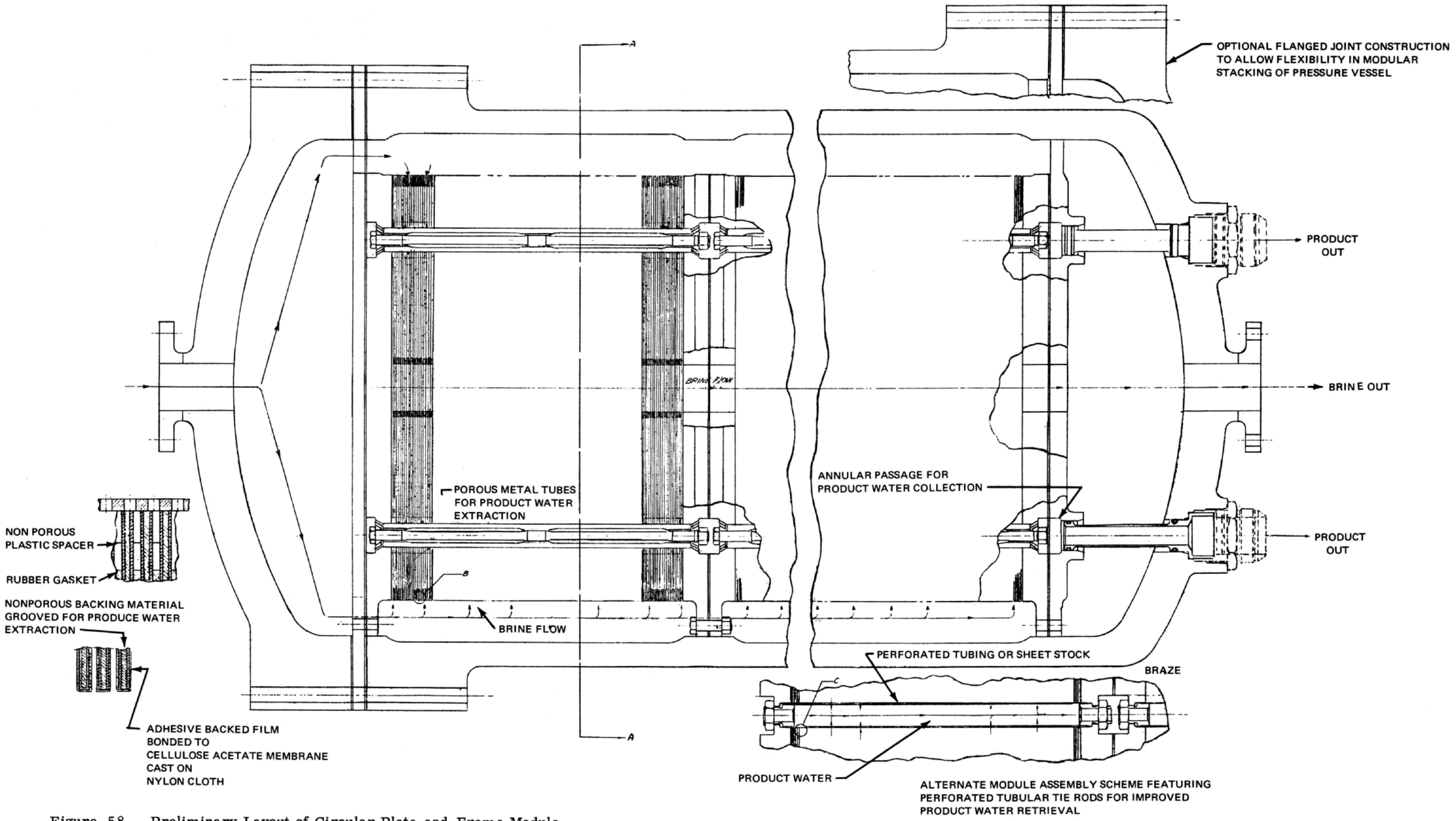

Figure 58 Preliminary Layout of Circular Plate-and-Frame Module

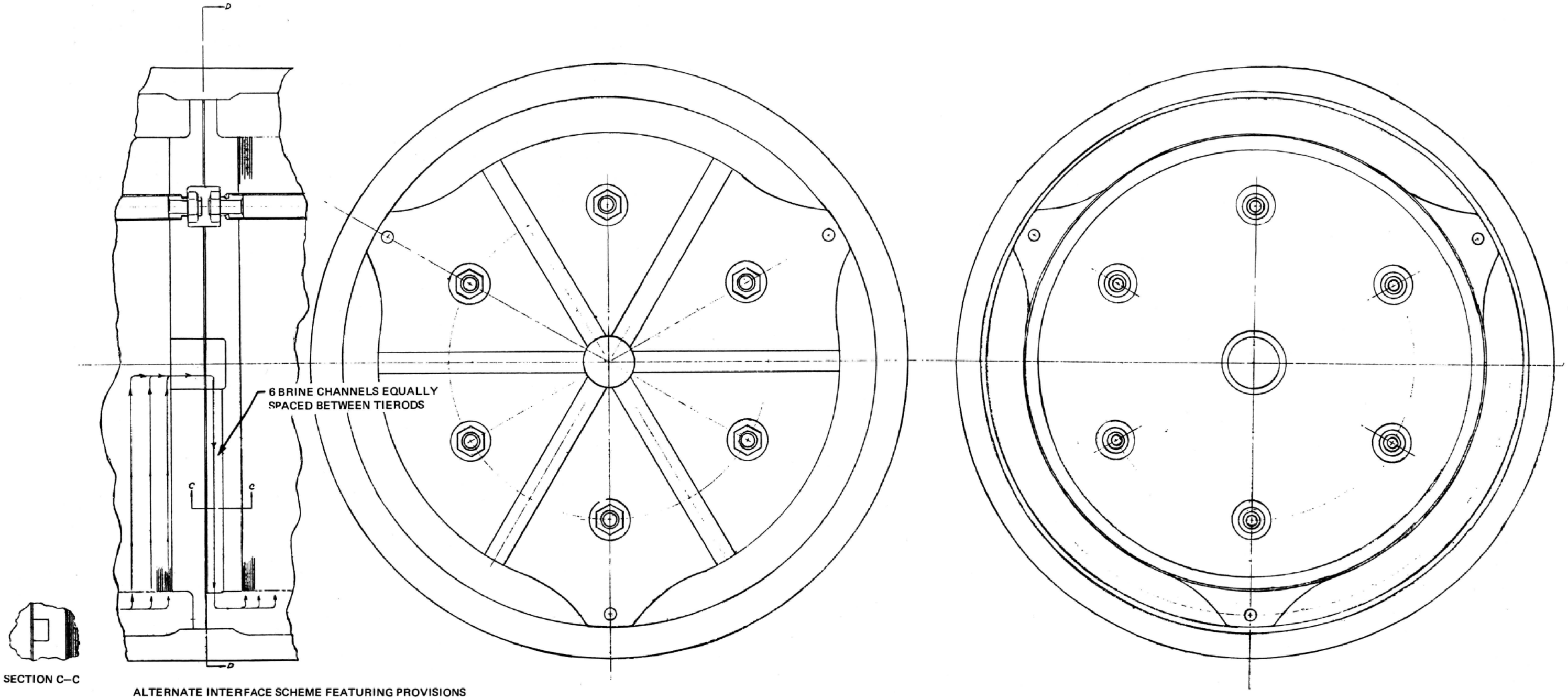

ALTERNATE INTERFACE SCHEME FEATURING PROVISIONS FOR BRINE RECIRCULATION BETWEEN COMPOSITE MEMBRANE CARTRIDGES

Figure 59 Preliminary Layout of Circular Plate-and-Frame Module

structural integrity of the cartridge. Enlarged views B and C show possible sealing techniques and composite details. Section D-D in Figure 59 gives an end view of the cartridge which shows the approximate size and orientation of the product-water collection tubes and other composite details. Also shown in Figure 59 is an alternate interface scheme to connect two cartridges in series. This scheme would enable one to get longer path lengths and hence, a higher recovery factor.

In order to evaluate the cartridge concept shown in Figures 58 and 59, specific characteristics, namely, dimension, and membrane constant, were assumed. The assumed characteristics of each cartridge are given in Table 24 and the calculated values for a module containing four compact cartridges are summarized in Table 25.

TABLE 24

Assumed Characteristics for a Circular Plate-and-Frame Compact Cartridge

diameter	18 inches
length	12 inches
brine outlet hole	2-inch diameter
end plates (2)	1-inch diameter
composite-membrane thickness	0.030 inch
spacing (turbulator thickness)	0.030 inch
number	200
membrane constant	0.0313 gfd/psi

TABLE 25

Design Specifications and Performance
Summary for Circular Plate-and-Frame Cartridge

Cartridge

composite	
spacing	0.030 inch
thickness	0.030 inch
diameter	18.0 inches
brine outlet	2.0 inches
membrane area	2.7 ft^2
dimensions	
length	12.0 inches
end plates	1.0 inch each
total length	14.0 inches
number of composites	200
total membrane area	540 ft^2
total volume	2.06 ft^3
packing density	262 ft^2/ft^3
total water production	13,500 gpd
water production/volume	6,550 gpd/ft^3

Module

number of cartridges	4
total membrane area	2160 ft^2
dimensions:	
overall length	80 inches
diameter	24.0 inches
type heads	3-1 ellipitical
total volume	23.0 ft^3
packing density	93.9 ft^2/ft^3
total product-water production	54,000 gpd
product water volume	2350 gpd/ft^3
average Reynolds number	20
recovery factor	50 percent
pressure drop	10 psi
average velocity	0.04 ft/sec

Considering the assumed cartridge characteristics and the performance summary as given in Tables 24 and 25, several measures of the value of a circular plate-and-frame cartridge can be obtained. A packaging density of 262 ft^2/ft^3 is obtainable with a compact cartridge whose volume is 2.06 ft^3, and contains 540 ft^2 of membrane area. The water production per volume for a cartridge of this size is 6550 gpd/ft^3. However, the packaging density of a system is greatly reduced when a number of cartridges are installed within a pressure vessel. For instance, a pressure vessel containing 23.0 ft^3 of volume is required to contain four circular compact plate-and-frame cartridges. This unit contains 2160 ft^2 of membrane area and has a packaging density of 93.9 ft^2/ft^3. The water production per volume for a module of this size is 2350 gpd/ft^3. The reduction in the packaging density and water production per volume is a direct result of unusable volume in the pressure vessel heads, and between the outside diameter of the cartridge and the inside diameter of the pressure vessel barrel. Nineteen modules of this size would be required to produce one million gallons of water per day.

Another important characteristic of the system is the energy required. This is composed of two parts; the hydraulic energy required, i. e., the pressure drop in the system, and the energy required to remove the product from the brine. Calculations indicate a pressure drop through the system of approximately 10 psi with a Reynolds number of about 20. This is an energy requirement of 0.6 kw-hr/kgal with a 50 percent recovery factor. In addition, the energy required to separate the product from the brine was calculated. The minimum energy required for standard brackish water (10,000 ppm NaCl at 77°F) is approximately 0.1 kw-hr/kgal and is independent of the method of separation. For an actual reverse-osmosis system the energy requirement is more like 5.8 kw-hr/kgal or a total energy requirement of 6.4 kw-hr/kgal for a 50 percent recovery. This value is calculated for a system in which concentration polarization is less than a factor of two. If there is more polarization than this in the system, the energy requirement would be correspondingly higher. It is believed that the use of turbulators and a small channel spacing will keep concentration polarization to this value.

An alternate design was chosen for further study. A layout of a tubular configuration is shown in Figures 60 and 61. Referring to Figure 60 the feedwater enters the system and flows into seven parallel tubes, each of which is 0.250 inch in inside diameter, 0.500 inch outside diameter, and ten feet long. The system is composed of seven sets of seven tubes in parallel for a total path length of seventy feet, a membrane area of 4.6 ft^2 (total of 32.2 ft^2). This system then would produce approximately 800 gpd. The design specifications and performance characteristics are summarized in Table 26. It is possible to increase the size of this system either by adding tubes in series or sets of

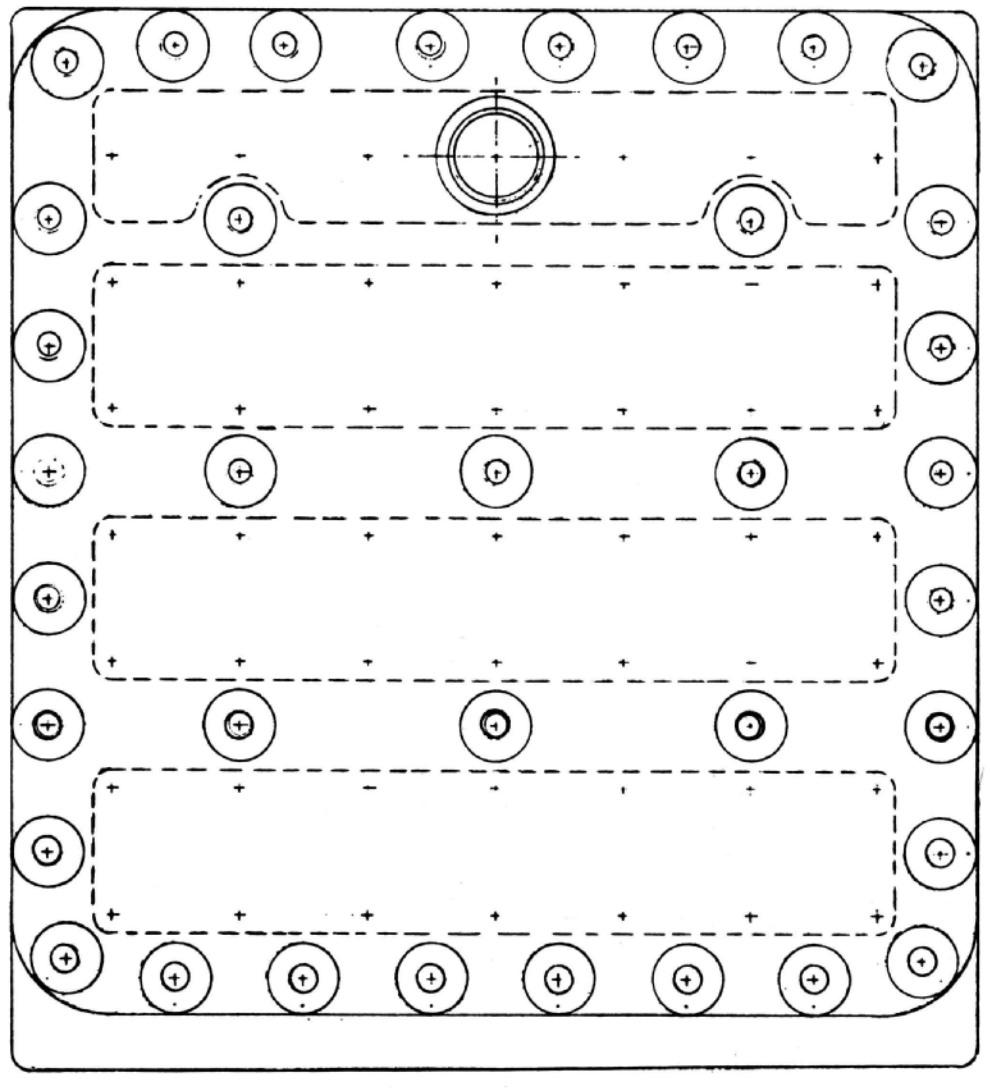

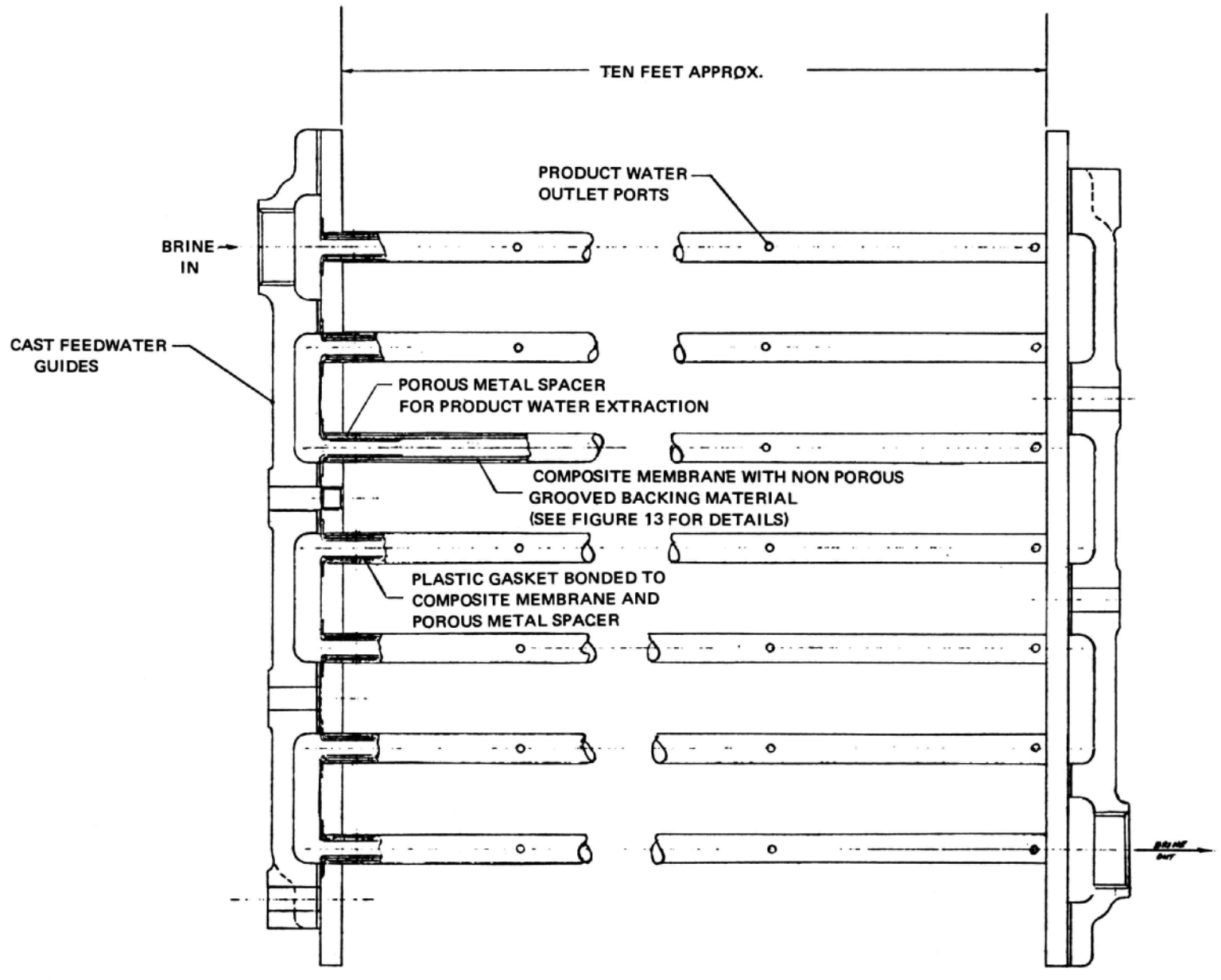

Figure 60 Preliminary Layout of Tubular Module

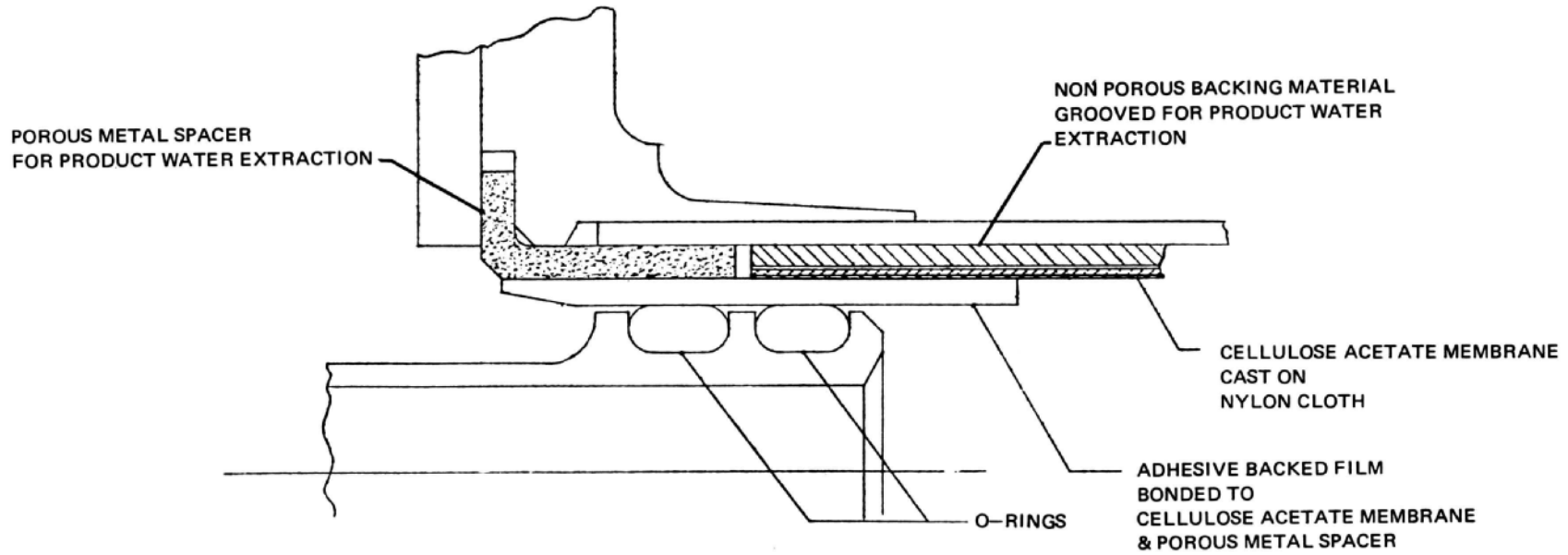

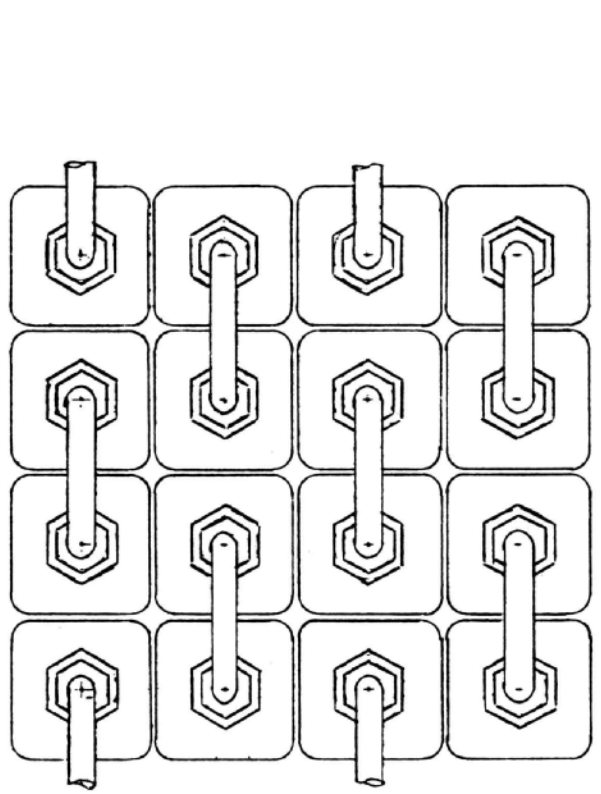

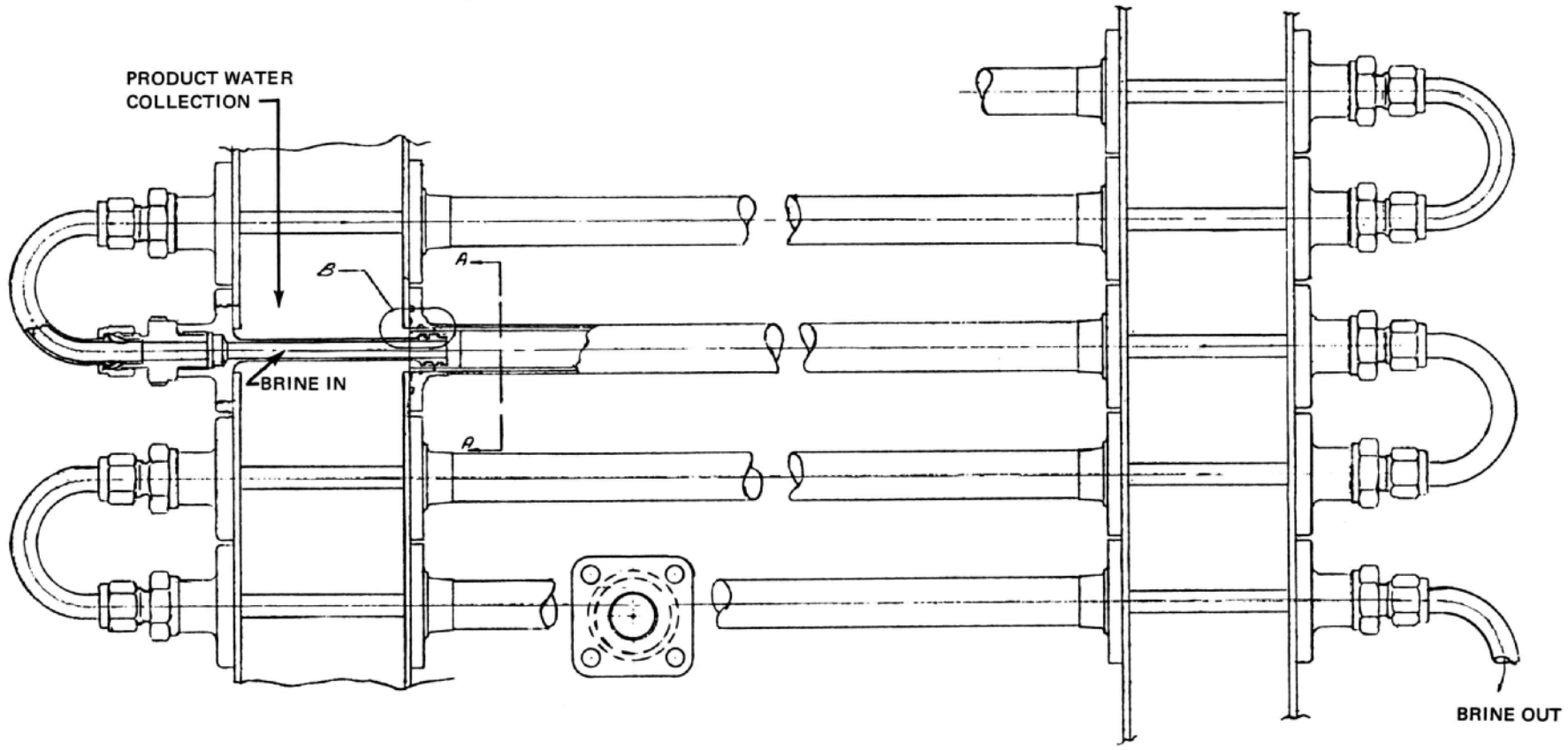

Figure 61 Preliminary Layout of Tubular Module

tubes in parallel. Figure 61 shows an alternate design of a tubular configuration. Whereas the design shown in Figure 60 uses cast end plates, this design uses commercial tube fittings. Also shown in this figure is a possible product-water withdrawal scheme. Both designs would use the same kind of membrane tubes and supports.

TABLE 26

Design Specifications and Performance
Summary for Tubular Cartridge

number of tubes	49 (seven series x seven parallel)
membrane area/tube	0.66 ft^2
length	10 ft
tube diameter	
inside	0.250 inch
outside	0.500 inch
total volume	13.7 ft^3
total membrane area	32.2 ft^2
packing density	2.4 ft^2/ft^3
water production volume	58.6 gpd/ft^3
total water production	800 gpd
Reynolds number	5000 - 6050
recovery factor	20 percent
pressure drop	20 psi
average velocity	2.8 ft/sec

In order to evaluate this design the packing density and the energy requirements were calculated. For a system having a total volume of 13.7 ft^3, this system has a packing density of 2.4 ft^2/ft^3, and hopes are small for increasing it by much more than an order of magnitude. The energy requirements for this design are strongly dependent on the number of tubes in series and the recovery factor. Assuming the system as shown in Figure 60 and demanding turbulent flow at the exit which specifies a recovery factor of 20 percent, the pressure drop is approximately 20 psi. This is an energy loss of about three-quarters of a kilowatt-hour per 1000 gallons of product; somewhat higher than that estimated for the plate-and-frame configuration. The energy required to separate product water from the brine is the same as for the plate-and-frame configuration, i.e., 5.8 kw-hr/kgal. This gives a total energy requirement of 6.55 kw-hr/kgal.

VIII. CONCLUSIONS AND RECOMMENDATIONS

This section summarizes the results of a two-year research program performed for Office of Saline Water. The major findings are listed and the areas requiring further research and development to make a practical and economical reverse-osmosis desalination system are identified.

A. Modified Cellulose-Acetate Membranes

1. Modified cellulose-acetate membranes remain the best type for a reverse-osmosis system, although considerable research has been performed to obtain better membranes. In view of this, compaction studies (lifetime measurements) should be extended in order to determine if membrane performance decay is either linear or logarithmic with respect to time. An endurance test of between fifteen hundred and five thousand hours would be required to properly identify the mode of decay. The endurance program should be performed on the compact cartridge as well as on membrane specimens.

2. Membrane-processing studies indicate that acceptable membrane performance is obtained using the formulation developed by Manjikian. Membrane performance of 25 to 30 gfd with a salt rejection of 98 to 95 percent was obtained when evaluated at standard brackish-water test conditions. The membrane is cast on a nylon fabric instead of a glass plate. The membrane formulation and processing conditions are as follows:

   a) Membrane Formulation - percent by weight:

cellulose acetate	- 25 percent
acetone	- 45 percent
formamide	- 30 percent

   b) Processing Conditions:

cellulose acetate type	- Eastman Kodak E-398-3 or 10
reinforced membrane thickness	15 mils
cast temperature	70°F
evaporation time	30 seconds
cold-bath temperature	35°F
cold-bath time	1 hour

hot-bath temperature	185°F
hot-bath time	4 minutes

3. Travis Mills Nylon 5055, 7.5 mils thick, was used for the membrane studies performed during this program. Thinner nylon fabrics as well as alternate fabrics should be evaluated, as a thinner reinforcing membrane would improve the packaging density of desalination systems.

4. Diffulties have been encountered in obtaining membranes with reproducible characteristics of water flux and salt rejection. Studies indicate that these difficulties may be attributed to the membrane-formation procedure, to some unidentified variable in the raw materials involved, or possibly to the membrane evaluation apparatus.

   a) Overall process control is extremely critical in the fabrication of high-performing membranes. Factors that affect the preparation of membranes include the molecular weight of the cellulose acetate, its water content, the quality of the acetone and formamide, storage time, and the atmosphere in which the basic membrane cast solution is prepared and cast. Membranes should be processed in a facility with a fully-controlled environment.

   b) Raw material specifications should be established as studies indicate that nonreproducible membranes have been produced from cast solutions whose molecular weight and viscosity varied. This leads to the conclusion that standard formulations, fabrication techniques and procedures are not always suitable for a given cast solution. Perhaps a rigid specification of the acetyl content of the cellulose acetate would eliminate these variations.

   c) Test cells having a well-defined feedwater flow should be employed for the evaluation of all membranes. The test cells used throughout the entire program were 2.5 inches in diameter. They did not provide a uniform feedwater flow pattern over the membrane surface, even though turbulent flow conditions existed. It seems doubtful but possible, that the lack of a uniform feedwater flow may have affected membrane performance.

5. Membrane testing should be performed on actual brackish waters rather than on synethic waters. A true picture of membrane performance will then be established. Feedwater pretreatment, such as filtration and bacteria removal, should be incorporated into all test systems as membrane fouling and/or scale buildup may affect membrane performance. Feedwater pretreatment will undoubtedly increase plant operation costs, however the

lifetime characteristics of the membranes may be greatly extended. Since the performance of membranes is strongly dependent on the temperature of the feedwater (approximately 0.4 gfd/°F), preheating of the feedwater will probably be economical. The cost of any reverse-osmosis system should take into account the energy requirements required to preheat the feedwater. Membrane performance at the standard test temperature of 77°F is between 25 to 30 gfd. Membrane performance would be reduced to approximately 17 gfd without preheating, since most ground water is cooler than 57°F.

B. Compact Cartridge Concept

1. The compact reverse-osmosis cartridge concept investigated has the potential of being developed into an acceptable water purification system. Performance characteristics similar to those of laboratory controlled specimens were obtained, even though the cartridges were not designed for optimum operation and application.

2. In any compact disposable cartridge the feedwater flow channel must be small and consequently the flow conditions will be laminar. It does not now appear practical either from a volume or pumping power standpoint to design a reverse-osmosis cartridge for turbulent flow. It may however, be practical to introduce mechanical devices to promote mixing. The mechanical devices previously described as turbulators can be integrated with the membrane spacers and may be required to maintain feedwater flow geometry.

3. The zero-loss membrane-support plates provide negligible product-water pressure drop and make it possible to consider a much wider range of materials to support the reverse-osmosis membranes. Support plates can be made economically in large quantities from inexpensive plastics. Thermosetting and thermoplastic materials could be used as long as they could withstand the desalination system operating pressures. Injection molding or pressing are two possible ways of forming the support plates.

4. The composite membrane developed during this contract was formed by attaching a reinforced membrane to both sides of a zero-loss support plate by means of a tape and cement seal. To obtain an inexpensive disposable cartridge the cost of the composite membranes must be low. Further work should be directed towards the development of a cheap and reliable composite membrane as the technique employed is time-consuming and expensive.

5. The membrane-coated porous material work demonstrated that acceptable performance could be obtained by directly casting a membrane on a porous material. A sizable reduction in the composite membrane fabrication cost would result if the direct-cast technique could be developed.

REFERENCES

1. Green, L. Jr., "Heat, Mass and Momentum Transfer in Flow through Porous Media", ASME Paper No. 57-HT-19, August 1957

2. Manjikian, S., S. Loeb, and J. W. McCutchan, "Improvements in Fabrication Techniques for Reverse-Osmosis Desalination Membranes", First International Symposium on Water Desalination, Washington, D. C., October 1965

3. Merten, Ulrich, ed. "Desalination by Reverse Osmosis," M.I.T. Press, Cambridge, Mass., 1966

4. Brian, P.L.T., "Concentration Polarization in Reverse-Osmosis Desalination with Variable Flux and Incomplete Salt Rejection", Dept. No. DSR-4647, Mass. Inst. of Tech., Dept. of Chem. Engr., Desalination Research Laboratory, May 12, 1965

5. International Critical Tables, McGraw-Hill, New York, 1928

6. Sherwook, T. K., P.T.L. Brian, R. E. Fisher, and L. Dresner, "Salt Concentration at Phase Boundaries in Desalination by Reverse-Osmosis", Industrial and Engineering Chemistry Fundamentals, Vol. 4, No. 2, pp. 113-118, May 1965

7. Rohsenow, W. M., and H. Choi, "Heat, Mass and Momentum Transfer, Prentice-Hall, Englewood Cliffs, New Jersey, pp. 67-71, 1961

APPENDIX 1

Hydrodynamics of Porous Media

APPENDIX 1

Hydrodynamics of Porous Media

The study of the hydrodynamics of porous media required the evaluation of potential support materials under conditions simulating those that would exist in a reverse-osmosis desalting system. This appendix describes the experimental evaluation equipment that was used to simulate a reverse-osmosis desalting system. The equipment consisted of two major components, an evaluation cell and a test system. The principal function of the experimental evaluation system was to obtain the necessary data to define the flow resistance coefficient of various materials.

The evaluation cell that was constructed to obtain this data is shown in Figure 62. A rectangular specimen 4.0 x 1.5 x 0.06 inch was encapsulated in RTV silicone rubber. The encapsulated specimen was inserted between the upper and lower sections of the cell. Water entered and left the support material specimen through slots in the end flanges. The water pressure was measured at each end flange so that the pressure drop across the specimen could be determined. A fitting in one flange of the cell was used for temperature instrumentation. The pressure and temperature fittings are not visible in the figure. A partially-assembled evaluation cell is shown in Figure 63. The lower part of this figure represents the end flange, and the hole in the center is the water entrance port. The lower section of the cell adjacent to the test sample was rigidly mounted during operation. Pressure was applied by a hydraulic system to the upper section to simulate the effect of brine pressure, and to force a positive seal between the specimen and the cell components.

The test system was constructed to accept six of the evaluation cells simultaneously. A photograph of the system is shown in Figure 64. The evaluation cells were located directly beneath the pressure gages which read hydraulic piston pressure as shown in Figure 65. The system used deaerated distilled water that was maintained at the desired temperature. Individual pumps and appropriate valving were used to independently control the pressure and flow rate to each evaluation cell.

A more complete description of this system is given below and can be followed readily by referring to the system schematic shown in Figure 66. The accumulator tank was a standard one-gallon high-pressure hydropneumatic-transfer-barrier accumulator. During operation, deaerated water only came in contact with the Buna-N bladder or the stainless-steel inserts and fittings associated with the bladder. Pump pulsations were held to a minimum by nitrogen gas pressure applied to the outer surface of the flexible bladder. A polypropylene filter of 10-micron pore size and 95 percent removal rate was

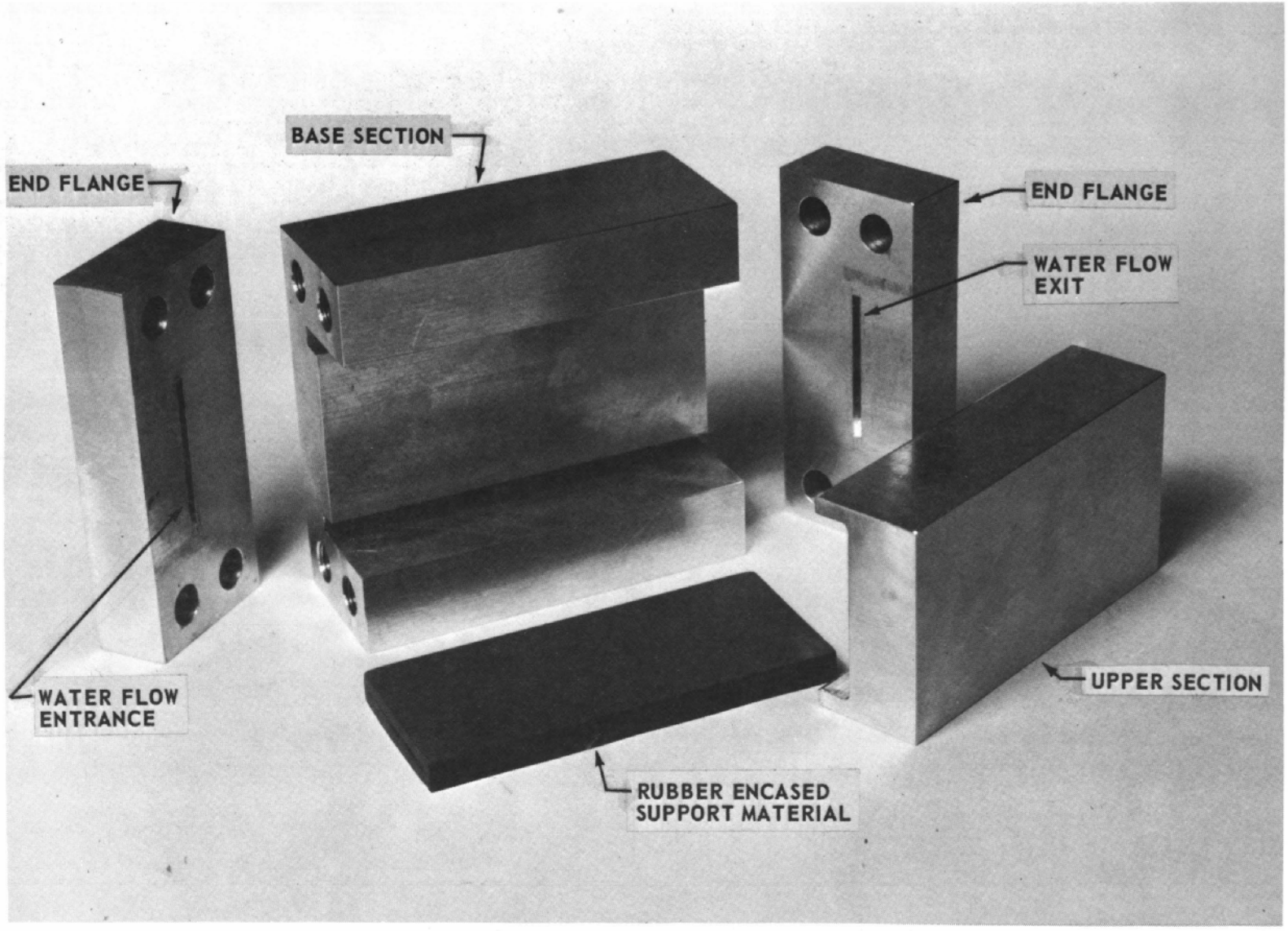

Figure 62 Details of Support-Material Evaluation Cell XP-68946

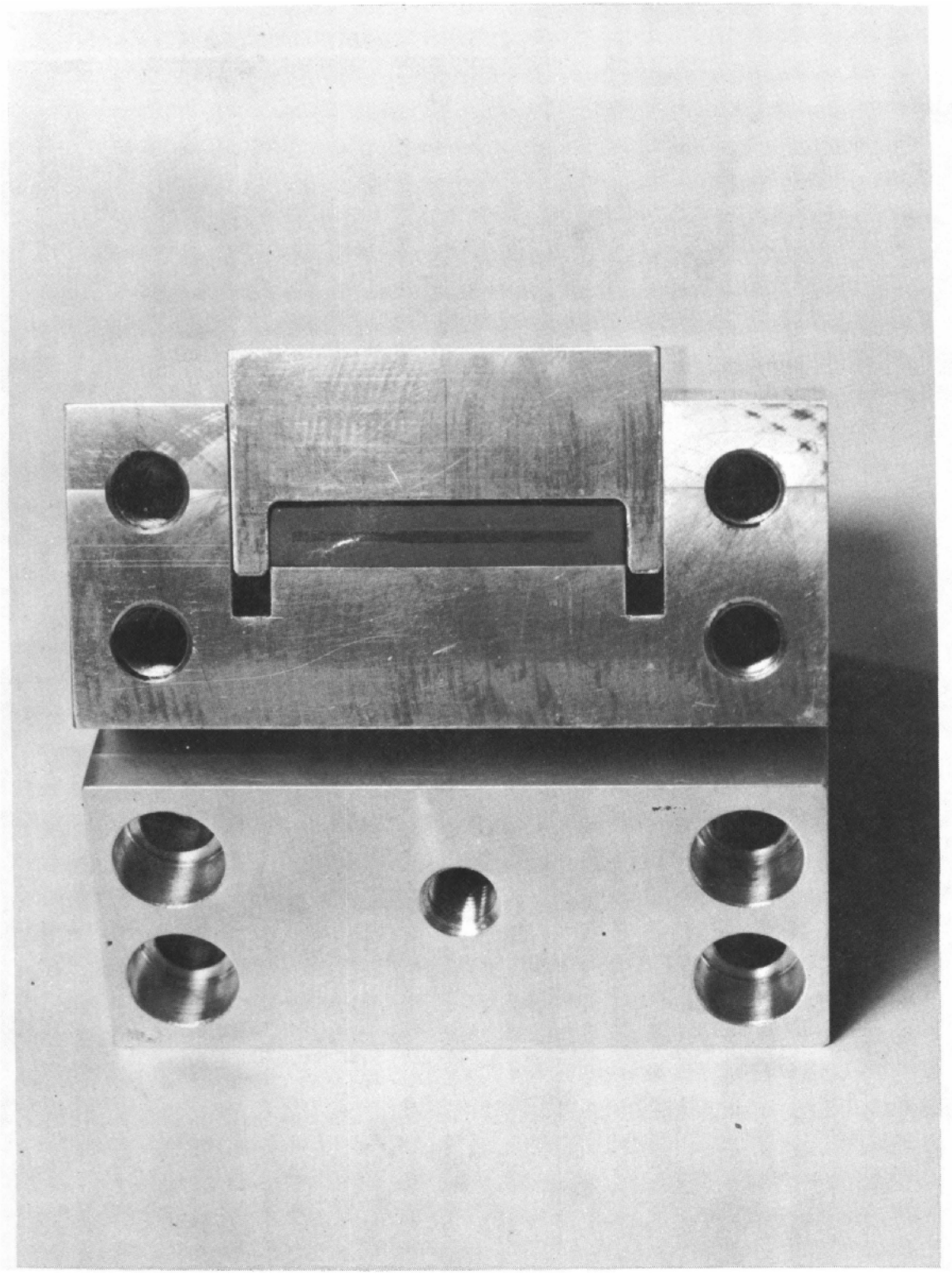

Figure 63 Support-Material Evaluation Cell Partially Assembled XP-68951

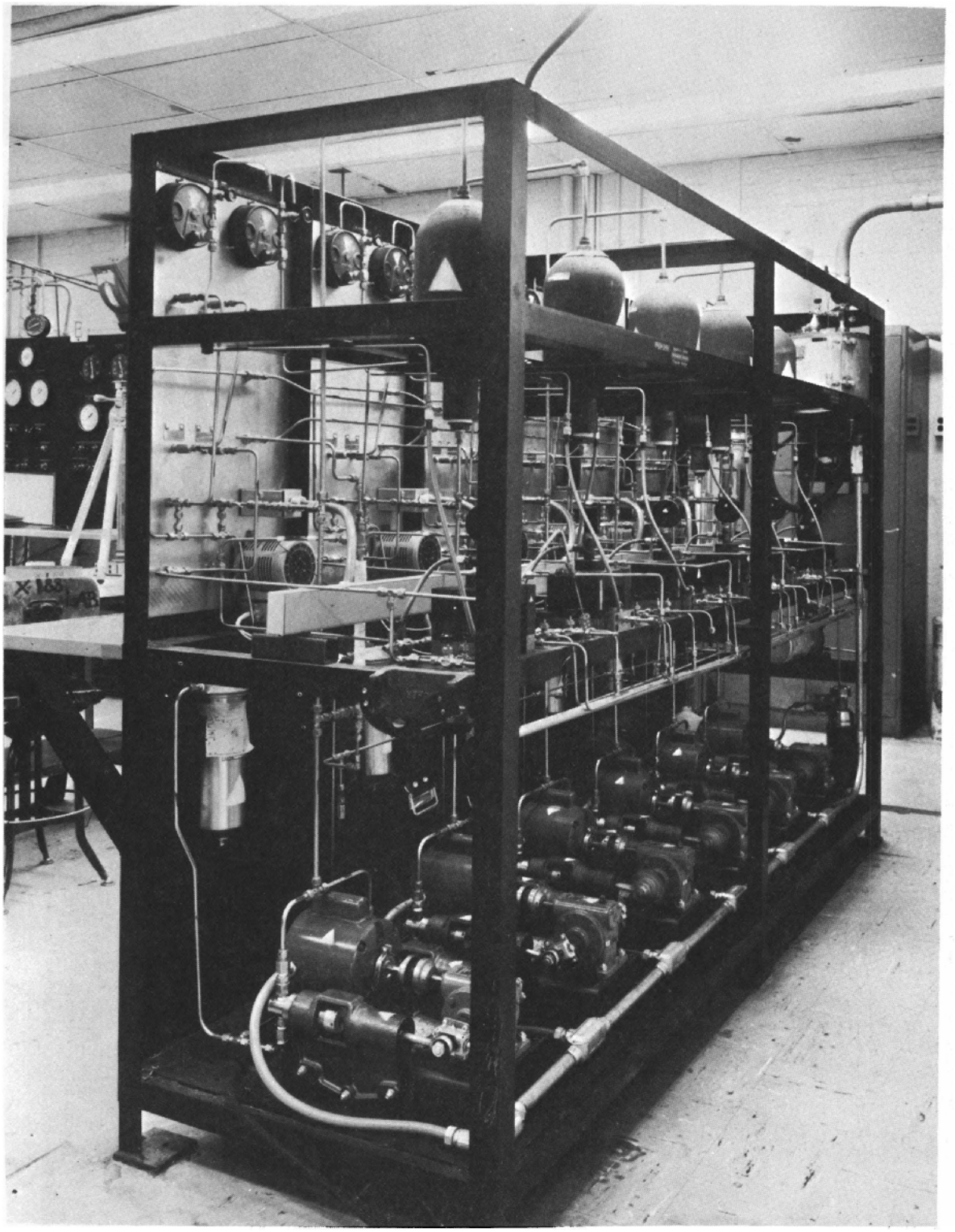

Figure 64 Porous Material Evaluation System XP-76953

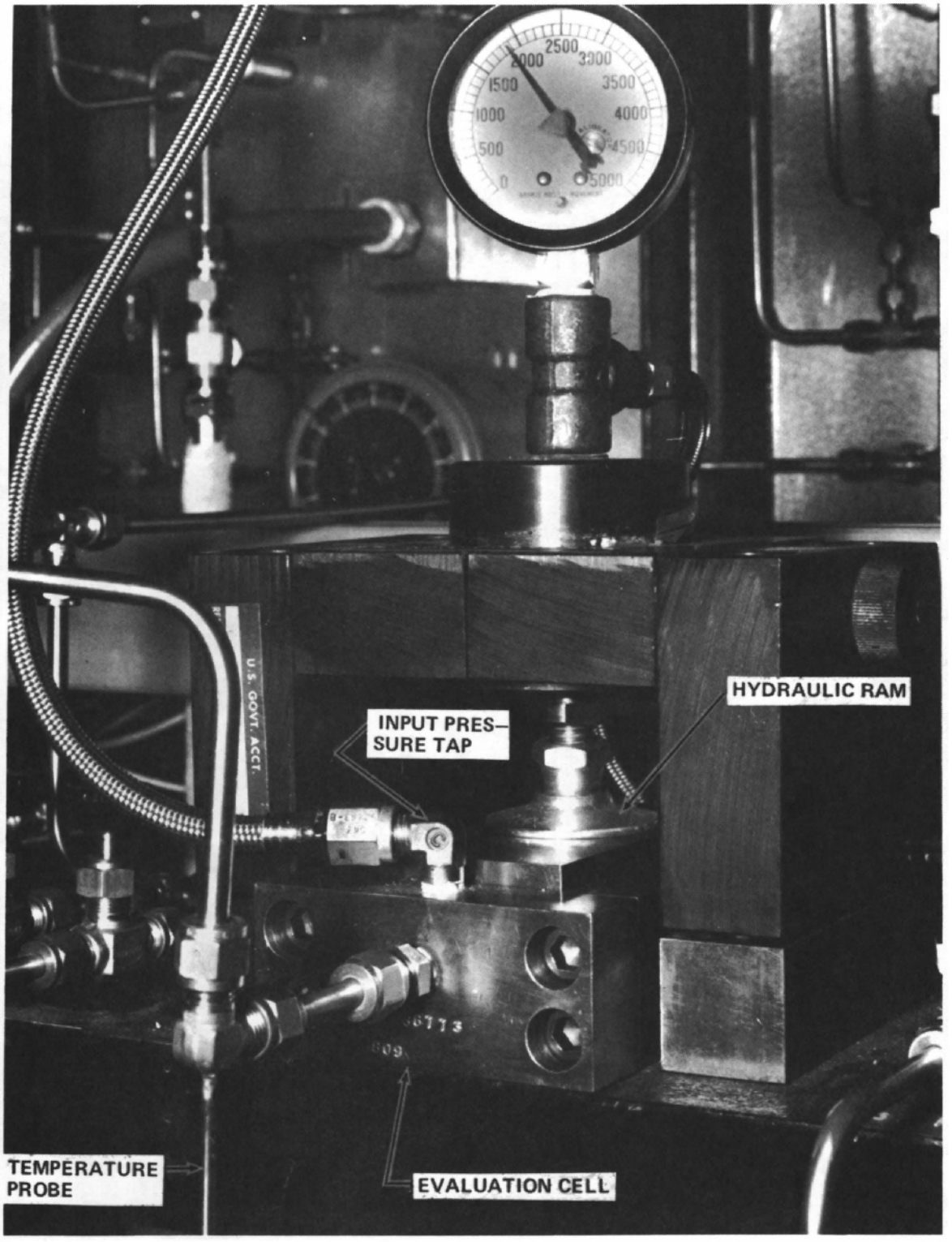

Figure 65 Hydraulic Ram for Simulated Brine Pressure Loading XP-25296

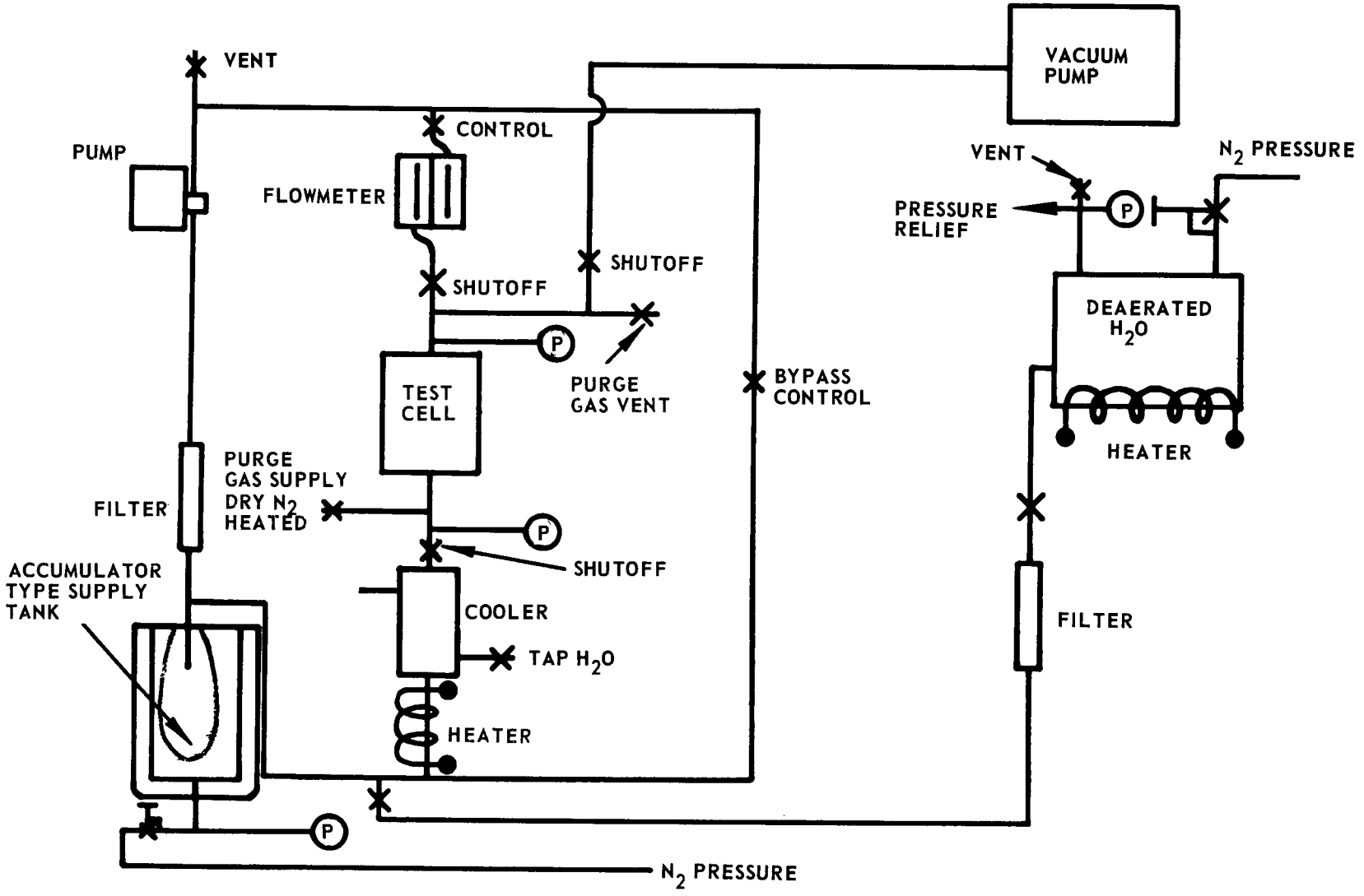

Figure 66 Schematic Diagram of Support-Material Evaluation System

employed for removal of foreign material. The high-density filter medium was contained in Type 316 stainless steel. The pump was a BIF positive-displacement duplex type, made of Type 316 stainless steel. Two flowmeters connected in series measured the desired flow range. The Fisher-Porter tri-flat flowmeters had ranges of 0.004 to 0.28 gph and 0.008 to 1.0 gph. Bourdon-tube-type pressure gages with a range of 0 to 300 psig were used. A heater and cooler of Type 316 stainless steel were used to control and vary the water temperature. These components were interconnected by 1/4-inch tubing and valves as shown in the schematic diagram.

The distilled water was deaerated by passing it through several boiling and condensing cycles. The deaerated water then was maintained at a temperature near its boiling point to maintain low gas solubility until it was introduced into the evacuated test system. A vacuum pump evacuated the entire system before introducing the deaerated water. The vacuum equipment was capable of achieving a vacuum of 10^{-5} mm of mercury. The transfer of the deaerated water to the operating section of the system was performed by using the vacuum created within the operating system, or pressure created in the deaeration section of the system. Once the system had been initially charged, further deaeration could be accomplished by using the system heater. The gas generated during this operation could be removed by venting. The bypass line and control valve permitted regulation of the flow through the evaluation cell. The system could also be run without deaerated water.

Details of the porous-material screening tests are shown in Table 27.

TABLE 27

Porous Material Screening Test Summary

Mat'l Type	Material	Code	400 psi ΔP, psi	400 psi W_f, gph	400 psi ft^{-2}	400 psi Time, hrs	750 psi ΔP, psi	750 psi W_f, gph	750 psi ft^{-2}	750 psi Time hrs	1500 psi ΔP, psi	1500 psi W_f, gph	1500 psi ft^{-2}	1500 psi Time, hrs	THICKNESS, inches PRE-TEST	THICKNESS, inches POST-TEST
engineered material	sand-phenolic	3R-5	243.0	0.054	1.99×10^{12}	10.0	231.4	0.047	2.17×10^{12}	12.0					0.068	0.068
		3R-7	234.1	0.045	2.19×10^{12}	10.0	142.0	0.033	1.70×10^{12}	9.5					0.061	0.061
							210.0	0.042	1.98×10^{12}							
	sand-phenolic-Fiberglas	3R-8					87.8	0.516	8.30×10^{10}	12.0	96.3	0.316	8.92×10^{10}	10.0	0.073	0.073
		3R-9					37.2	0.50	4.02×10^{10}	12.0	203.0	0.49	2.27×10^{11}	10.0	0.083	0.082
	sand-phenoxy	3R-62					300	0		3.0					0.044	0.044
		3R-63					300	0		2.0					0.035	0.035
	sand-cement	3R-55					300	0		2.0					0.094	0.093
	sand-cement-asbestos	3R-59					300	0		0.25					0.075	0.075
		3R-60					300	0		1.0					0.076	0.075
	sand-terpolymer(1)	3R-85	40.1	0.516	4.42×10^{10}	10.0	19.8	0.50	2.24×10^{10}	12.0					0.087	0.085
		3R-86	20.4	0.516	2.24×10^{10}	10.0	23.8	0.511	2.71×10^{10}	12.0					0.087	0.080
	sintered glass, 20-25μ	CORN3	247.6	0.18	4.87×10^{11}	10.0	235.0	0.18	4.97×10^{11}	12.0					0.059	0.058
		CORN4	241.7	0.12	8.15×10^{11}	10.0	171.0	0.03	2.32×10^{11}	10.0					0.063	0.062
commercial material	sintered stainless-steel screen-rigmesh	Rig 1					9.5	0.516	8.11×10^{9}	12.0	7.4	0.516	6.37×10^{9}	10.0	0.066	0.066
		Rig 5					1.13	0.528	9.45×10^{9}	12.0	1.16	0.504	1.01×10^{10}	10.0	0.067	0.067
	sintered stainless steel 10μ	MOTT2					70.9	0.50	5.15×10^{10}	12.0	96.7	0.516	7.11×10^{10}	10.0		
		MOTT4					76.6	0.516	5.84×10^{10}	12.0	137.2	0.486	1.05×10^{11}	10.0	0.059	0.058
	battery separator, W. R. Grace	D-60-1	245.4	0.198	1.74×10^{11}	5.0	252.3	0.05	7.08×10^{11}	12.0					0.022	N.A.
		D-60-2	245.1	0.24	1.36×10^{11}	10.0	215.4	0.27	1.10×10^{11}	12.0					0.021	N.A.
	porous ceramic, 10μ	COORS5	247.5	0.015	2.51×10^{12}	10.0	225.0	0.03	2.18×10^{12}	12.0					0.046	0.045
		COORS7	243.3	0.015	5.37×10^{12}	10.0	240.0	0.036	2.17×10^{12}	8.0					0.051	0.051
	porous ceramic, 100μ	COORS9					9.12	0.516	6.05×10^{9}	12.0	50.0	0.504	3.30×10^{10}	10.0	0.051	0.051
		COORS10					20.71	0.516	2.30×10^{9}	12.0	31.9	0.50	2.05×10^{10}	10.0	0.050	0.050
		COORS11	18.2	0.516	1.21×10^{10}	10.0	17.2	0.516	1.09×10^{10}	12.0					0.051	0.051
		COORS12	26.9	0.516	1.76×10^{10}	10.0	23.8	0.516	1.53×10^{10}	12.0					0.051	0.052
zero-loss material	phenolic	ZL-11					20.0	0.488		14.0	16.3	0.516		10.0	0.063	0.063
		ZL-10									16.3	0.516		10.0	0.063	0.062
	polyethylene	could-not be-machined														
	sintered glass, 10μ	ZL-6					200.5	0.516		12.0					0.062	0.062
		ZL-7					98.6	0.511		12.0					0.062	0.064
	Flexboard	ZL-8					45.0	0.516		14.0	45.5	0.501		10.0	0.059	0.059
		ZL-9					98.7	0.504		14.0	105.2	0.516		11.0	0.060	0.059

(1) May be misleading since some material squeezed out of both ends

N.A. Thickness not available

APPENDIX 2

Membrane Manufacturing Facilities

APPENDIX 2

Membrane Manufacturing Facilities

The membrane-coated material specimens produced on this program were processed in two facilities for membrane formation. The first facility was used for the earlier efforts in screening membrane-coated materials. The cast method was manual and no attempt was made to control the cast environment. In the second facility the cast process was mechanized and a controlled-environment chamber was used. This appendix describes the membrane-formation process in both facilities.

The facility used during the screening effort on membrane-coated materials is shown in Figure 67. The casting area is at the left of the photograph. The cold-water bath was an epoxy-lined wooden box and ice was used to cool the water to 35°F. The hot-water bath was an insulated glass jar which contained a stirrer and an immersion heater. A temperature-control regulator was used to maintain the water temperature to within 0.2°F of the desired temperature. This facility permitted rapid experimentation in the new casting techniques required for membrane-coated materials. Various methods of supporting reinforcing fabrics and porous materials during the various steps of the membrane-formation process could be readily evaluated. The cast-process variables were adequately controlled to produce specimens satisfactory for screening studies.

The cast facility used for the later studies was considerably more complex than that used for the screening tests. It offered two marked advantages, mechanized casting and controlled and variable cast environment. A photograph of the mechanized cast facility is shown in Figure 68. The temperature inside the chamber could be varied from 0 to 70°F and controlled within 2°F by an internal refrigeration/heater system. Normally, air conditioned to control the moisture content was used for the cast atmosphere. However, provisions had been made to permit the use and treatment of other atmospheric compositions within this chamber. The moisture content of the air was controlled by using a dew-point coil which permitted variation of the relative humidity from 0 to 40 percent within ±5 percent. A variable-drive reversible motor located outside of the chamber provided power for the drive screw. The drive screw forced the cast knife to move across the substrate surface (a glass plate for example) and deposit the film. The substrate was located within a cold-bath pan which could be flooded with the cold-bath solution by opening a valve located outside of the chamber. A cam lifted the cast knife above the edge of the pan after the film deposition process. A gravity-actuated valve automatically permitted the cast solution to flow from the cast knife when in contact with the substrate surface. As the cam lifted the assembly off the

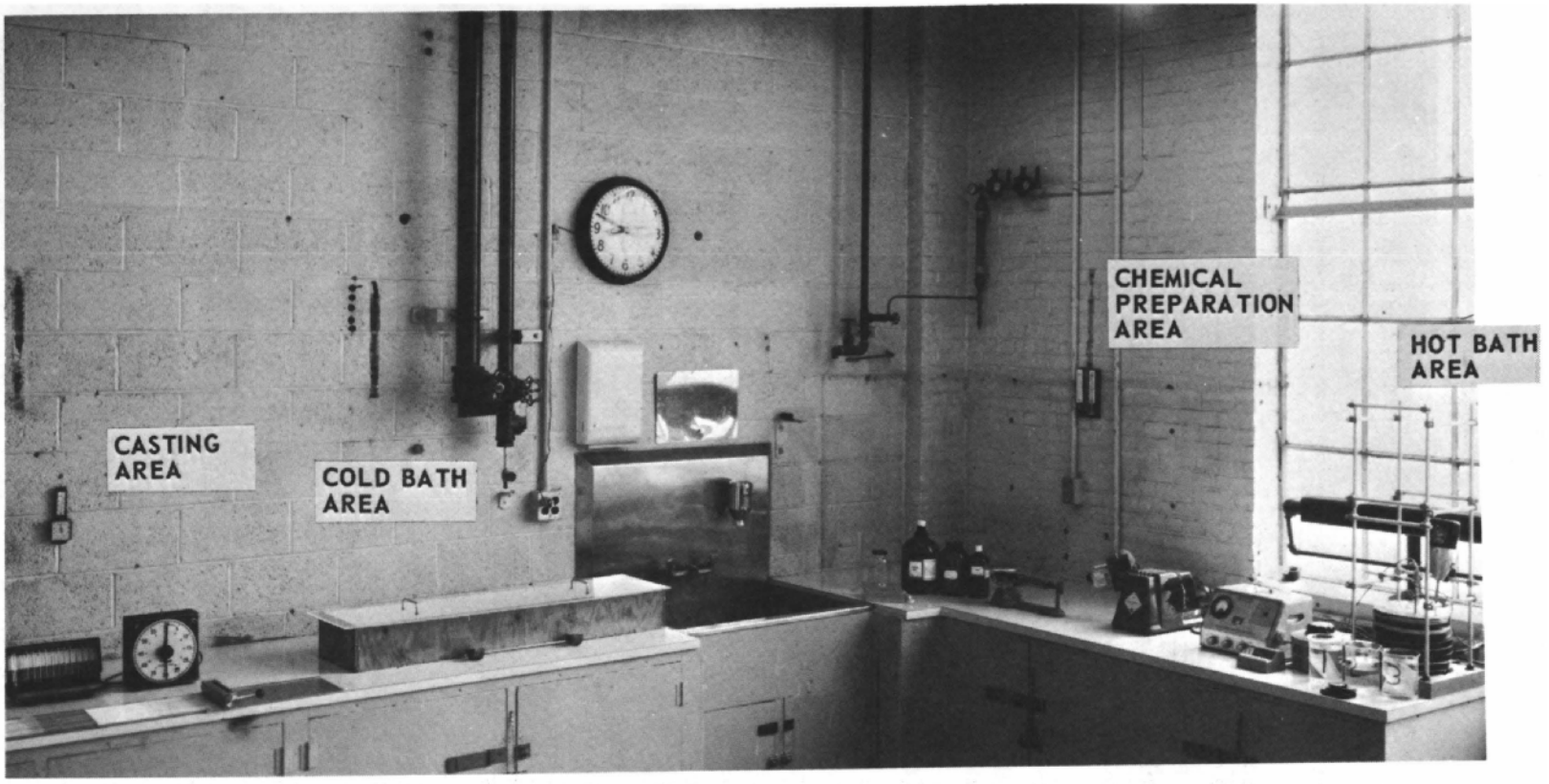

Figure 67 Membrane Formation Area H-58820

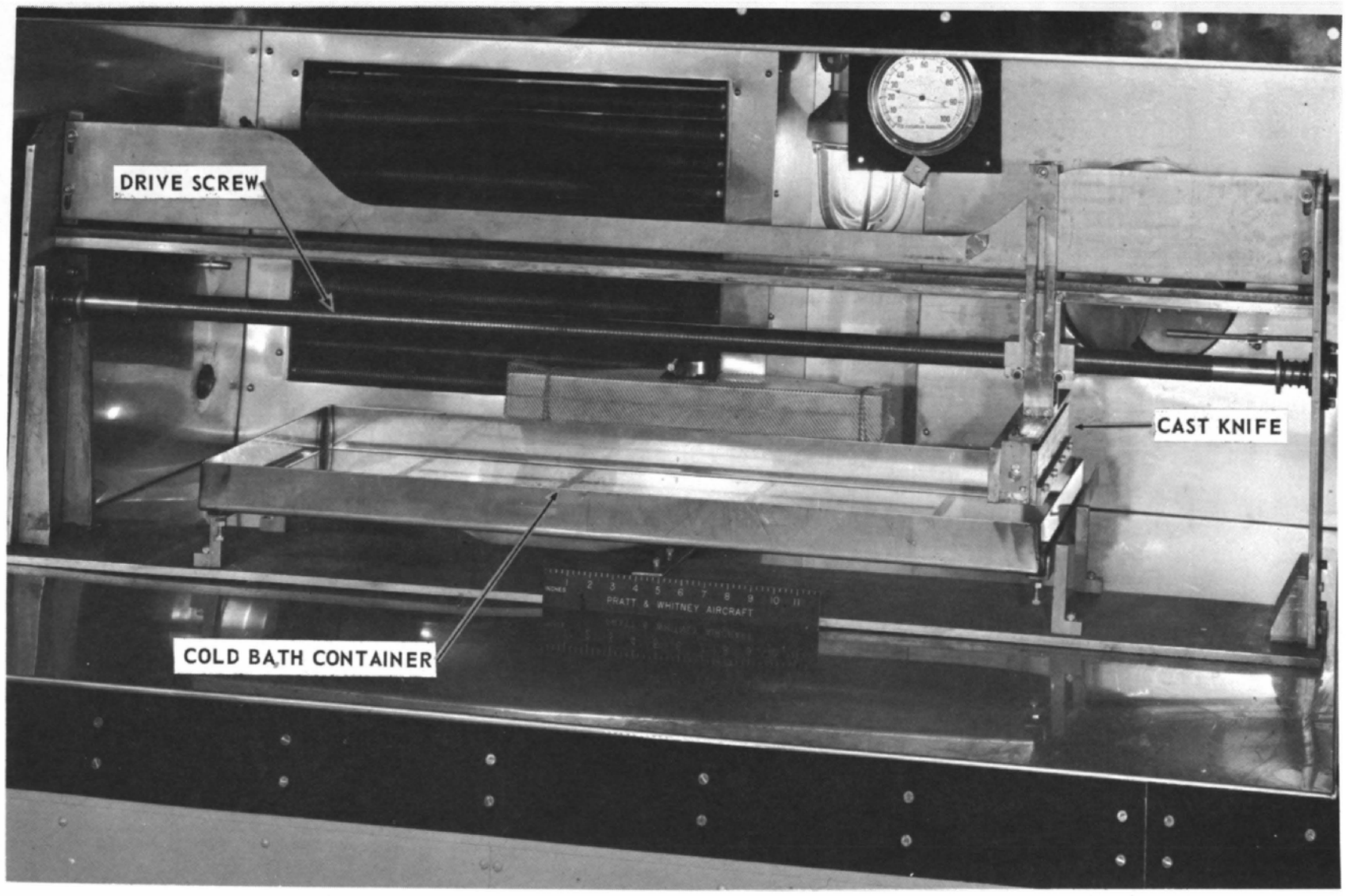

Figure 68 Automatic Cast Facility H-61783

substrate, the valve rotated into a closed position. A tube not shown in the photograph permitted the introduction of the cast solution into the cast knife without opening the chamber door. This eliminated the need for reconditioning the cast atmosphere after introducing the cast solution into the knife assembly. The chamber atmosphere could be reconditioned within 20 minutes. The operating characteristics of the cast chamber were as follows:

temperature - variable from 0° to 70°F
relative humidity - variable from 20 to 40 percent above 35°F
less than 20 percent below 35°F
cast speed - variable from 0.1 to 8.0 ft/sec

The membrane specimen contained within the cold-bath pan could be stored in the freezer. An external view of the cast chamber and cold-bath chamber is shown in Figure 69. The hot-bath chamber for this system is shown in Figure 70.

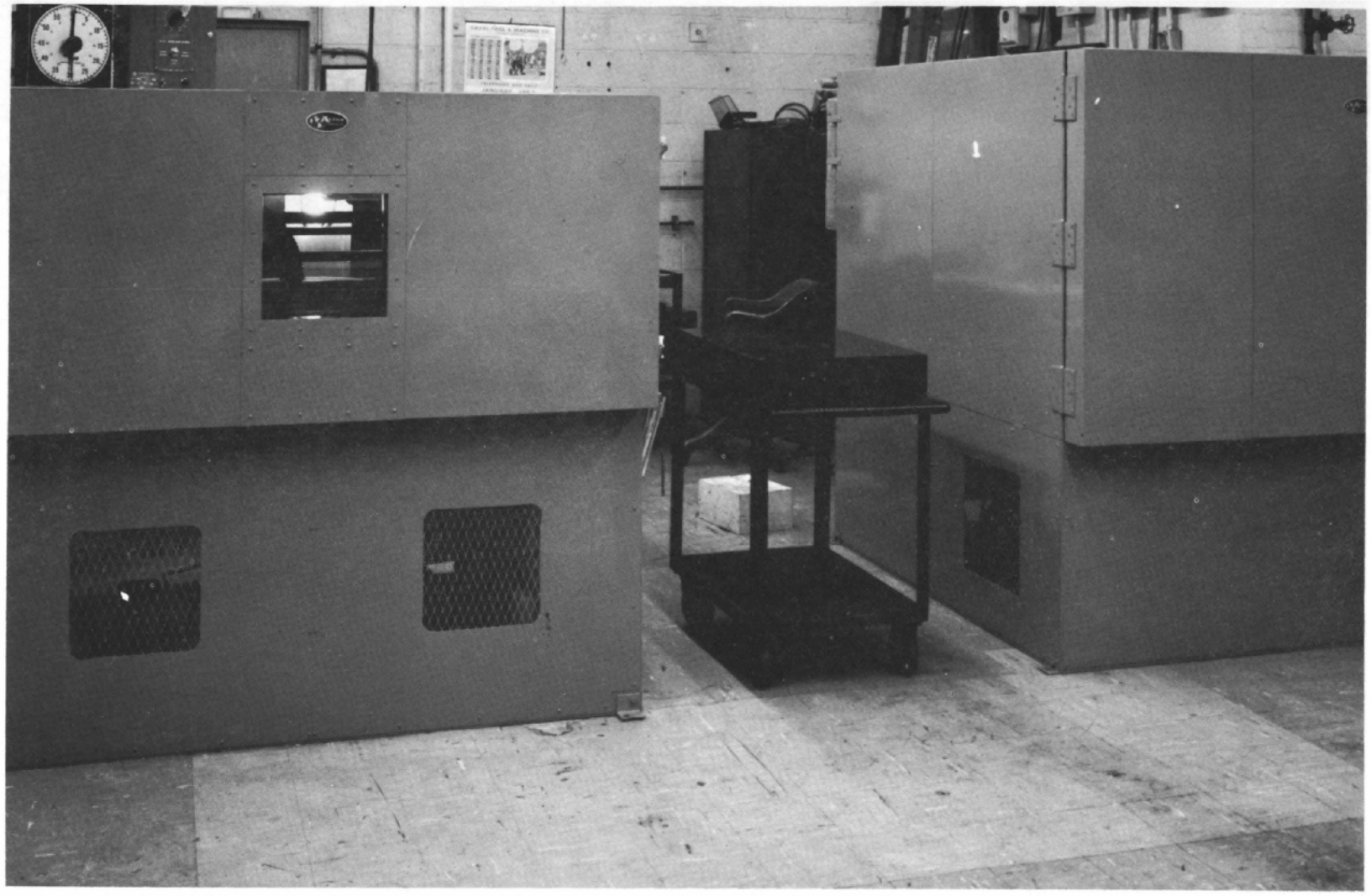

Figure 69 Environmental Control Chamber and Cold-Bath Chamber H-61779

Figure 70 Hot-Bath Chamber XP-69661

APPENDIX 3

Membrane Evaluation Facilities

APPENDIX 3

Membrane Evaluation Facilities

Two test systems were in operation during this contract for membrane evaluation:

1) a test system for the experimental evaluation of membrane-coated materials, and
2) a test system for the experimental evaluation of a compact membrane reverse-osmosis cartridge concept.

These systems were capable of measuring performance as a function of brine pressure, temperature, flow rate and concentration.

Evaluation of Membrane-Coated Materials

A photograph of the reverse-osmosis test system is shown in Figure 71 and schematically in Figure 72. The system consisted of three evaluation cells that could be individually controlled with respect to brine (feedwater) flow rate and pressure, but used a common pumping system and brine supply. A heat exchanger controlled the brine temperature. The operating variables of the evaluation cells and their ranges of variation were as follows:

feedwater pressure	-	200-1500 psi
feedwater flow rate	-	0-3 gpm
feedwater temperature	-	70° - 150°F
feedwater concentration	-	as desired

The system was designed to permit endurance operation. Any evaluation cell could be removed from the system without interrupting operation of the other two cells.

The evaluation cell would accept a membrane or membrane-coated material specimen 2.5 inches in diameter. A photograph of the evaluation cell is shown in Figure 73. The two stainless-steel flanges were connected by four 1-inch bolts from the outer shell of the cell. The brine feedwater entered and left the cell through two 1/2-inch diameter holes in the upper flange of the assembly. A smaller hole directly in the center of this flange was a pressure-sensing port. A porous sintered stainless-steel disc was inserted into a cavity in the lower flange to support the membrane and a membrane-coated material specimen. An O-ring seal inserted between the membrane and the upper flange contained the pressurized brine. Product water passed through the porous support into a circular groove which was connected to a product-water drain tube.

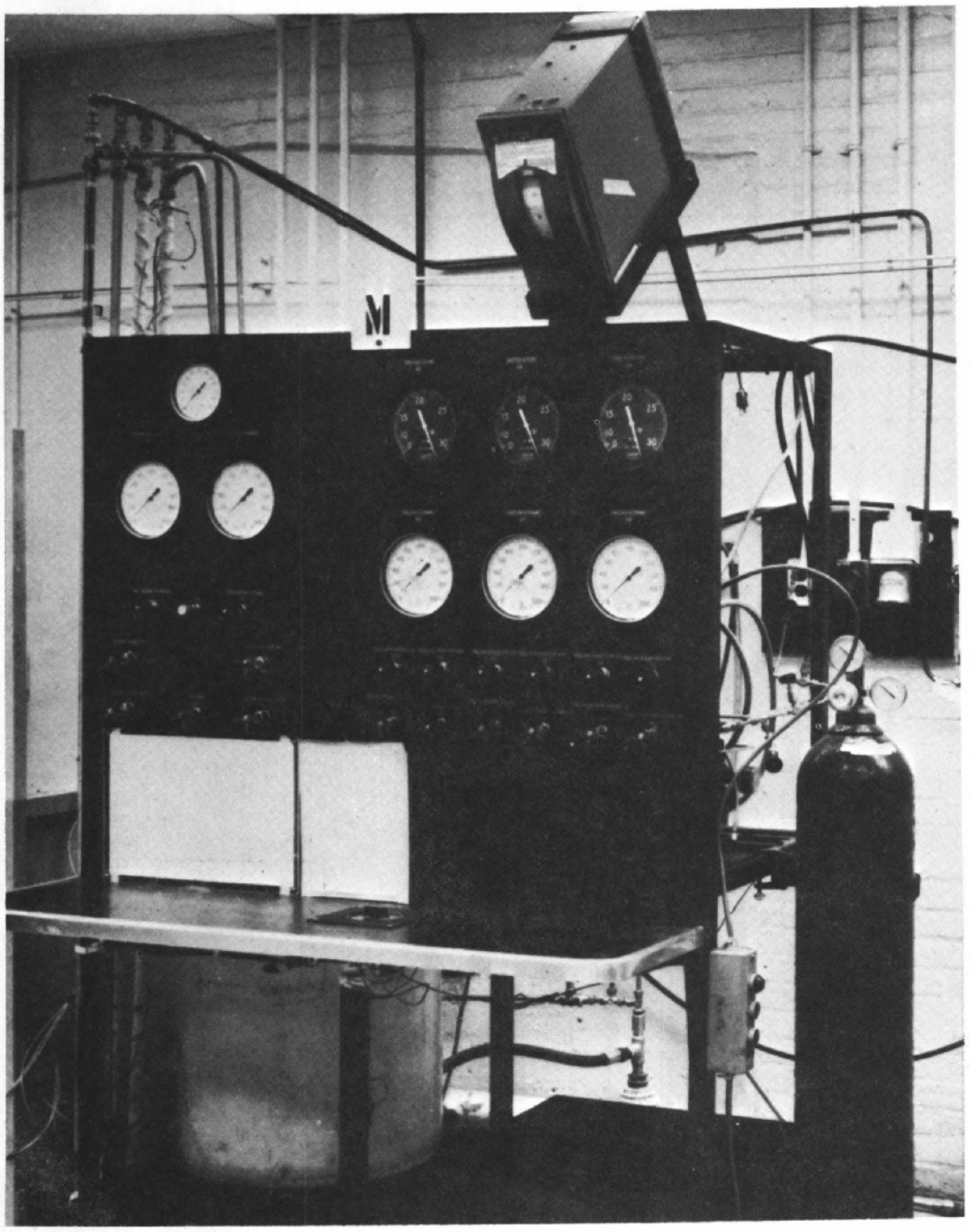

Figure 71 Photograph of Test System for Reverse-Osmosis Membranes XP-59686

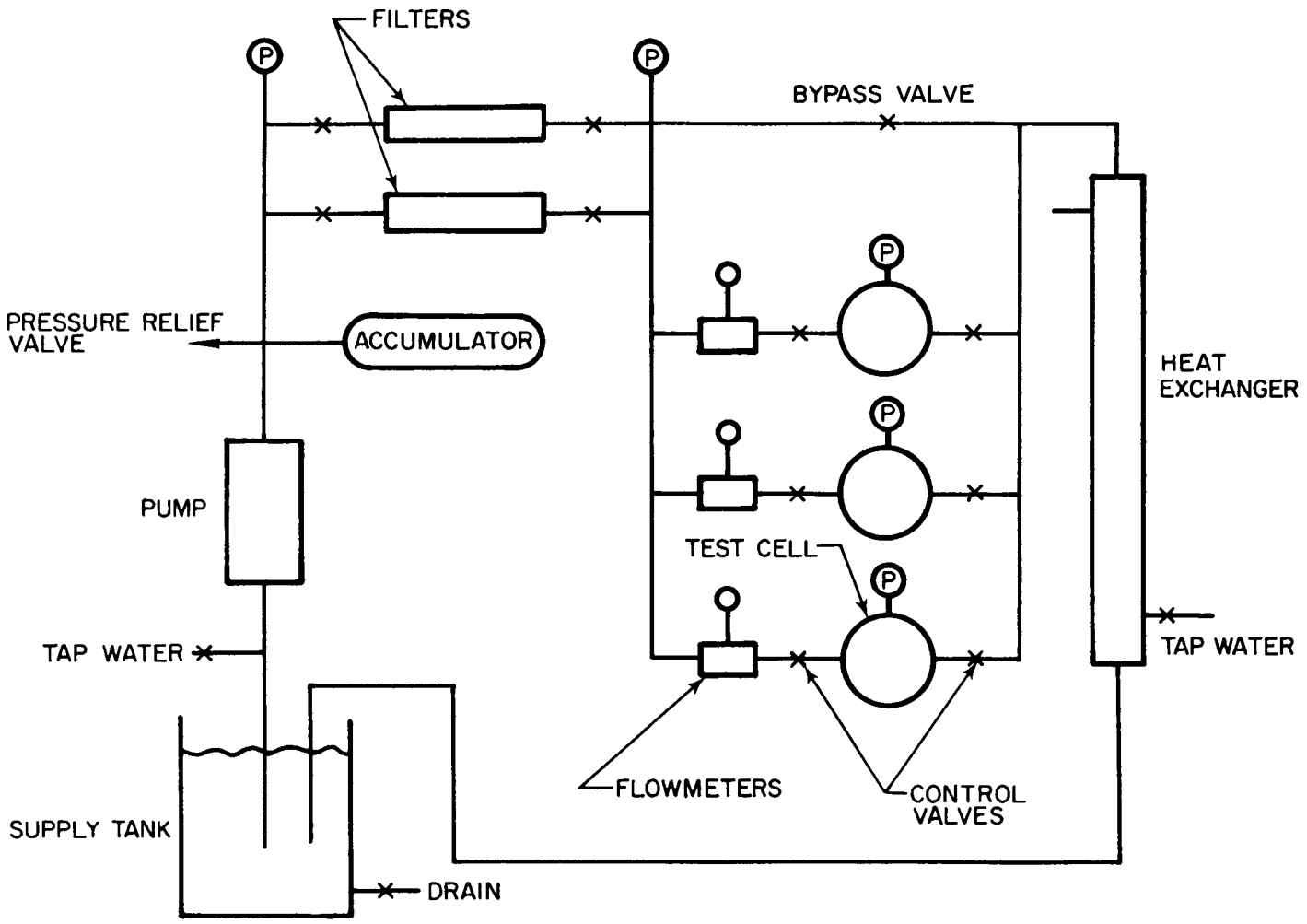

Figure 72 Schematic Diagram of Test System for Reverse-Osmosis Membranes

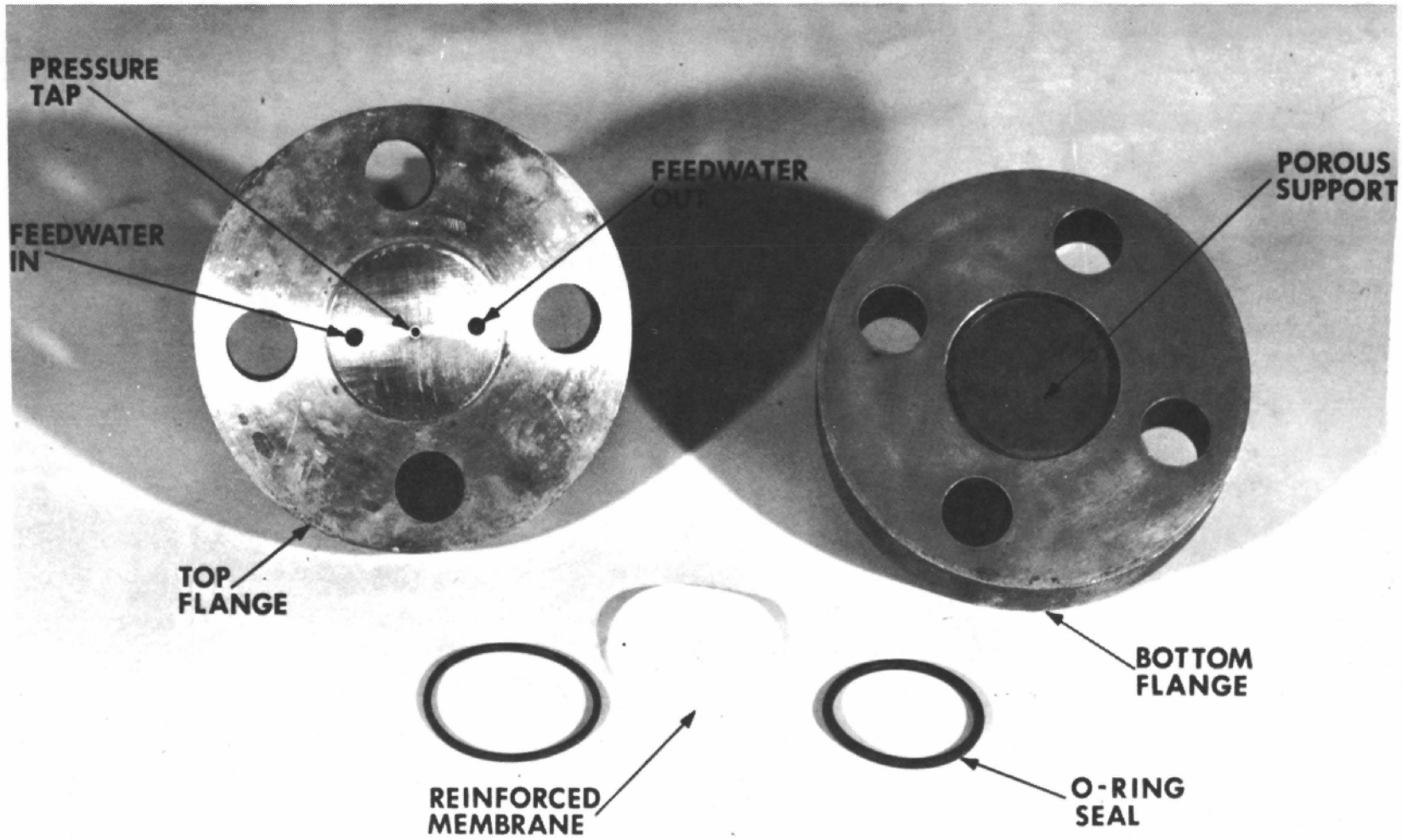

Figure 73 Membrane Evaluation Test Cell M-59559

Calculations indicated that the average brine velocity was 3.5 feet per second within the cell cavity for a brine flow rate of 2 gallons per minute. The Reynolds number at this condition of approximately 6000 was well above the value of 3600 required to achieve stable turbulent flow conditions. The existence of turbulent flow provides sufficient agitation of the brine solution that the salt concentration gradient adjacent to the membrane surface over the entire membrane surface area was minimized.

The entire system was connected by stainless-steel tubing. Noncorrosive metal valves were used throughout.

Salinity measurements of the feedwater and product water were determined by the Volhard titration method.

Evaluation of Reverse-Osmosis Cartridge

The reverse-osmosis cartridge test system employed during this contract is shown photographically in Figure 74 and schematically in Figure 75. The test system consisted of two basic items, a control console and a pressure vessel.

The test system was designed to permit operation with minimum attention by test personnel. System pressure was controlled automatically by means of a pneumatic controller while the feedwater flow rate was regulated by means of a positive-displacement duplex pump with an adjustable stroke. A heat exchanger controlled the brine temperature. Salinity measurements of the feedwater and product water were obtained by means of an electrical conductivity cell and a 1000 cps bridge. The system was connected with stainless-steel tubing. It operated at the following ranges:

feedwater pressure	-	300-1500 psi
feedwater flow rate	-	0 - 1.9 gpm
feedwater temperature	-	20-100°F
feedwater concentration	-	as desired

The pressure vessel used to contain the compact cartridge is shown in Figure 76. It was designed and constructed to the AMS Unfired Pressure Vessel Code. The vessel was constructed for a maximum operating pressure of 1650 psi at 300°F and was hydrostatic-pressure tested at 2475 psi. It was constructed of SA 515-70 carbon steel and coated with a corrosion-resistant paint. The paint began to break down when exposed to the brine solution as its operating temperature was higher than that recommended by the pressure-vessel manufacturer. Cracking at weld joints of dissimilar metals was feared. To prevent further breakdown of the paint and subsequent rusting, all internal parts of the pres-

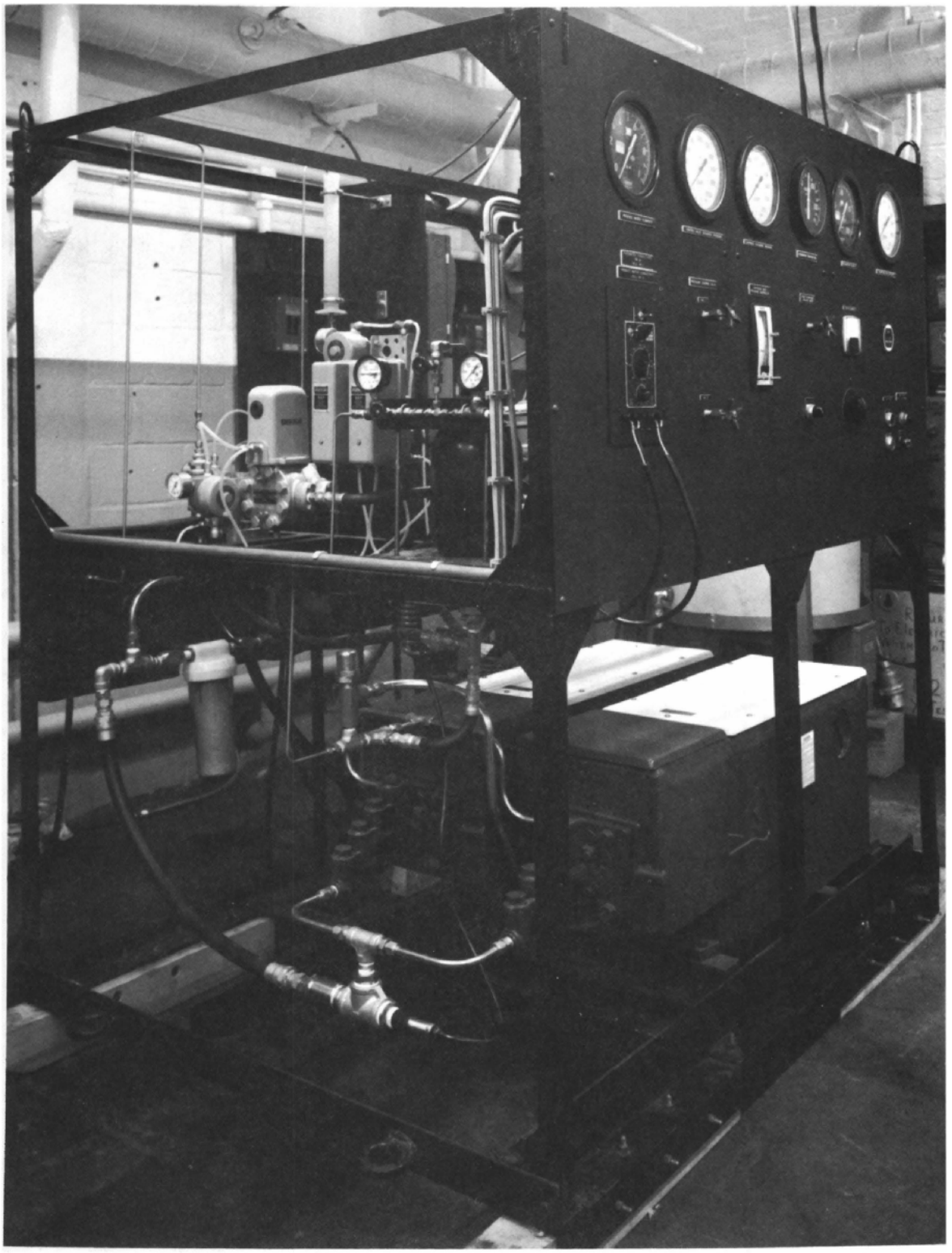

Figure 74 Reverse-Osmosis Test System XP-85099

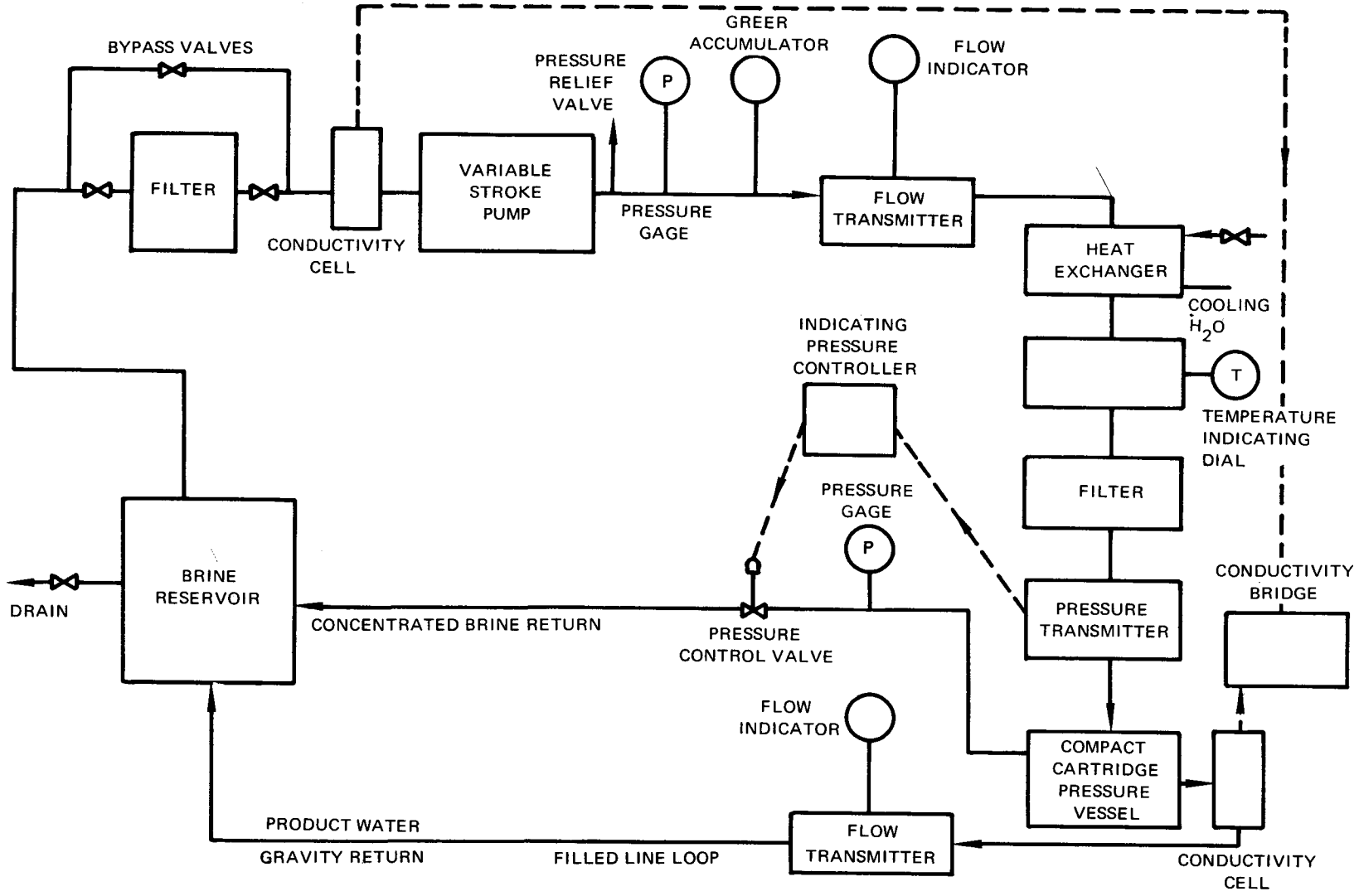

Figure 75 Reverse-Osmosis Test System Schematic

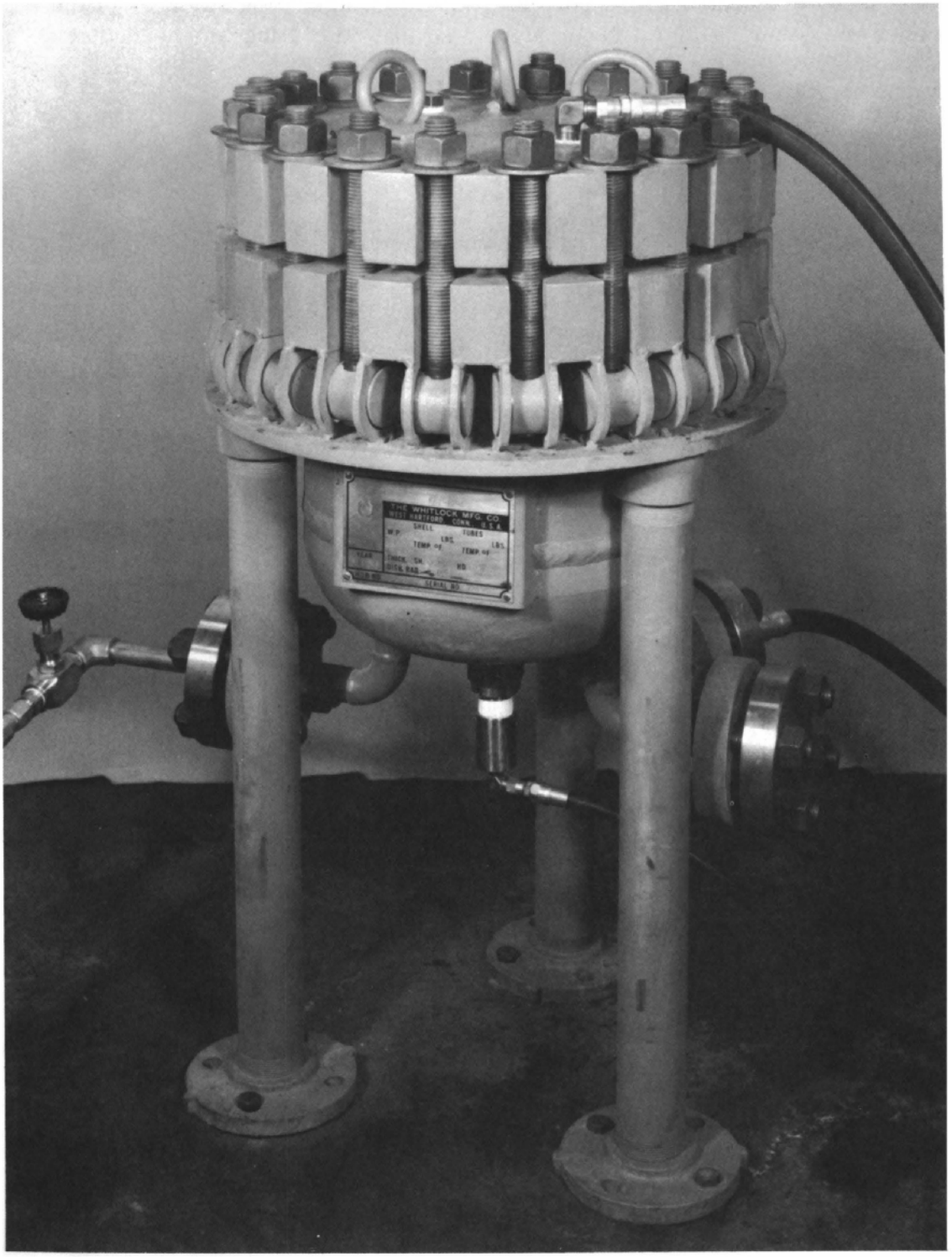

Figure 76 Pressure Vessel XP-84969

sure vessel were coated with a polyester tape. The sealing surfaces of the vessel were either 70-30 Cu-Ni or Monel, so that no coating was needed at these points.

APPENDIX 4

Nomenclature

NOMENCLATURE

A	-	membrane constant, gfd/psi
C	-	bulk concentration, ppm
C_{in}	-	bulk concentration of brine entering an increment, ppm
C_{out}	-	bulk concentration of brine leaving an increment, ppm
C_{pw}	-	concentration of product water ppm
C_w	-	concentration of brine at membrane surface, ppm
$\bar{C}$	-	average bulk concentration of brine for an increment, ppm
D_s	-	diffusion coefficient of salt
F	-	flow rate, gpm
h	-	channel height, inches
j	-	product-water flux, gfd
$\bar{j}$	-	average product-water flux, gfd
P	-	brine pressure - psi
P_{in}	-	pressure of brine entering an increment, psi
P_{out}	-	pressure of brine leaving an increment, psi
$\bar{P}$	-	average brine pressure for an increment, psi
Sr	-	membrane salt rejection
V	-	brine velocity, ft/sec
V_{in}	-	velocity of brine entering an increment, ft/sec
V_{out}	-	velocity of brine leaving an increment, ft/sec
$\bar{V}$	-	average brine velocity for an increment, ft/sec

V_o - velocity of brine at inlet of channel, ft/sec

w - width of channel, inches

x - axial distance from inlet of channel, inches

X - dimensionless axial length, $jx/V_o h$

δ_x - length of increment, inches

α - dimensionless variable defined by Equation (14)

Γ - polarization factor defined by Equation (10)

μ - dynamic viscosity, lb/ft sec

ξ - dimensionless variable defined by Equation (13)

π - osmotic pressure, psi

π_{pw} - osmotic pressure of product water, psi

π_w - osmotic pressure of brine at membrane surface, psi

ρ_{in} - density of brine entering an increment, lb/ft^3

ρ_{out} - density of brine leaving an increment, lb/ft^3

ρ_{pw} - density of product water, lb/ft^3

gfd - gallons per day per square foot of membrane area

gpm - gallons per minute

ppm - parts per million

psi - pounds per square inch

LIST OF INVENTIONS

In accordance with Article V of the contract, the subject inventions resulting from work done under the contract and reported to the Government are summarized as follows:

P&WA Project Number	Title	Date Reported	Interior Department Case No.
EH-1780	Regeneratable Reverse-Osmosis Membranes	2/23/67	none
EH-1805	Reverse-Osmosis Membrane Sandwich	3/23/67	none
EH-1437	Porous Backup Plates for Desalination	6/16/67	SAL 1216
EH-2025	Direct Casting of Reverse-Osmosis Membranes on Porous Support Materials	6/16/67	SAL 1217

☆ U.S. GOVERNMENT PRINTING OFFICE : 1969 O—336-970